Self-assembly of carbohydrate-based brush-like block copolymers : colored biomaterials and photonic crystals

Hong Li

THÈSE

Pour obtenir le grade de

DOCTEUR DE L'UNIVERSITÉ GRENOBLE ALPES

École doctorale : CSV- Chimie et Sciences du Vivant
Spécialité : Sciences des Polymères
Unité de recherche : CEntre de Recherche sur les MAcromolécules Végétales

Auto-assemblage de copolymères à blocs en peigne à base de carbohydrates : biomatériaux colorés et cristaux photoniques

Self-assembly of carbohydrate-based brush-like block copolymers: colored biomaterials and photonic crystals

Présentée par :

HONG LI

Direction de thèse :

Redouane BORSALI directeur de l'institut Carnot Polynat, Université Grenoble Alpes	Directeur de thèse

Rapporteurs :

Sophie GUILLAUME
DIRECTRICE DE RECHERCHE, CNRS délégation Bretagne et Pays de la Loire
Toshifumi SATOH
PROFESSEUR, Hokkaido University

Thèse soutenue publiquement le **6 décembre 2022**, devant le jury composé de :

Redouane BORSALI DIRECTEUR DE RECHERCHE, CNRS délégation Alpes	Directeur de thèse
Sophie GUILLAUME DIRECTRICE DE RECHERCHE, CNRS délégation Bretagne et Pays de la Loire	Rapporteure
Toshifumi SATOH PROFESSEUR, Hokkaido University	Rapporteur
Daniel GRANDE DIRECTEUR DE RECHERCHE, CNRS Ile-de-France Villejuif	Président
Christophe SINTUREL PROFESSEUR DES UNIVERSITES, Université dOrléans	Examinateur
Karine GORGY MAITRE DE CONFERENCES HDR, Université Grenoble Alpes	Examinatrice
Marc ZELSMANN CHARGE DE RECHERCHE HDR, CNRS délégation Alpes	Examinateur
Yu OGAWA CHARGE DE RECHERCHE, CNRS délégation Alpes	Examinateur

Acknowledgements

First of all, it is my honor to invite Sophie GUILLAUME, Toshifumi SATOH, Daniel GRANDE, Christophe SINTUREL, Karine GORGY, Marc ZELSMANN and Yu OGAWA to be my jury members. I also appreciate my jury members accepting to engage in the evaluation of my Ph.D. thesis.

I would like to thank sincerely my thesis supervisor Redouane BORSALI for receive me as a member of A2G group in CERMAV under foundation of CSC scholarship. Without his guidance and support over the past four years, my Ph.D. project wouldn't be carried out successfully. Under his endless advice and patience, it is great helpful for me to find a solution to dissolve the encountering issue. I am very grateful to Muhammad MUMTAZ for his great help and teaching of synthesis part. I am happy to integrate quickly into our group with his accompany. Special thanks to Karine GORGY, Jean-luc PUTAUX, Isabelle JEACOMINE, Marc ZELSMANN, Jean-Hervé TORTAI and Yu OGAWA to be my CSI jury from 2018-2022.

I would also like to thank Yoshiharu NISHIYAMA, Franck Dahlem, Hugues BONNET, Issei OTSUKA, Sami HALILA and Christophe TRAVELET for kind discussion and suggestions. Thanks to the big CERMAV family including technical and administrative staffs for their consistent support. Thanks to my friends and colleagues: Robin, Pier, Yao, Bing, Steve, Anais, Monica, Paulo, Armelle, Anny, Ahlem, Docas, Fransior, Kamilla, Rubal, Aicha, Noah, Ping-jui, Ender, Ge, Dan Chan, Kaifeng, Tianzheng, Zhongkuan and others for their friendship and help.

Lastly, I am deeply thankful to my parents, brother, sister, and girlfriend for their forever support and trust no matter how far away between us. Without this sincere love and consistent support for every single day from them, I cannot go far and accomplish my Ph.D. project.

Table of Contents

General Introduction

Carbohydrates constitute a sustainable source of materials that has attracted a growing interest due to their "green" aspects, biocompatibility, biodegradability and bio-recognition properties. Their industrial applications at the macroscopic scale are offering new solutions for biobased materials and they find applications in different sectors such as cosmetics, health, packaging, or microelectronics. Recently, novel class of nanostructured systems obtained from the self-assembly of carbohydrate-based brush block copolymers (BRs) has been developed to achieve periodic organizations (a few hundred nm in domain spacings) resulting in materials exhibiting structural colors. They are the so-called one-dimensional photonic crystals 1D-PCs, or Bragg stacks, that consist of alternating layers of high-and low-refractive index materials. At the specific wavelength for which the optical periodicity of the material matches the path length of a photon, a photonic band gap is formed, which prevents this frequency of light from propagating. At this wavelength, all reflected signals are in phase and add constructively, generating a reflected signal. Consequently, an iridescence can be observed in a similar way to the natural structurally-colored tissues, for instance, natural opals, the wings of some butterflies, the cuticles of beetles and a variety of other animal and plant species.

Based on the above consideration, my Ph.D. project was to explore the properties of colored materials made from the self-assemblies of a series of brush-like block copolymers made with polystyrene (PS) and maltoheptaose (MH) as side chains attached a polynorbornene backbone. Those systems were synthesized by the "self-assembly glycopolymer group of CERMAV" with different molecular weight (MW) and targeting lamellar phases and therefore colored materials. The results that are presented in the thesis describes those results, namely, full-color display of the one-dimensional photonic crystals (1D-PCs) fabricated from the self-assembly of brush-like glycopolymers and their blends can be obtained exhibiting colorless, blue, green, orange to grey covering the entire UV-vis. spectrum range. Impressively, the optical appearance of these films can be quickly (with controlled and reproducible manner)

changed from colorless to blue, green, yellow and orange within few seconds by simply controlling solvent atmosphere.

In colloidal suspension, highly homogenous core-shell glyconanoparticles can be easily obtained via the self-assembly of BRs under the water vapor environment. Those spherical glyconanoparticles can be tunable into multiple morphologies including rod, cubic, donut and honeycomb nanostructures after thermal annealing treatments, which may put forward new insight into the design and synthesis of functional materials with unique structures, properties, and applications by using post-treatments of the glyconanoparticles.

In the rest of the Ph.D. work, a series of BRs were used to investigate their morphologies on surface (mica) or highly oriented pyrolytic graphite (HOPG) as a function of time using atomic force microscopy (AFM). Expectedly, an increase in the average length from about 25 nm, 35 nm to 100 nm can be observed along with increasing molar mass on mica, which were consistent with increasing the backbone polymerization of BRs. Impressively, multiple morphologies including worm-like, S- or C-shape, tadpole-like, helical-like, globular-like, hair-like, droplet-like and island-like, were observed at high dilution solution by spin coating on mica. In contrast, globe-shape, tadpole-shape, toroid-shape, rod-shape and pearl-necklacelike conformations are obtained by spin coating on the HOPG substrate. Herein, diverse of conformation and dynamic shape-changing of BRs hierarchical molecular architecture, show a potential in different applications.

In the end, these novel carbohydrate-based brush block copolymers (BRs) can rapidly self-assemble into highly ordered nanostructures as compared to linear high molar weight block copolymers (BCPs), due to their dense functionality, low entanglement, to achieve lamellar organizations with few hundred nm in domain spacings. They are attracting a lot of attention as potential candidates for various optoelectronic applications, including their use as filters, low- and high-reflection coatings, gratings

and resonant cavities due to their intrinsic capability to manipulate and control the propagation of visible light. Accordingly, there is a huge interest especially in the field of structural color materials, where the optical properties can be tuned upon application of external triggers (such as solvent vapor, UV etc…).

List of Abbreviations

BRs	Brush block copolymers
PCs	Photonic crystals
1D	One-dimensional
2D	Two-dimensional
3D	Three-dimensional
1D-PCs	One-dimensional photonic crystals
2D-PCs	Two-dimensional photonic crystals
3D-PCs	Three-dimensional photonic crystals
CMC	Critical micelle concentration
ROMP	Ring open metathesis polymerization
PBGs	Photonic bandgaps
PS	Polystyrene
PLA	Polylactide
MH	Maltoheptaose
MT	Maltotriose
MW	Molecular weight
HOPG	Highly oriented pyrolytic graphite
BCPs	Block copolymers
GNCs	Glyconanoparticles
AFM	Atomic force microscopy
SAXS	Small-angle X-ray ccattering
BrBCPs	Brush diblock copolymers
PEO	Poly(ethylene oxide)
PEG	Poly(ethylene glycol)
LA	Lactide
EO	Ethylene oxide
SDEMS	Solvent diffusion-evaporation-mediated self-assembly
DMAP	4-(Dimethyamino) pyridine

TEA	Trimethylamine
THF	Tetrahydrofuran
DMF	*N*, *N*-Dimethylformamide
CaH_2	Calcium hydride
NbBOH	N-(4-hydroxybutyl)-cis-5-norbornene-exo-2, 3-dicorboxiimide
NbCOOH	N-(hexanoic acid)-cis-5-norbornene-exo-2, 3-dicorboxiimide
PS-OH	ω-Hydroxyl terminated polystyrene
NbPS	2-Polystyrylethyl-6-(cis-5-norbornene-exo-2, 3-dicorboxiimide) hexanoate
NbBBBr	N-(4-bromobutanoate butyl)-cis-5-norbornene-exo-2, 3-dicorboxiimide
NMWDs	Narrow molecular weight distributions
PDMS	Polydimethylsiloxane
DLS	Dynamic light scattering
PVA	Polyvinyl achohol
SDS	Sodium dodecyl sulfate
NCs	Nanoparticles
nm	Nanometer
PDI	Polydispersity index
μm	Micrometer
NMR	Nuclear magnetic resonance
FT-IR	Fourier transform infrared spectroscopy
TEM	Transmission electronic microscopy
Cryo-TEM	Cryogenic transmission electronic microscopy
SEC	Size exclusion chromatography
SEM	Scanning electron microscopy

Chapter 1： Literature Review

1.1. Introduction

Photonic crystals (PCs),[1] capable of interfering the light waves that propagate through this structure, are able to reflect specific-frequency wavelength due to their periodically organized structures, in which domains composed of variation of dielectric constant are regularly repeated. Consequently, photonic bandgaps (PBGs)[2] are created in PCs comparable to the energy bandgap of wavelengths so that destructive interference of certain wavelengths scattered from dielectric lattice (Bragg scattering)[3] takes place in PCs. Taking advantage of the feasibility of creating a PBG, it is possible to adjust the light propagation happened in PCs. Therefore, PCs are engaged in some of particular interest applications, including use as lasers,[4] polarizers,[5] solar absorbers,[6] sensing,[7] imaging,[8] self-collimation,[9] negative refraction,[10] optical diode[11] and light bending[12] so on. (Figure 1) Even though the emergence of an interdisciplinary field of technology and science gains increasing attention shown in Figure 2a by the publication rate.[13] Since the concept of the PCs was firstly documented by Yablonovitch[14] and John[15] in 1987, research on PCs has been eruptive for over three decades shown in Figure 2b in which there is a persistently increasing tendency in the number of published papers every year except for 2020 due to COVID-19 limiting research activities (Scopus database).[16]

To date, PCs have been achieved by a variety of strategies such as traditional “top-down”[17] and “bottom-up” approaches[18]. In comparison with the “top-down” approaches, “bottom-up” approaches as a relatively cheaper and fast techniques to prepare PCs under moderate conditions,[19] have been received a lot of attention including self-assembly of linear and brush block copolymers (Figure 2). Based on these polymers fabricated into PCs, brush polymers have several superior advantages over other polymers due to their unique architecture: (1) highly dense and regularly spaced side chains attached to the backbone.[20-22] (2) extended wormlike or cylindrical backbone conformations.[23-25] (3) reduced chain entanglement compared to their linear block polymers.[26, 27] In addition, the optical properties of PCs can be further enhanced

and diversified by introducing additives (namely polymers,[28] nanoparticles[29] and solvents[30]) to fulfill multifunctional performances. Therefore, a large number of articles have been reported on the synthesis strategies of brush polymers for applications in photonic devices,[31] imaging,[32] tumor detection[33] and lithographic patterning[34] so on. Recently, the exotic properties promised by photonic materials have added a new growth area.[13] In the continued development of photonics, structures and components of brush polymers will play an increasingly critical role, and it is therefore timely for designing a precisely and well-defined brush polymers in fabrication and application of photonic crystals.

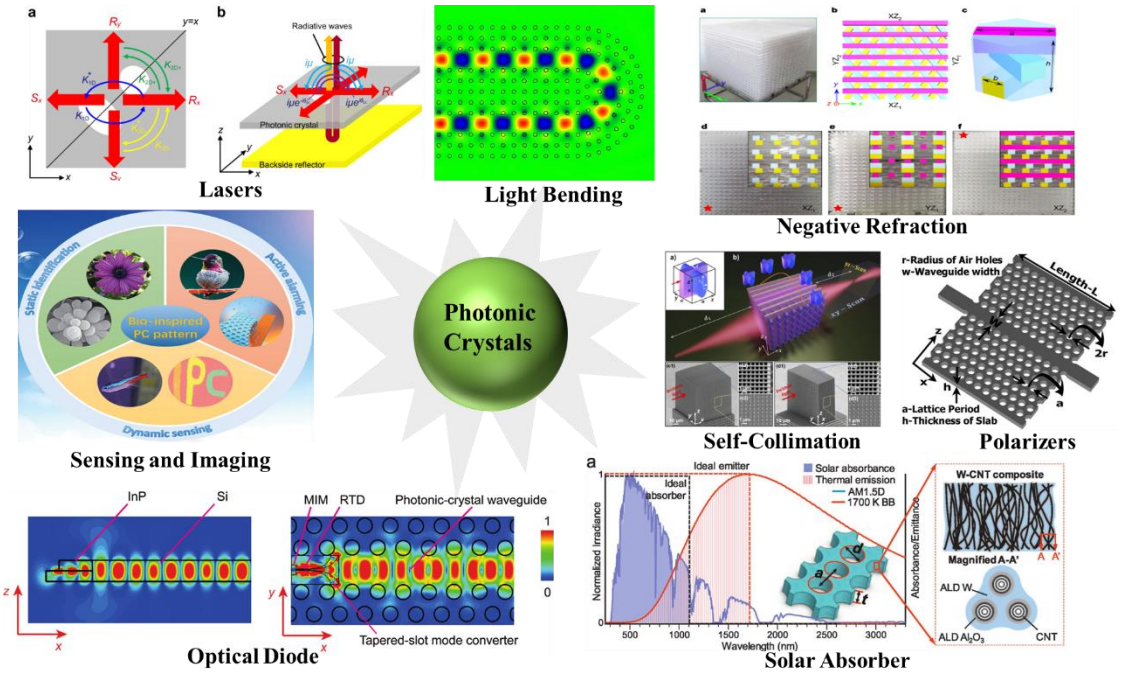

Figure 1. The scheme representation of photonic crystals applications in lasers,[4] polarizers,[5] solar absorbers,[6] sensing,[7] imaging,[8] self-collimation, [9] negative refraction, [10] optical diode[11] and light bending.[12]

Inspired by such distinctive properties of the carbohydrate molecules due to their natural abundance, good biocompatibility and renewable availability,[35-37] the combination of synthetic polymers with the carbohydrate molecules, leading to a variety of liner block copolymers polymers, has been exploited[38-43] . However, to date, little attention has been paid to the development of carbohydrate-decorated brush block

copolymers (BRs) with resonant optical properties such as photonic band gaps, as they require structures with large periodicities, comparable to the wavelengths (λ) of light being manipulated. In previous studies of our group, the self-assemblies of a number of carbohydrate-based liner block copolymers that consisted of various hydrophobic synthetic polymers with oligo- or polysaccharides involving amylose, maltotriose (MT) and maltoheptaose (MH), were adequately and systematically investigated the desired nano-organized thin films and nanoparticles[40, 44-51]. With this useful information in hand, from an application point of view, we are currently attempting to design a novel carbohydrate-decorated brush block copolymer to obtain a predictable morphology and size thin films, photonic crystals and nanoparticles, which could be applied in optical elements and drug carrier, respectively. Based on the above consideration including well-studied on the assembly of linear PS-block-MH in our group and UV cross-linking capability of PS,[52-54] in my Ph.D. project, a series of bottlebrush block copolymers with polystyrene (PS) and maltoheptaose (MH) as side chains attached the backbone polynorbornene, were successfully synthesized with different molecular weight (MW) tuned by backbone degree of polymerization under the help of Muhammad Mumtaz in our group (Scheme 1, see synthetic part in chapter 2). Subsequently, the preparation of photonic crystals and glyconanoparticles (GNCs) from these bottlebrush block glycol-polymers were investigated in the following chapter 3 and chapter 4.

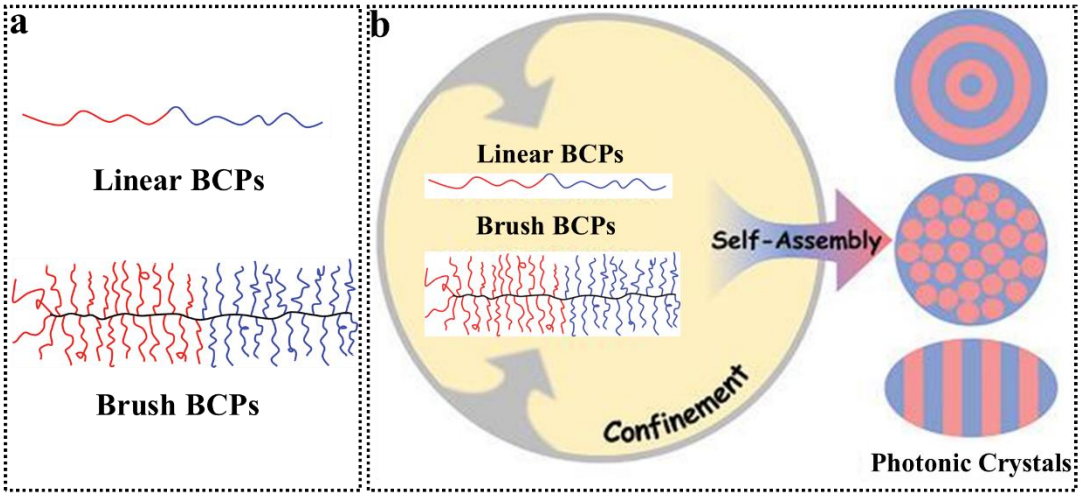

Figure 2. (a) Comparison of linear (top) and brush (bottom) block copolymers (BCPs).[55] (b) The schematic illustration of the self-assembly of BCPs into photonic materials.[56]

1.2 History of photonic crystal

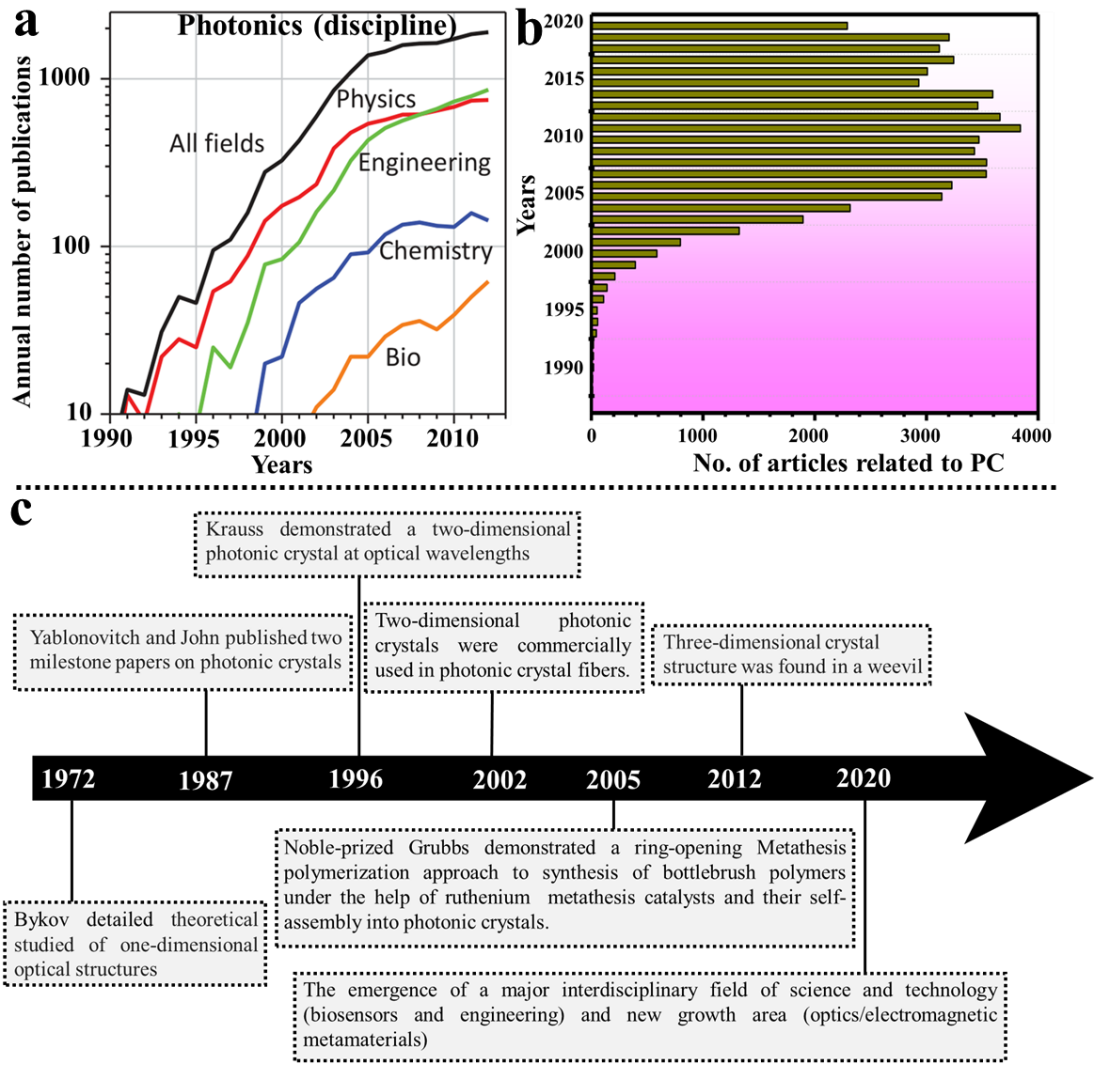

Figure 3. (a) Annual photonic crystal research papers produced by different disciplines.[13] (b) The number of research publications related to PC indexed in the Scopus database.[16] (c) Timeline in the history of photonic crystals.[13-15, 58-62]

In fact, the history of photonic crystals studies can be traced back to the 1887,[57] when Raylaigh Lord investigated theoretically these one-dimensional periodic structures termed as one-dimensional photonic crystals (1D-PCs) today by showing a one-dimensional photonic bandgap (PBG) in the 1D-PCs. By 1972,[58] Bykov studied firstly the issue of the spontaneous radiation in one-dimensional optical structures with a PBG. Then two or three dimensional periodic optical structures were also studied by Bykov in 1975.[59] However, scientists did not pay attention appropriately to these studies due to ahead of their time. Until 1987 (over 100 years later), two milestone articles of PCs

documented by Yablonovitch[14] and John[15] respectively, were recognized as one of landmark developments in physics. After 1987, research on PCs grew exponentially as depicted in Figure 3b. In 2002, commercial two-dimensional PCs were applied in photonic crystal fibres.[60] Three year later (2005),[61] noble-prized Grubbs created a novel ruthenium metathesis catalysts used as a ring-opening metathesis ruthenium approach to synthesis of bottlebrush polymers, which provided a powerful method to prepare PCs from the self-assembly of bottlebrush polymers. To better understand and design in PCs from nature, in 2012,[62] biomimetics study of natural structures in a diamond crystal structure was discovered in a weevil. Today, significant development and capability of PCs has greatly promoted the development of interdisciplinary including biosensors and engineering, even the emergence of new research area[13] (Figure 3a).

1.3 Types of photonic crystals

According to the periodic arrangement of dielectric material along one, two, and three axis, photonic crystals can be mainly characterized into one dimensional (1D), two dimensional (2D) and three dimensional (3D) PCs, respectively.[63] Figure 4a demonstrated the schematic illustrations of 1D-PCs, 2D-PCs, and 3D-PCs in which materials with different refractive indices were revealed by the different color. 1D-PCs as the simplest case scenario (Bragg reflectors), is made up of alternating layers with varied refractive indices. 2D-PCs can be formed in a planar crystal structure where the columns of dielectric materials are periodic in arrangement. 3D-PCs consisted of materials with varying refractive indices in all three directions, can create a complete PBG where light propagation is not allowed at certain range of wavelength along any direction of the 3D lattice structure. In this context, 2D and 3D-PCs have been widely applied in chemical, biomolecular wearable sensors, communication, solar cells, and laser propagation so on.[64, 65] However, it is still challenging for integrating other structures into 2D-PCs and 3D-PCs because of their complex structure, which limits to mass production during fabrication processes.[66-68] In contrast, 1D-PCs with a simple structure and ease fabrication process, relative easily prediction of their optical properties, and high reflectivity have been always received lots of consideration by

researchers over last three decades. In 2016, B. Yang reported that a relatively flexible and convenient way based on 1D layers was discussed about the possibility of constructing 3D staked structures by chemical routes.[69] In 2018, P. Lova showed that advances in functional solution processed planar 1D-PCs, providing a promising method to scale-up the fabrication in the low cost integrated optoelectronic devices.[70] In 2021, L. Torrijos-Morán revealed slow light bimodal interferometry in 1D-PC waveguides with the significant performance improvement.[1] In the continuous efforts for years by researchers and inspired by natural creatures, it greatly expands the range of applications of 1D-PCs shown in Figure 4b. In my Ph.D. project, 1D-PCs was focused to study by the self-assembly of brush block glycol-copolymers and the properties of 1D-PCs was detailly investigated in the chapter 3.

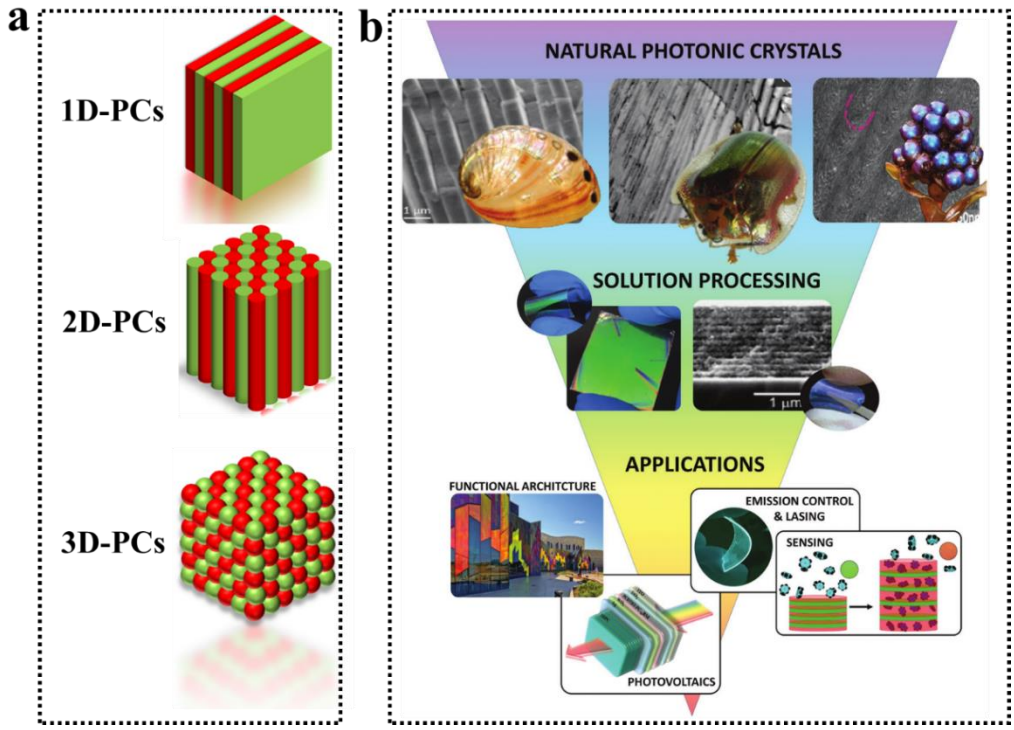

Figure 4. (a) Schematic illustration of 1D-PCs, 2D-PCs, and 3D-PCs. (b) Evolution of distributed Bragg reflectors technologies.[70] Digital images and electron microscopy and of natural PCs structures from top to bottom: Panamanian Tortoise beetle[71], Mother of pearl[72] and Pollia Condensata Berries[73]. Scheme photographs of distributed Bragg reflectors applications.[70, 74-76]

1.4 Properties of one-dimensional photonic crystals.

At each interface of the alternating layers of varying refractive indices in 1D-PCs, interference of incident light takes place when the path length of a photon is equal to the periodicity of PBG, leading a strong reflected signals at the specific wavelength. In the following equations, Bragg's law and Snell's law (Equation 1) can be applied to estimate the reflected wavelength of light (λ_{Bragg}).[70, 77]

$$\textbf{Equation 1: } m\lambda_{Bragg} = 2D \times (\eta^2_{eff} - \sin^2\Theta)^{1/2}$$

Where θ is the incident angle, η is the effective index, D is the layer thickness ($D = d_1 + d_2$, the thickness of the two constituent layers is d_1 and d_2, respectively), m is the order of Bragg diffraction.[55]

$$\textbf{Equation 2: } \eta_{eff} = (n_1d_1 + n_2d_2)/(d_1 + d_2)$$

Equation 2 can be used to calculate the effective refractive index. n_{eff} is the effective refractive index, and $n_1 + n_2$ is the refractive index of the two layers. The reflected wavelength peak (λ_{Bragg}) for a normal incidence, can be simplified as the following equation 3.[78, 79]

$$\textbf{Equation 3: } m\lambda = 2(n_1d_1 + n_2d_2)$$

Based on the above equation 3, the reflected wavelength of light is dependent on the optical thickness of each layer. Thus, altering the thickness or refractive index of the constituent layers, are mostly applied to adjust the reflected wavelength peak. According to the above mechanism, practically many samples as sensing by swelling[80] or pore filling[81] were achieved based on a photonic bandgap change. For angle of incidence θ, the reflected wavelength peak can be simplified as the following equation $m\lambda = 2nd\sin\Theta$ as shown in Figure 5.[78,79]

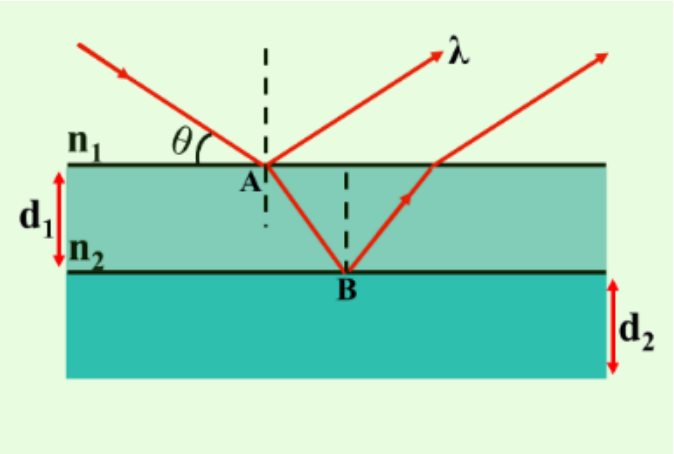

Figure 5. Illustration of Bragg's law. **m** is the diffraction order; **λ** is the wavelength of the reflected light; **n** is the mean refractive index; **d** is the lattice period; **Θ** is the angle of incident light.

1.5 Fabrication of Photonic Crystals

Photonic crystals can be fabricated by kinds of strategies including as "top-down" and "bottom up" approaches shown in Figure 6.[55] For instance, electrochemical etching,[82] phase mask lithography,[83] and layer-by-layer stacking,[84] termed as "top-down" technologies, have been widely applied to manufacture photonic crystals precisely. However, these approaches are usually in need of complicated sets of procedures and complex equipment.[85] In contrast, "bottom-up" approaches accomplished by the self-assembly of polymers or colloidal crystals, have been attracting people's attention due to their fast processes, relative inexpensiveness and mild processing conditions.[19] Unfortunately, it is usually necessary for colloidal photonic crystals to integrate with inorganic materials,[86] leading to increase series of fabrication procedures and costs, and typical colloidal materials with low refractive index contrast impose restrictions on applications of colloidal templates.[87-89] Moreover, face-centered cubic or hexagonal closely packed geometries are generally found in the assembly of colloidal photonic crystals, limiting geometric diversities of colloidal materials.[90]

Thanks to the advance of modern polymerization technologies, it is possible for scientists to design and synthesize the polymers with different chain architectures and molecular weights, providing fascinating PCs based on polymeric multilayer structures.[91] These polymeric materials are easily moldable and flexible so that series

of geometrical forms have been achieved by controlling mechanical properties, compositions and structures of soft materials.[92-95] Although polymeric components suffer from the relatively small refractive index contrast[96] in comparison with inorganic dielectrics[97], this hindrance can be compensated for by functionalizing polymeric materials with an intrinsic high refractive index[98], loading with high index components[99] and increasing layers in large numbers[78]. In this context, brush polymers as a kind of soft material, also termed as bottlebrushes, have come to fore due to their unique architecture, that is, polymeric side chains with a highly-grafted density attached to the linear backbone.[20-22] In the chapter 2, we will discuss about the classification of brush polymers and general synthetic methods to prepare brush polymers.

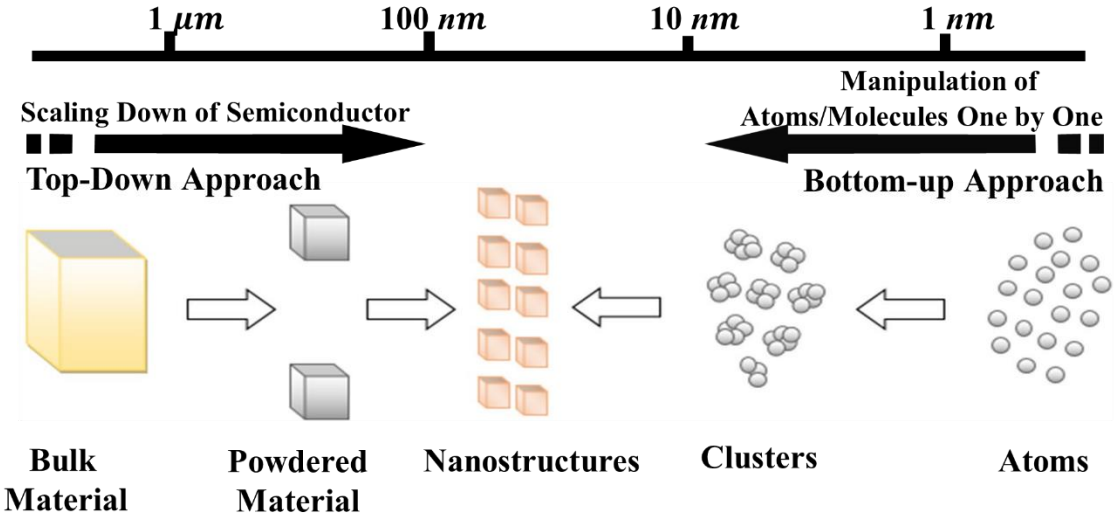

Figure 6. Schematic illustration of "top-down" and "bottom-up" approaches for synthesis of nanostructures.[100]

References:

1. Torrijos-Moran, L.; Griol, A.; Garcia-Ruperez, J., Slow light bimodal interferometry in one-dimensional photonic crystal waveguides. *Light Sci Appl* **2021,** *10* (1), 16.
2. Wu, F.; Lyu, K.; Hu, S.; Yao, M.; Xiao, S., Ultra-large omnidirectional photonic band gaps in one-dimensional ternary photonic crystals composed of plasma, dielectric and hyperbolic metamaterial. *Opt Mater* **2021,** *111*, 110680.
3. Rybin, M. V.; Filonov, D. S.; Samusev, K. B.; Belov, P. A.; Kivshar, Y. S.; Limonov, M. F., Phase diagram for the transition from photonic crystals to dielectric metamaterials. *Nat Commun* **2015,** *6*, 10102.
4. Inoue, T.; Yoshida, M.; Gelleta, J.; Izumi, K.; Yoshida, K.; Ishizaki, K.; De Zoysa, M.; Noda, S., General recipe to realize photonic-crystal surface-emitting lasers with 100-W-to-1-kW single-mode operation. *Nat Commun* **2022,** *13* (1), 3262.
5. Prakash, C.; Sen, M., Optimization of silicon-photonic crystal (PhC) waveguide for a compact and high extinction ratio TM-pass polarization filter. *J Appl Phys* **2020,** *127* (2), 023101.
6. Cui, K.; Lemaire, P.; Zhao, H.; Savas, T.; Parsons, G.; Hart, A. J., Tungsten-carbon nanotube composite photonic crystals as thermally stable spectral-selective Absorbers and Emitters for Thermophotovoltaics. *Adv Energy Mater* **2018,** *8* (27), 1801471.
7. Wu, P.; Wang, J.; Jiang, L., Bio-inspired photonic crystal patterns. *Mater Horiz* **2020,** *7* (2), 338.
8. Pitruzzello, G.; Krauss, T. F., Photonic crystal resonances for sensing and imaging. *J Opt* **2018,** *20* (7), 073004.
9. Xia, C.; Gutierrez, J. J.; Kuebler, S. M.; Rumpf, R. C.; Touma, J., Cylindrical-lens-embedded photonic crystal based on self-collimation. *Opt Express* **2022,** *30* (6), 9165.
10. He, H.; Qiu, C.; Ye, L.; Cai, X.; Fan, X.; Ke, M.; Zhang, F.; Liu, Z., Topological negative refraction of surface acoustic waves in a Weyl phononic crystal. *Nature* **2018,** *560* (7716), 61.
11. Yu, X.; Kim, J. Y.; Fujita, M.; Nagatsuma, T., Efficient mode converter to deep-subwavelength region with photonic-crystal waveguide platform for terahertz applications. *Opt Express* **2019,** *27* (20), 28707.
12. Zhang, Y.; Li, B., Photonic crystal-based bending waveguides for optical interconnections. *Opt Express* **2006,** *14* (12), 5723.
13. Lee, J. H.; Koh, C. Y.; Singer, J. P.; Jeon, S. J.; Maldovan, M.; Stein, O.; Thomas, E. L., 25th anniversary article: ordered polymer structures for the engineering of photons and phonons. *Adv Mater* **2014,** *26* (4), 532.
14. Yablonovitch, E., Inhibited spontaneous emission in solid-state physics and electronics. *Phys Rev Lett* **1987,** *58* (20), 2059.
15. John, S., Strong localization of photons in certain disordered dielectric superlattices. *Phys Rev Lett* **1987,** *58* (23), 2486.
16. Butt, M. A.; Khonina, S. N.; Kazanskiy, N. L., Recent advances in photonic crystal optical devices: A review. *Opt Laser Technol* **2021,** *142*, 107265.

17. Takahashi, S.; Suzuki, K.; Okano, M.; Imada, M.; Nakamori, T.; Ota, Y.; Ishizaki, K.; Noda, S., Direct creation of three-dimensional photonic crystals by a top-down approach. *Nat Mater* **2009,** *8* (9), 721.
18. Wang, J.; Pinkse, P. W. H.; Segerink, L. I.; Eijkel, J. C. T., Bottom-up assembled photonic crystals for structure-enabled label-free sensing. *ACS Nano* **2021,** *15* (6), 9299.
19. Galisteo-Lopez, J. F.; Ibisate, M.; Sapienza, R.; Froufe-Perez, L. S.; Blanco, A.; Lopez, C., Self-assembled photonic structures. *Adv Mater* **2011,** *23* (1), 30-69.
20. Xia, Y.; Olsen, B. D.; Kornfield, J. A.; Grubbs, R. H., Efficient synthesis of narrowly dispersed brush copolymers and study of their assemblies: the importance of side chain arrangement. *J Am Chem Soc* **2009,** *131* (51), 18525.
21. Hadjichristidis, N.; Pitsikalis, M.; Pispas, S.; Iatrou, H., Polymers with complex architecture by living anionic polymerization. *Chem Rev* **2001,** *101* (12), 3747.
22. Zhang, M.; Müller, A. H. E., Cylindrical polymer brushes. *J Polym Sci A Polym Chem* **2005,** *43* (16), 3461.
23. Wintermantel, M.; Gerle, M.; Fischer, K.; Schmidt, M.; Wataoka, I.; Urakawa, H.; Kajiwara, K.; Tsukahara, Y., Molecular bottlebrushes. *Macromolecules* **1996,** *29* (3), 978.
24. Sheiko, S. S.; Moller, M., Visualization of macromolecules-a first step to manipulation and controlled response. *Chem Rev* **2001,** *101* (12), 4099.
25. Henn, D. M.; Fu, W.; Mei, S.; Li, C. Y.; Zhao, B., Temperature-induced shape changing of thermosensitive binary heterografted linear molecular brushes between extended wormlike and stable globular conformations. *Macromolecules* **2017,** *50* (4), 1645.
26. Sveinbjornsson, B. R.; Weitekamp, R. A.; Miyake, G. M.; Xia, Y.; Atwater, H. A.; Grubbs, R. H., Rapid self-assembly of brush block copolymers to photonic crystals. *Proc Natl Acad Sci U S A* **2012,** *109* (36), 14332.
27. Liang, H.; Grest, G. S.; Dobrynin, A. V., Brush-like polymers and entanglements: from linear chains to filaments. *ACS Macro Lett* **2019,** *8* (10), 1328.
28. Miyake, G. M.; Piunova, V. A.; Weitekamp, R. A.; Grubbs, R. H., Precisely tunable photonic crystals from rapidly self-assembling brush block copolymer blends. *Angew Chem Int Ed Engl* **2012,** *51* (45), 11246.
29. Song, D. P.; Li, C.; Colella, N. S.; Lu, X.; Lee, J. H.; Watkins, J. J., Thermally tunable metallodielectric photonic crystals from the self-assembly of brush block copolymers and gold nanoparticles. *Adv Opt Mater* **2015,** *3* (9), 1169.
30. Xu, Y.; Hickey, R. J., Solvent-responsive and reversible structural coloration in nanostructured block polymer films. *Macromolecules* **2020,** *53* (14), 5711.
31. Wei, M.; Gao, Y.; Serpe, M. J., Polymer brush-based optical device with multiple responsivities. *J Mater Chem B* **2015,** *3* (5), 744.
32. Zhang, X.; Yang, P.; Dai, Y.; Ma, P. a.; Li, X.; Cheng, Z.; Hou, Z.; Kang, X.; Li, C.; Lin, J., Multifunctional up-converting nanocomposites with smart polymer brushes gated mesopores for cell imaging and thermo/pH dual-responsive drug controlled release. *Adv Funct Mater* **2013,** *23* (33), 4067.

33. Wang, J.; Wang, Y.; Chen, H.; Xu, H.; Wang, W.; Bai, L., Sensitive and simultaneous detection of tumor markers assisted by novel functional polymer brush/Au nanoparticles composite. *Sens Actuators B Cheml* **2018,** *258*, 998.
34. Chen, T.; Amin, I.; Jordan, R., Patterned polymer brushes. *Chem Soc Rev* **2012,** *41* (8), 3280.
35. Morris, J.; Bietsch, J.; Bashaw, K.; Wang, G., Recently developed carbohydrate based gelators and their applications. *Gels* **2021,** *7* (1), 24.
36. Solanki, A.; Das, M.; Thakore, S., A review on carbohydrate embedded polyurethanes: an emerging area in the scope of biomedical applications. *Carbohydr Polym* **2018,** *181*, 1003.
37. Vankar, Y. D.; Schmidt, R. R., Chemistry of glycosphingolipids-carbohydrate molecules of biological significance. *Chem Soc Rev* **2000,** *29* (3), 201.
38. Hung, C. C.; Nakahira, S.; Chiu, Y. C.; Isono, T.; Wu, H. C.; Watanabe, K.; Chiang, Y. C.; Takashima, S.; Borsali, R.; Tung, S. H.; Satoh, T.; Chen, W. C., Control over Molecular Architectures of Carbohydrate-based block copolymers for stretchable electrical memory devices. *Macromolecules* **2018,** *51* (13), 4966.
39. Kumar, S.; Maiti, B.; De, P., Carbohydrate-conjugated amino acid-based fluorescent block copolymers: their self-assembly, pH responsiveness, and/or lectin recognition. *Langmuir* **2015,** *31* (34), 9422.
40. Isono, T.; Kawakami, N.; Watanabe, K.; Yoshida, K.; Otsuka, I.; Mamiya, H.; Ito, H.; Yamamoto, T.; Tajima, K.; Borsali, R.; Satoh, T., Microphase separation of carbohydrate-based star-block copolymers with sub-10 nm periodicity. *Polym Chem* **2019,** *10* (9), 1119.
41. Stenzel, M. H.; Davis, T. P.; Fane, A. G., Honeycomb structured porous films prepared from carbohydrate based polymers synthesized via the RAFT process. *J Mater Chem* **2003,** *13* (9), 2090.
42. Chen, G., The Past Ten Years of Carbohydrate Polymers in ACS Macro Letters. *ACS Macro Lett* **2021,** *10* (9), 1145.
43. Chen, J.; Kamitakahara, H.; Edgar, K. J., Synthesis of polysaccharide-based block copolymers via olefin cross-metathesis. *Carbohydr Polym* **2020,** *229*, 115530.
44. Otsuka, I.; Tallegas, S.; Sakai, Y.; Rochas, C.; Halila, S.; Fort, S.; Bsiesy, A.; Baron, T.; Borsali, R., Control of 10 nm scale cylinder orientation in self-organized sugar-based block copolymer thin films. *Nanoscale* **2013,** *5* (7), 2637.
45. Liao, Y.; Chen, W. C.; Borsali, R., Carbohydrate-based block copolymer thin films: ultrafast nano-organization with 7 nm resolution using microwave energy. *Adv Mater* **2017,** *29* (35), 1701645.
46. Isono, T.; Miyachi, K.; Satoh, Y.; Nakamura, R.; Zhang, Y.; Otsuka, I.; Tajima, K.; Kakuchi, T.; Borsali, R.; Satoh, T., Self-assembly of maltoheptaose-block-polycaprolactone copolymers: carbohydrate-decorated nanoparticles with tunable morphology and size in aqueous media. *Macromolecules* **2016,** *49* (11), 4178.
47. Zepon, K. M.; Otsuka, I.; Bouilhac, C.; Muniz, E. C.; Soldi, V.; Borsali, R., Glyco-nanoparticles made from self-assembly of maltoheptaose-block-poly(methyl methacrylate): micelle, reverse micelle, and encapsulation. *Biomacromolecules* **2015,** *16* (7), 2012.

48. Hung, C. C.; Lin, Y. C.; Chuang, T. H.; Chiang, Y. C.; Chiu, Y. C.; Mumtaz, M.; Borsali, R.; Chen, W. C., Harnessing of spatially confined perovskite nanocrystals using polysaccharide-based block copolymer systems. *ACS Appl Mater Interfaces* **2022,** *14* (26), 30279.
49. Liao, Y.; Goujon, L. J.; Reynaud, E.; Halila, S.; Gibaud, A.; Wei, B.; Borsali, R., Self-assembly of copper-free maltoheptaose-block-polystyrene nanostructured thin films in real and reciprocal space. *Carbohydr Polym* **2019,** *212*, 222.
50. Liao, Y.; Liu, K.; Chen, W. C.; Wei, B.; Borsali, R., Robust sub-10 nm pattern of standing sugar cylinders via rapid "microwave cooking". *Macromolecules* **2019,** *52* (22), 8751.
51. Gross, A. J.; Chen, X.; Giroud, F.; Travelet, C.; Borsali, R.; Cosnier, S., Redox-active glyconanoparticles as electron shuttles for mediated electron transfer with bilirubin oxidase in solution. *J Am Chem Soc* **2017,** *139* (45), 16076.
52. Li, L.; Zhong, Y.; Li, J.; Chen, C.; Zhang, A.; Xu, J.; Ma, Z., Thermally stable and solvent resistant honeycomb structured polystyrene films via photochemical cross-linking. *J Mater Chem* **2009,** *19* (39), 7222.
53. Yaseen, A. A.; Al-Tikrity, E. T. B.; Yousif, E.; Ahmed, D. S.; Kariuki, B. M.; El-Hiti, G. A., Effect of ultraviolet irradiation on polystyrene containing cephalexin schiff bases. *Polymers (Basel)* **2021,** *13* (17), 2982.
54. Friess, F. V.; Hu, Q.; Mayer, J.; Gemmer, L.; Presser, V.; Balzer, B. N.; Gallei, M., Nanoporous block copolymer membranes with enhanced solvent resistance via UV-mediated cross-linking strategies. *Macromol Rapid Commun* **2022,** *43* (3), 2100632.
55. Liberman-Martin, A. L.; Chu, C. K.; Grubbs, R. H., Application of bottlebrush block copolymers as photonic crystals. *Macromol Rapid Commun* **2017,** *38* (13), 1700058.
56. Wang, Z.; Chan, C. L. C.; Zhao, T. H.; Parker, R. M.; Vignolini, S., Recent advances in block copolymer self-assembly for the fabrication of photonic films and pigments. *Adv Opt Mater* **2021,** *9* (21), 2100519.
57. Rayleigh, L. J. T. L., Edinburgh,; Magazine, D. P.; Science, J. o., XXVI. On the remarkable phenomenon of crystalline reflexion described by Prof. Stokes. **1888,** *26* (160), 256.
58. Dyachenko, P. N.; Miklyaev, Y. V., One-dimensional photonic crystal based on nanocomposite of metal nanoparticles and dielectric. *Opt Mem Neural Netw* **2007,** *16* (4), 198.
59. Bykov, V. P.; Spontaneous emission from a medium with a band spectrum. *J. Quantum Electron* **1975,** *4* (7), 861.
60. Jennifer, O. Seeing the future in photonic crystals, *American Institute of Physics*, **2001**
61. Choinopoulos, I., Grubbs' and schrock's catalysts, ring opening metathesis polymerization and molecular brushes-synthesis, characterization, properties and applications. *Polymers (Basel)* **2019,** *11* (2), 298.

62. Wilts, B. D.; Michielsen, K.; Kuipers, J.; De Raedt, H.; Stavenga, D. G., Brilliant camouflage: photonic crystals in the diamond weevil, Entimus imperialis. *Proc Biol Sci* **2012,** *279* (1738), 2524.
63. Vaz, R.; Frasco, M. F.; Sales, M. G. F., Photonics in nature and bioinspired designs: sustainable approaches for a colourful world. *Nanoscale Adv.* **2020,** *2* (11), 5106.
64. Cai, Z.; Smith, N. L.; Zhang, J. T.; Asher, S. A., Two-dimensional photonic crystal chemical and biomolecular sensors. *Anal Chem* **2015,** *87* (10), 5013.
65. Yadav, A.; Kaushik, A.; Mishra, Y. K.; Agrawal, V.; Ahmadivand, A.; Maliutina, K.; Liu, Y.; Ouyang, Z.; Dong, W.; Cheng, G. J., Fabrication of 3D polymeric photonic arrays and related applications. *Mater Today Chem* **2020,** *15*,100208.
66. Cersonsky, R. K.; Antonaglia, J.; Dice, B. D.; Glotzer, S. C., The diversity of three-dimensional photonic crystals. *Nat Commun* **2021,** *12* (1), 2543.
67. Deparis, O.; Vigneron, J. P., Modeling the photonic response of biological nanostructures using the concept of stratified medium: the case of a natural three-dimensional photonic crystal. *Mater Sci Eng B* **2010,** *169* (1-3), 12.
68. Bahraminasab, M., Challenges on optimization of 3D-printed bone scaffolds. *Biomed Eng Online* **2020,** *19* (1), 69.
69. Shen, H.; Wang, Z.; Wu, Y.; Yang, B., One-dimensional photonic crystals: fabrication, responsiveness and emerging applications in 3D construction. *RSC Adv* **2016,** *6* (6), 4505.
70. Lova, P.; Manfredi, G.; Comoretto, D., Advances in functional solution processed planar 1D photonic crystals. *Adv Opt Mater* **2018,** *6* (24), 1800730.
71. Vigneron, J. P.; Pasteels, J. M.; Windsor, D. M.; Vertesy, Z.; Rassart, M.; Seldrum, T.; Dumont, J.; Deparis, O.; Lousse, V.; Biro, L. P.; Ertz, D.; Welch, V., Switchable reflector in the Panamanian tortoise beetle Charidotella egregia (Chrysomelidae: Cassidinae). *Phys Rev E Stat Nonlin Soft Matter Phys* **2007,** *76* (3), 031907.
72. Choi, S. H.; Byun, K. M.; Kim, Y. L., Lasing interactions disclose hidden modes of necklace states in the anderson localized regime. *ACS Photonics* **2017,** *5* (3), 881.
73. Vignolini, S.; Rudall, P. J.; Rowland, A. V.; Reed, A.; Moyroud, E.; Faden, R. B.; Baumberg, J. J.; Glover, B. J.; Steiner, U., Pointillist structural color in Pollia fruit. *Proc Natl Acad Sci U S A* **2012,** *109* (39), 15712.
74. Lova; Cortecchia; Soci; Comoretto, Solution processed polymer-ABX4 perovskite-like microcavities. *Appl Sci* **2019,** *9* (23), 5203.
75. Calvo, M. E.; Míguez, H., Flexible, adhesive, and biocompatible bragg mirrors based on polydimethylsiloxane infiltrated nanoparticle multilayers. *Chem Mater* **2010,** *22* (13), 3909.
76. Yu, W.; Jia, X.; Long, Y.; Shen, L.; Liu, Y.; Guo, W.; Ruan, S., Highly efficient semitransparent polymer solar cells with color rendering index approaching 100 using one-dimensional photonic crystal. *ACS Appl Mater Interfaces* **2015,** *7* (18), 9920.

77. Chen, X.; Mayama, H.; Matsuo, G.; Torimoto, T.; Ohtani, B.; Tsujii, K., Effect of ionic surfactants on the iridescent color in lamellar liquid crystalline phase of a nonionic surfactant. *J Colloid Interface Sci* **2007,** *305* (2), 308.
78. Yue, Y.; Gong, J. P., Tunable one-dimensional photonic crystals from soft materials. *J Photochem Photobiol C Photochem Rev* **2015,** *23*, 45.
79. Alfrey, T.; Gurnee, E. F.; Schrenk, W. J., Physical optics of iridescent multilayered plastic films. *Polym Eng Sci* **1969,** *9* (6), 400.
80. Kou, D.; Zhang, S.; Lutkenhaus, J. L.; Wang, L.; Tang, B.; Ma, W., Porous organic/inorganic hybrid one-dimensional photonic crystals for rapid visual detection of organic solvents. *J Mater Chem C* **2018,** *6* (11), 2704.
81. Calvo, M. E.; Colodrero, S.; Hidalgo, N.; Lozano, G.; López-López, C.; Sánchez-Sobrado, O.; Míguez, H., Porous one dimensional photonic crystals: novel multifunctional materials for environmental and energy applications. *Energy Environ Sci* **2011,** *4* (12), 4800.
82. Dang, Z.; Breese, M. B.; Recio-Sanchez, G.; Azimi, S.; Song, J.; Liang, H.; Banas, A.; Torres-Costa, V.; Martin-Palma, R. J., Silicon-based photonic crystals fabricated using proton beam writing combined with electrochemical etching method. *Nanoscale Res Lett* **2012,** *7* (1), 416.
83. Sarkar, S.; Samanta, K.; Joseph, J., Method for single-shot fabrication of chiral woodpile photonic structures using phase-controlled interference lithography. *Opt Express* **2020,** *28* (3), 4347.
84. Ma, W.; Kou, Y.; Zhao, P.; Zhang, S., Bioinspired structural color patterns derived from 1D photonic crystals with high saturation and brightness for double anti-counterfeiting decoration. *ACS Appl Polym Mater* **2020,** *2* (4), 1605.
85. Liddle, J. A.; Gallatin, G. M., Nanomanufacturing: a perspective. *ACS Nano* **2016,** *10* (3), 2995.
86. Hou, J.; Li, M.; Song, Y., Patterned colloidal photonic crystals. *Angew Chem Int Ed Engl* **2018,** *57* (10), 2544.
87. Pan; Wang; Dou; Zhao; Xu; Wang; Zhang; Li; Pan; Li, Recent advances in colloidal photonic crystal-based anti-counterfeiting materials. *Crystals* **2019,** *9* (8), 417.
88. Li, M.; Lyu, Q.; Peng, B.; Chen, X.; Zhang, L.; Zhu, J., Bioinspired colloidal photonic composites: fabrications and emerging applications. *Adv Mater* **2022**, 2110488.
89. Wang, Y.; Shang, L.; Bian, F.; Zhang, X.; Wang, S.; Zhou, M.; Zhao, Y., Hollow colloid assembled photonic crystal clusters as suspension barcodes for multiplex bioassays. *Small* **2019,** *15* (13), 1900056.
90. Chen, S.; Bu, D.; Hu, Y.; Xiao, X.; Yang, D.; Ma, D.; Huang, S., Photonic crystals with tunable lattice structures based on anisotropic metal-organic framework particles and their application in anticounterfeiting. *Adv Photonics Res* **2021,** *3* (2), 2100246.
91. Edrington, A. C.; Urbas, A. M.; DeRege, P.; Chen, C. X.; Swager, T. M.; Hadjichristidis, N.; Xenidou, M.; Fetters, L. J.; Joannopoulos, J. D.; Fink, Y. J. A. M., Polymer-based photonic crystals. **2001,** *13* (6), 421.

92. Kim, E.; Lee, H., Mechanical characterization of soft microparticles prepared by droplet microfluidics. *J Polym Sci* **2022,** *60* (11), 1670.
93. Shang, J.; Le, X.; Zhang, J.; Chen, T.; Theato, P., Trends in polymeric shape memory hydrogels and hydrogel actuators. *Polym Chem* **2019,** *10* (9), 1036.
94. Zhang, L.; Shi, X. L.; Yang, Y. L.; Chen, Z. G., Flexible thermoelectric materials and devices: from materials to applications. *Mater Today* **2021,** *46*, 62.
95. Zhang, T.; Li, K.; Li, C.; Ma, S.; Hng, H. H.; Wei, L., Mechanically durable and flexible thermoelectric films from PEDOT:PSS/PVA/Bi0.5Sb1.5Te3 nanocomposites. *Adv Electron Mater* **2017,** *3* (4), 1600554.
96. Lova, P.; Megahd, H.; Stagnaro, P.; Alloisio, M.; Patrini, M.; Comoretto, D., Strategies for dielectric contrast enhancement in 1D planar polymeric photonic crystals. *Appl Sci* **2020,** *10* (12), 4122.
97. Do, Y. R.; Kim, Y. C.; Song, Y. W.; Cho, C. O.; Jeon, H.; Lee, Y. J.; Kim, S. H.; Lee, Y. H., Enhanced light extraction from organic light-emitting diodes with 2D SiO2/SiNx photonic crystals. *Adv Mater* **2003,** *15* (14), 1214.
98. Higashihara, T.; Ueda, M., Recent progress in high refractive index polymers. *Macromolecules* **2015,** *48* (7), 1915.
99. Lü, C.; Cui, Z.; Li, Z.; Yang, B.; Shen, J., High refractive index thin films of ZnS/polythiourethane nanocomposites. *J Mater Chem* **2003,** *13* (3), 526.
100. Tharmavaram, M.; Rawtani, D.; Pandey, G., Fabrication routes for one-dimensional nanostructures via block copolymers. *Nano Converg* **2017,** *4* (1), 12.

Chapter 2: Synthesis and Characterization of Carbohydrate-based Brush Block Copolymers

2.1 Introduction

Brush polymers, also termed as bottlebrushes or cylindrical brush polymers, are a kind of grafted macromolecules in which side chains at a high grafting density are anchored to a linear backbone.[1] The side chains of brush polymers are so closed at high grafted densities that they prefer to stretch the backbone with a lower interchain entanglement compared to their linear block copolymers in solutions, resulting in unique structures including as a worm-like or cylindrical conformation.[2] This special architecture makes brush polymers endow with many unusual and novel properties. For instance, brush polymers are very different from linear block copolymers and are easily able to form architectures with large domain sizes over 100 nm via self-assembly.[1,2] In contrast to linear copolymers and surfactants, micelles prepared from brush polymers in selective solvents have a lower critical micelle concentration (CMC), thus allowing them apply for sensing and detecting in biology in a high diluting prerequisite.[3] Moreover, brush polymers can act as a nanoscale soft building block capable of tunable properties and wide applications due to the flexibility of their side chains and extending backbone.[4]

In the 1980s, the synthesis strategies of brush polymers were primarily studied by researchers.[5] Over the past four decades, effective synthetic approaches and characterizations for brush polymers have been achieved by the combination contributions of the development for polymerization techniques (ring opening metathesis polymerization and controlled radical polymerization)[6] and advanced characterization facilities[7] (scanning and transmission electron microscopies, atomic force microscope). Today, three main methods to synthesize brush polymers, referred to as grafting-to, grafting-through and grafting-from, have been widely used to obtain the diversity of brush polymers.[8, 9] Based on the structure, brush polymers can be basically divided into homo-,[10] random-,[11] block-,[12] Janus-[13] and core-shell-types[14]. Unique nano/microstructures and diverse applications have been successfully prepared

from the self-assembly of brush polymers at the interfaces, in solutions and in bulk (Figure 1).[15]

In previous studies of our group for the past decade, carbohydrate-based linear block copolymers have been well developed by using "click chemistry" for a series of glyconanoparticles and highly nanostructured sub-10 nm resolution thin films via self-assembly.[16] Click chemistry as a kind of atom-economy reactions, is frequency applied for joining two molecular units together. In our group, "click chemistry" has been commonly used to couple an azido-terminal synthetic polymer with an alkyne terminal polysaccharide block. Within hands of linear block copolymers, brush block copolymers are considered to prepare for comparing the properties and behaviors between linear and brush block copolymers. In this context, by hands of M. Mumtaz (Post Doc. in our group), a series of carbohydrate-based brush block copolymers were successfully synthesized by using aforementioned methods including as grafting-to and grafting-through. After synthesizing the carbohydrate-based brush block copolymers, photonic crystals and glyconanoparticles prepared from carbohydrate-based brush block copolymers will be presented in following chapter 3 and chapter 4, respectively.

2.2 Strategies to synthesize brush polymers

To date, three general approaches, termed as grafting-from,[17] grafting-to[18] and grafting-though,[19] are primarily used for the synthesis of brush polymers. Each method with its own's advantages and disadvantages have been well explored and explained.[2, 6, 7, 20, 21] Firstly, grafting-to approach needs to prepare the functional backbone and side chains independently. Nucleophilic substitution or coupling reactions are common following step to attach the side chains to the bottlebrush backbone.[18, 22] Because the steric effect between side-chains happens during these reactions, the grafting-to approach often produces the side chains at a low grafting density.[23] However, it is also a way to characterize the side chains and backbone independently, resulting in good control of side chain and backbone dispersity.[1] Grafting-from approach allows the side chains grow from a poly-initiator backbone, leading to the generation of bottlebrushes with a narrow backbone dispersity. But the dispersity of side chain can be not easily well-

controlled due to the steric hindrance growing with the side chain initiation growth. Moreover, multiple protection/deprotection steps are often required to synthesize brush polymers by using the grafting-from approach, resulting in the complication of synthesis.[6] Finally, Grafting-though approach can provide a method for macromonomers to construct the brush polymers via the polymerization. This approach allows for brush polymers with homogenous grafting density and side chains. As same

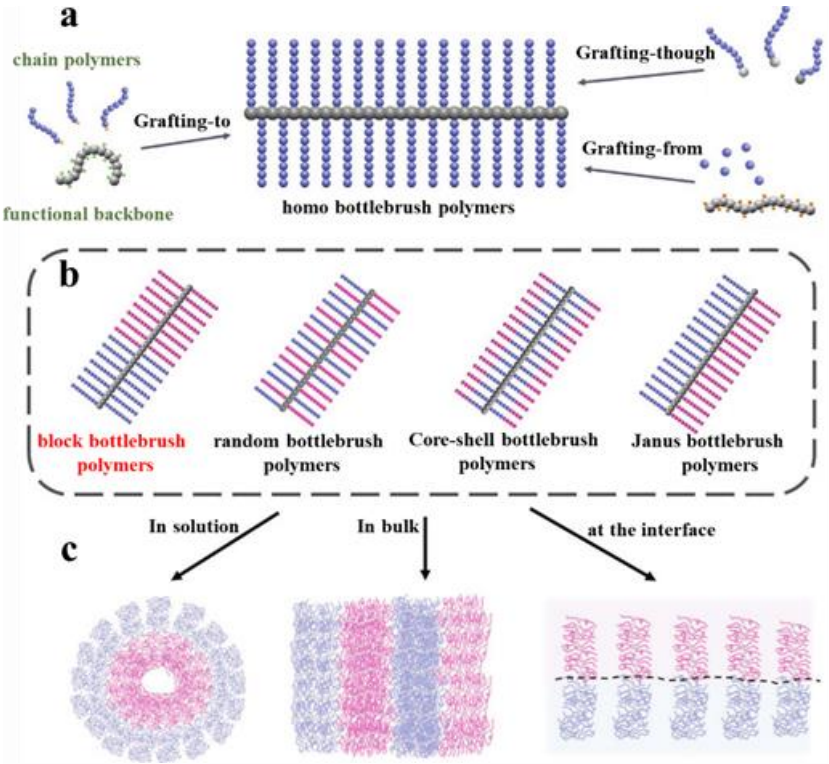

Figure 1. The synthetic approaches, polymer architectures, and applications of brush polymers via self-assembly. a) Scheme illustration of three approaches (grafting-through, grafting-to and grafting-from) to synthesize homo bottlebrush polymers. b) Examples of different brush polymers (block-, Janus-type, random- and core-shell-type). c) brush polymers are promising as a building block for applications via self-assembly (at the interface, in solution, and in bulk).[15]

as grafting-to approach, the side chains of brush polymers prepared from grafting-though approach, are able to be characterized before synthesizing completely brush polymers. Meanwhile, grafting-through approach meet same problem as grafting-to approach, that is, the increasing steric hindrance of the growing propagation of the poly-macromonomer. In addition, the possible presence of unreacted macromonomers is

difficult to be pacificated for the target product at the end. However, high efficiency catalyst and proper structure of the macromonomer are able to dissolve the issue.[6] Taking advantage of above routes and its combinations, researchers have been synthesized various brush polymers with diverse side chain architecture.[7] (Figure 1) Ultimately, application of rules for selecting the synthesis of approaches is dependent on the requirements. If it is necessary to obtain homogenous side chain length and high grafting density, it is our priority to choose the grafting-though approach. If the uniformity of grafting density of side chain is not essential, we must admit to a prejudice in favor of the grafting-from or -to approach due to their high modularity.[6]

Today, as shown in Figure 2, a series of brush polymers are well represented via the grafting-to,[24] grafting-from,[25] and grafting-though[26] approaches. Among them, grafting-though approach has drawn our attentions and the following experimental section shows that a set of brush block copolymers are successfully synthesized by the combination of grafting-though and grafting-to approaches.

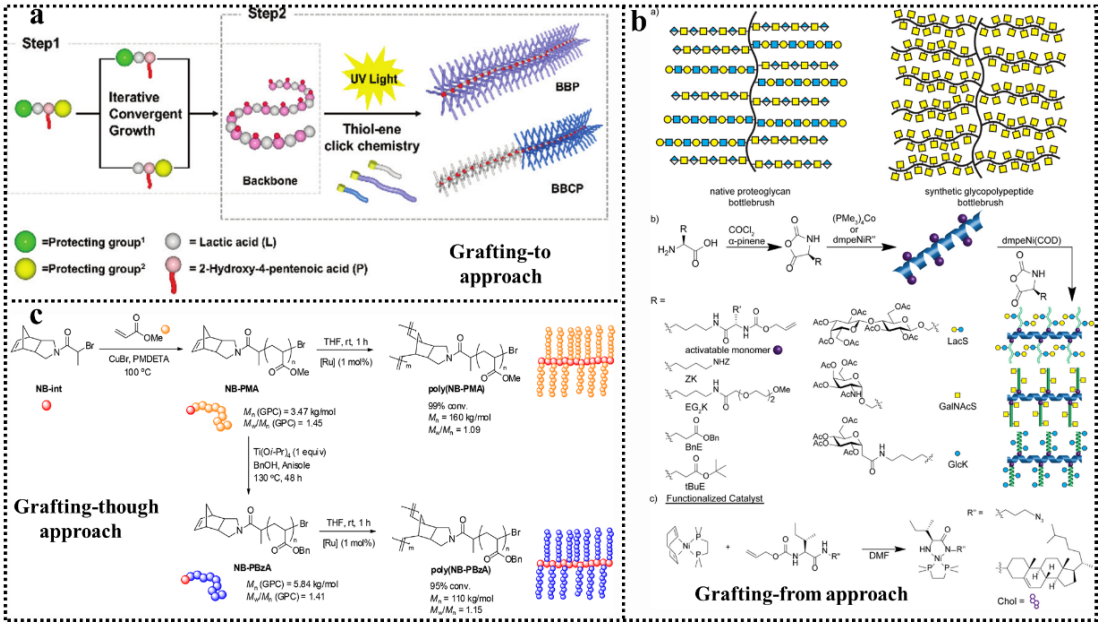

Figure 2. Examples of brush polymer synthesis approaches including as grafting-to, grafting-from, and grafting-though. (a) Schematic representation of brush polymers via the grafting-to approach.[24] (b) Schematic representation of brush polymers via the grafting-from approach.[25] (c) Schematic representation of brush polymers via the grafting-though approach.[26]

2.3 Self-assembly of brush polymers and its applications

Thanks to the advancement of the synthetic strategies of brush polymers mentioned above, especially the ring open metathesis polymerization (ROMP)[27-30] grafting-though synthesis, it has accelerated the development and progress of the architecture of brush polymers from the simplicity to the complexity to meet diverse demands. Currently, brush polymers have been widely used for diverse applications such as imaging[31] and nanofabrication.[32] The following part will focus on the various applications for brush polymers in thin and bulk films, at the interface, and in solutions (Figure 1c).

2.3.1 Self-assembly in thin and bulk films

In contrast to the linear block copolymers, the self-assembly of brush block copolymers in thin and bulk films into larger domain sizes (over 100 nm) and new morphologies have been attracted researchers' attention over the past two decades.

In 2013, a high-resolution and highly sensitive photoresist material fabricated from asymmetrical brush block copolymers was adequately investigated by the Wooly group.[32] In this article, the reversible addition-fragmentation chain transfer polymerization/ copolymerization was employed to synthesize two macromonomers followed by sequential ring opening metathesis polymerization as a grafting-through approach. Consequently, several asymmetrical brush block copolymers were made up of fluorinated poly(tetrafluoro-p-hydroxystyrene) and phenol functionalized poly(p-hydroxystyrene-co-N-phenylmaleimide) as side chains, and a rigid polynorbornene as the backbone. Then, the photoresist, crosslinker and bottlebrushes were mixed and spined casting on the silicon substrate, providing a vertically aligned bottlebrushes within thin films in which negative-tone resist characterizations at molecular scale can be constructed under the irradiation condition (Figure 3).

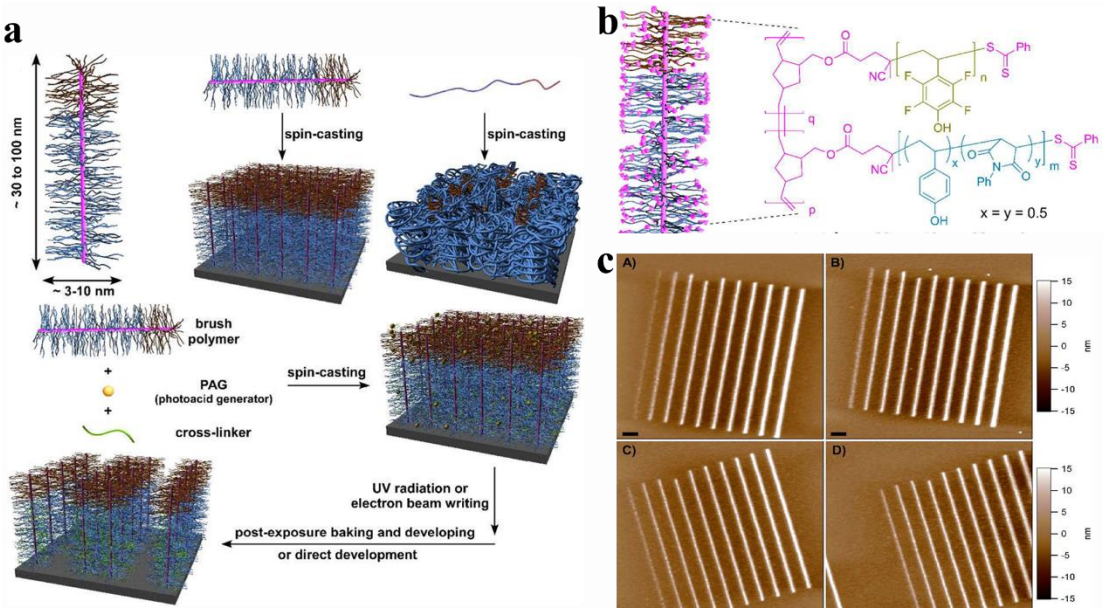

Figure 3. (a) A schematic illustration of the steps to afford highly sensitive photoresist thin films from asymmetrical brush block copolymers. (b) Structure of the asymmetrical brush block copolymers. (c) AFM height images of well-patterns films composed of asymmetrical brush block copolymers under irradiation.[32]

In 2020, D. F. Sunday and coworkers[33] reported a poly[(norbornene-graft-DL-lactide)-block-(norbornene-graft-styrene)] (gPLA-b-gPS) brush block copolymer (Figure 4) synthesized via a ROMP grafting-though route. The study found that there is significant thickness effect of confinement on the morphology and configuration of the brush block copolymer in thin films. These thin films with various thickness can be prepared from a blade coating technique. The lamellar periodicity of morphologies in blading-coated thin films showed a dependence on the film thickness, that is, the periodicity is increasing with decreasing the thickness of films. Mixtures of morphologies and orientations in blade-coating films can be observed after annealing by using the propylene glycol methyl ether acetate solvent, which were confirmed by grazing incidence small-angle X-ray scattering and atomic force microscope. This solvent was sensitive to the thickness of thin films in which the lamellar part had a thickness dependence property. Moreover, holes/islands happened frequency in thin films of linear block copolymers, cannot be observed but instead multiply morphologies emergence in the blade coating films fabricated from this brush block copolymers.

Based on above results, it is a promising candidate for a single brush block copolymer to obtain diverse morphologies and conformation by controlling processing conditions and thickness of thin films.

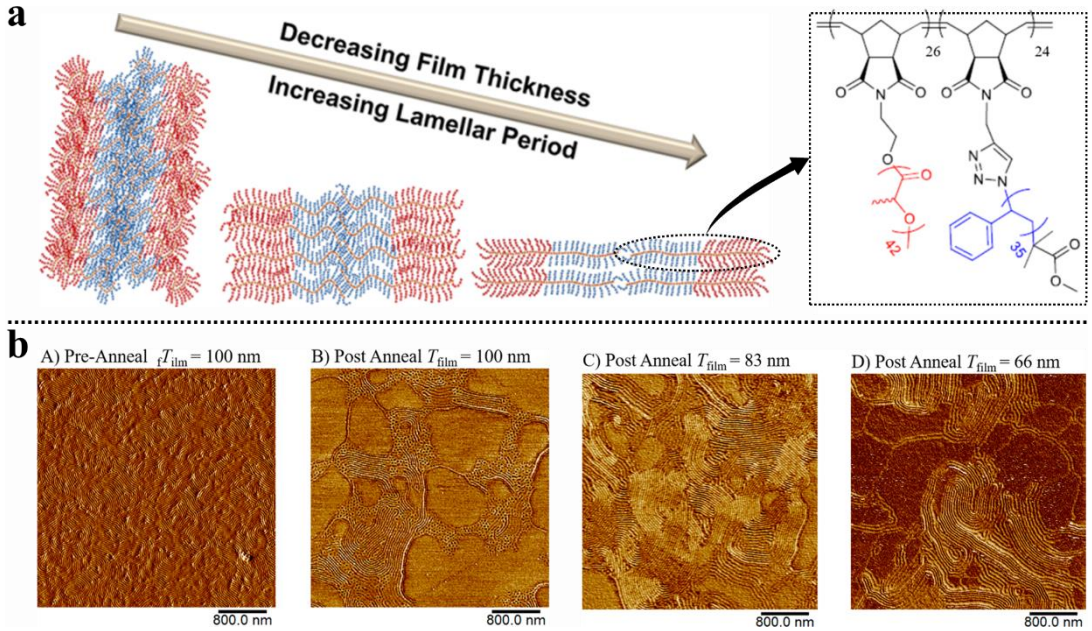

Figure 4. (a) Schematic illustration and structure of the brush block copolymer (gPLA-b-gPS, blue: PS and red: PLA) along with film thickness changes. (b) AFM phase images of gPLA-b-gPS blade-coating thin films by using solvent before and after annealing at 165 °C for 24 h.[33]

In regard to thin films, photonic crystals as one such application field have aroused scientists' interests. Among them, R. H. Grubbs and coworker[34] have made a big step toward fabricating photonic crystals by using brush block copolymers. In 2012, Grubbs and coworker synthesized a set of isocyanate-based brush block copolymers with different molecular weights (1512-7119 kDa) via the ROPM grafting-though method. The rapid self-assembly of these copolymers to one-dimensional photonic crystals from a volatile solvent, were able to reflect light covering large range of wavelength (from ultra-violet to near-infrared region). The primary peaks (λ_{max}) of reflectance wavelength showed a good linear relationship between the molecular weight of brush block copolymers and λ_{max} (R^2 = 0.990), providing a predictable way to obtain tunable bank gaps of photonic crystals by manipulating molecular weight of these polymers. (Figure 5)

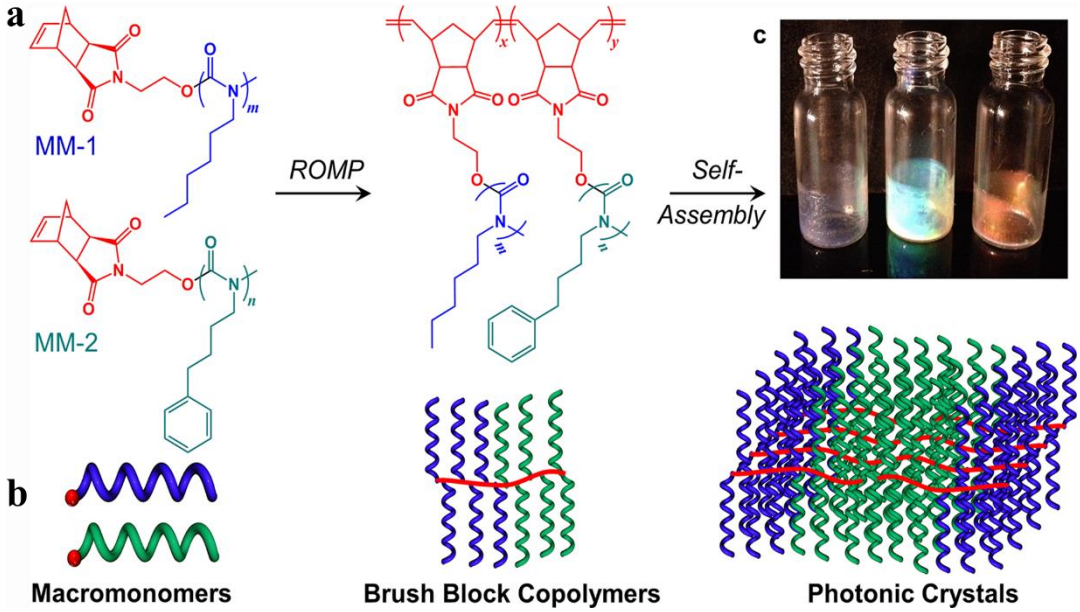

Figure 5. (a) Structures of isocyanate-based macromonomers and brush block copolymers via a ROMP grafting-though approach. (b) Scheme illustration of macromonomers, brush block copolymers and one-dimensional photonic crystals via the self-assembly. (c) Photograph of one-dimensional photonic crystals with various reflection colors (violet, green, and red).[34]

In following years (2013), R. H. Grubbs and co-workers[35] also synthesized successfully the symmetrical brush diblock copolymers BrBCPs with polystyrene and polylactide side chains and studied extensively on the self-assembly of BrBCPs in bulk state by using in situ small-angle X-ray scattering (SAXS) (Figure 6). Lamellar domains at range of 20 to 240 nm confirmed by SAXS, can be achieved in one minute at 130 ℃ from BrBCPs via the self-assembly. In contrast, lamellar domains cannot be clearly observed from a similar linear diblock copolymer at same condition even longer time. Interestingly, the domain spacing was near linear with the backbone length which was consistent with Monte Carlo simulations, providing a reference for designing brush block copolymers architecture that can rapidly form diverse nanostructure via self-assembly.

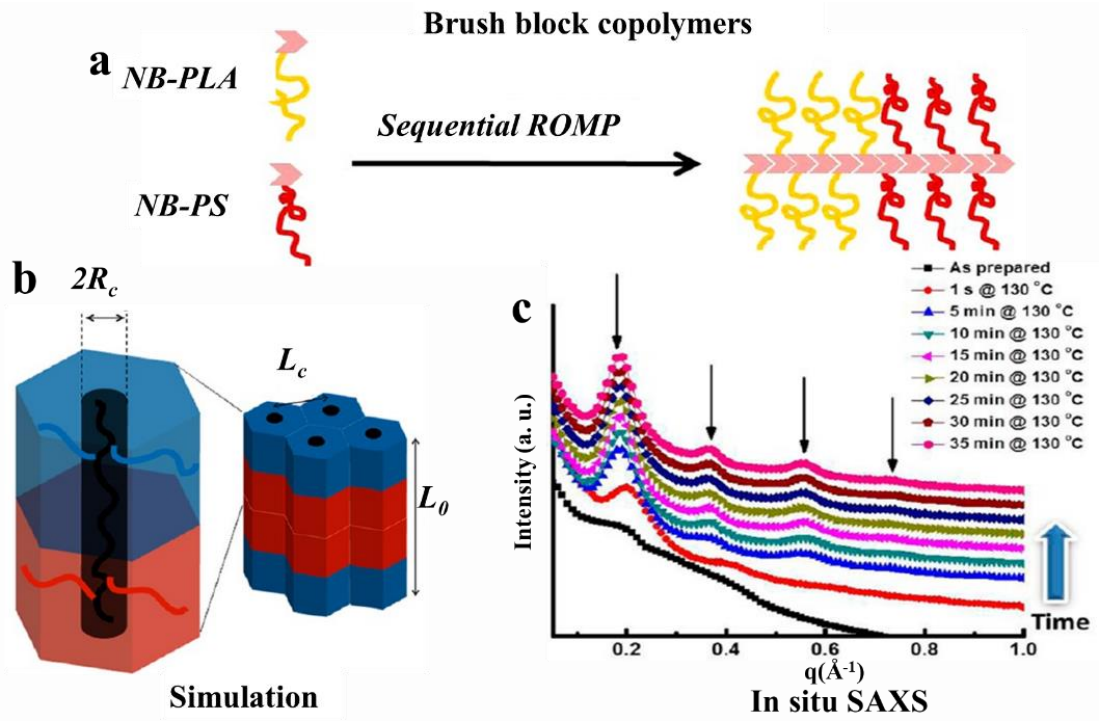

Figure 6. (a) Structure illustration of brush block copolymers BrBCPs via a ROMP grafting-though approach. (b) Scheme of the lattice of BrBCP lamellar structure. (c) Small-angle X-ray scattering of a BrBCP.[35]

2.3.2 Self-assembly in solution

Inspired by the distinct nature and diverse structure of brush polymers, researches were motivated to take advantage of them as a promising building block for the self-assembly into multi-morphologies in solution.

In 2014, Rzayev and coworkers[36] demonstrated that a series of amphiphilic brush block copolymers attached with various hydrophilic poly(ethylene oxide) (PEO) and hydrophobic polylactide (PLA) side chains, were obtained through a grafting-from approach. Under an aqueous environment, these amphiphilic polymers can be assembled into micelles with multiply morphologies including sphere, cylinder and bilayer. These micelle structures showed a shape-dependent property which was relate to the different interfacial curvatures between the hydrophilic and hydrophobic side chains. Less asymmetric brush polymers in composition had a preference to form the longer cylindrical micelles and aggregates without spherical shape. Compared to their linear analogues, the significant progress in thermodynamic stability of these micelle

aggregates can be achieved as well as a very low critical micelle concentration value (1mM). (Figure 7) Base on above results, these new giant brush block polymer surfactants can give us some inspiration on the design of diverse micelle architecture.

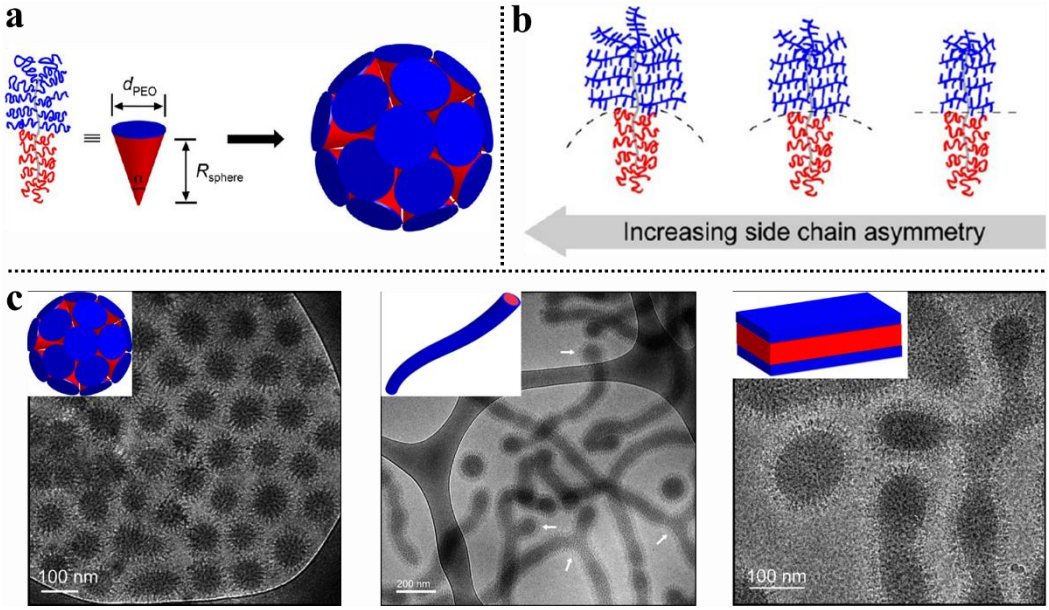

Figure 7. (a) Structure illustration of amphiphilic brush block copolymers as cones, and They assemble to pack into spheres. (b) Interfacial curvature controlled by side chain asymmetricity. (c) . Cryo-TEM images of spherical, cylindrical and bilayer micelle structures from amphiphilic brush block copolymers.[36]

As aforementioned in section 2.3.1., large periodic nanostructures can be prepared from brush block polymers via a self-assembly. However, it was rarely reported about the periodic nanostructures in solutions from the self-assembly of brush block polymers. Recently, Kim and coworkers[37] showed that a series of brush block copolymers with hydrophobic polystyrene (PS) and hydrophilic poly(ethylene glycol) (PEG) side chains, were synthesized by the ROMP grafting-though approach. Morphologies transition of brush block copolymers in the solution via a self-assembly, were able to observed clearly from spherical micelles to inverse mesophases along with the decreasing weight fraction of the PEG side chain. Interestingly, symmetrical icosahedral polymeric cubosomes with large periodic nanostructures, nanotubes and tubular networks, can be achieved from the self-assembly of various brush block copolymers in the solution by using the solvent diffusion-evaporation-mediated self-assembly (SDEMS) way (Figure

8), indicating the possible way to obtain diverse complicate nanostructures from the self-assembly of brush block copolymers in solution.

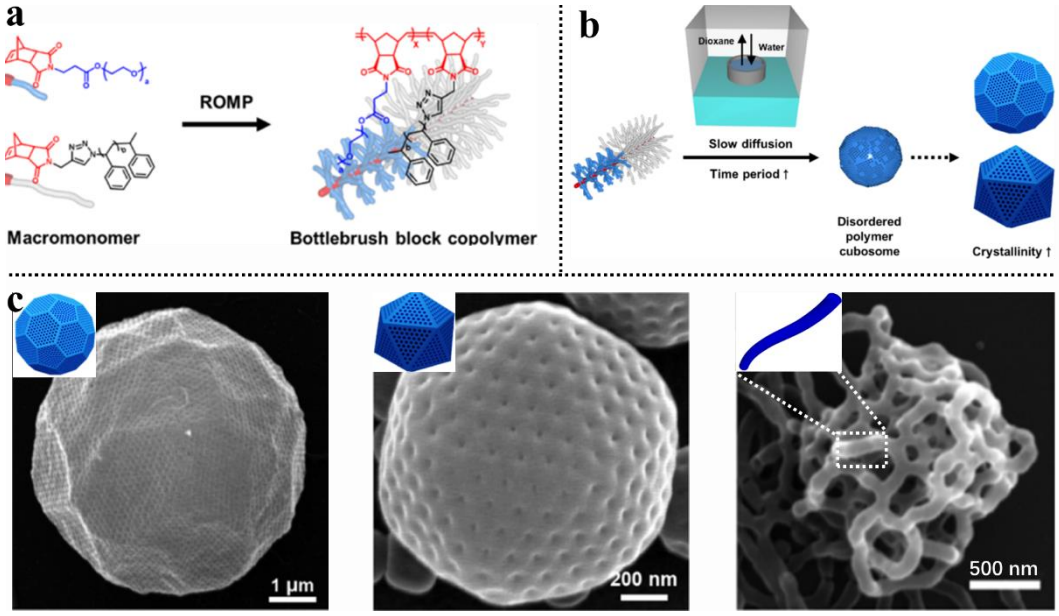

Figure 8. (a) Schematic illustration of brush block copolymers via a ROMP grafting-though approach. (b) Schematic illustration of brush block copolymers via self-assembly by the solvent diffusion-evaporation-mediated self-assembly (SDEMS). (c) SEM images of multiply morphologies including cubosomes and nanotubular networks from these brush polymers though the SDEMS way. The inset image represent scheme of the corresponding cubosomes and nanotubular networks.[37]

2.3.3 Self-assembly at the interface

The self-assembly behavior of Janus- and block-type brush polymers at the interface, is being growingly studied due to the pre-separating compartment of side chains. In 2012, Cheng and coworkers[38] reported that tandem polymeric reaction and sequential ring-opening polymerization were firstly used to the synthesis of amphiphilic norbornene-functionalized macromonomers with a hydrophobic lactide (LA) and a hydrophilic ethylene oxide (EO), the following ring-opening metathesis polymerization grafting-though approach was employed to afford the amphiphilic Janus-type brush polymers. In contrast to the corresponding macromonomers, several obvious advantages were accompanied with Janus brush polymers such as negligible intermolecular self-assembly and lower melting temperatures as well as lower

crystallinities, leading to a significant progress in stability as a kind of miniemulsions. (Figure 9) Potentially, a new giant polymeric surfactant may be achieved from these Janus-type brush polymers due to their unique structure and nanoscopic molecular sizes.

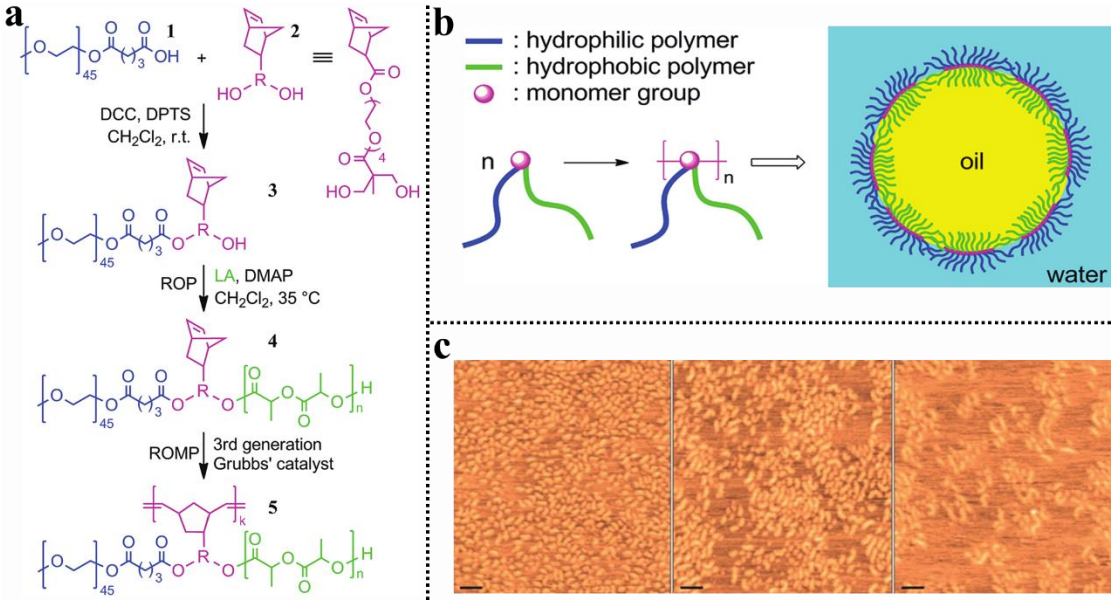

Figure 9. The synthesis route (a), schematic structure and application representations (b) of amphiphilic Janus brush polymers. (c) Tapping mode AFM height images of amphiphilic Janus brush polymers.[38]

The application of the block-type brush polymers at the interface was also investigated by Grubbs and coworkers.[39] In 2014, lamellar array can be obtained from the self-assembly of these block-type brush polymers. Furtherly, the domain spacing of lamellar structure were easily tunable by blending homopolymers (PLA and PS), exhibiting tunable optical spectra from 390 nm to 1410 nm. Interestingly, homopolymers cannot be macroscopic stratification in the presence of block-type brush polymers and even improve the overall order of lamellar array as a stabilizer agent in the interface between the domains of individual polymer (PLA and PS), indicating a possible compatibilizer in the mixture of polymers. (Figure 10) However, to date, the interface applications from block-type brush polymers via self-assembly have been rarely received consideration, and further continuous efforts should be paid in future.

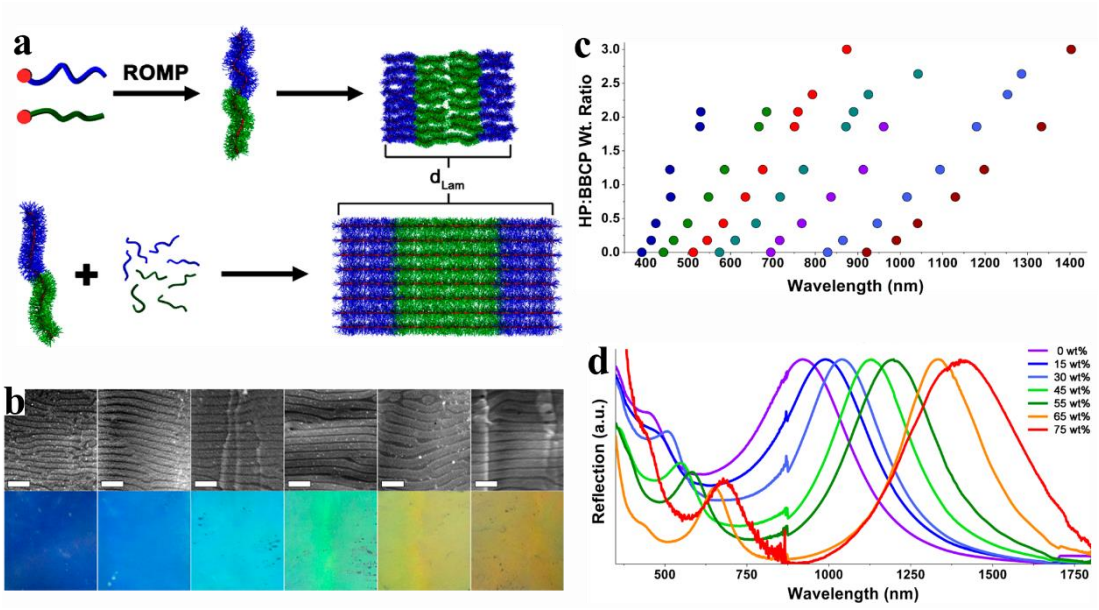

Figure 10. (a) Schematic representation of brush block copolymers with polylactic acid (PLA, green) and polystyrene (PS, blue) side chains. The domain size of lamellar array can be tunable by adding homopolymers (PLA and PS). (b) SEM images (up) and the corresponding color (down) of lamellar array along with the increasing weight ratio of homopolymers from 0-67.5%. (c) The tunable photonic band gap at range of 390-1410 nm can be achieved by adjusting the weight ratio of brush block copolymers/ homopolymers mixtures. (d) UV-vis reflection spectra of the brush block copolymer with the increasing weight ratio of the homopolymer.[39]

2.4 Results and Discussion

Synthesis of Bottle-brush block copolymers: The carbohydrate-based bottle-brush block copolymer was effectively achieved in multistep reactions, as illustrated in scheme 1. *N*-(hexanoic acid)-cis-5-norbornene-exo-2,3-dicorboxiimide (NbCOOH) and *N*-(4-hydroxybutyl)-cis-5-norbornene-exo-2,3-dicorboxiimide (NbBOH) were obtained by reaction of cis-5-norbornene-exo-2,3-dicorboxylic anhydride with 6-aminohexanoic acid and 4-amino-1-butanol respectively in toluene at 120 °C. 2-polystyrylethyl-6-(cis-5-norbornene-exo-2,3-dicorboxiimide) hexanoate (NbPS) was prepared by esterification of NbCOOH with home-made ω-hydroxyl-polystyrene (Figure 11-13) *N*-(4-bromobutanoate butyl)-cis-5-norbornene-exo-2,3-dicorboxiimide (NbBBBr) was obtained by reaction of NbBOH with 4-bromobutyryl chloride in CH_2Cl_2 (Figure 14). Several examples of (PNbBBBr-b-PNbHPS) were synthesized via metathesis ring opening polymerization by sequential addition of monomers using

Grubbs 3rd generation catalyst. Azido functionalization of PNbBBBr-b-PNbHPS samples was performed by treating the copolymer with NaN_3 in DMF at 60 °C. Finally, well-defined carbohydrate based bottle-brush block copolymer (PNbBBMH-b-PNHPS) was obtained by click chemistry of PNbBBN_3-b-PNbHPS with acetylene-functionalized maltoheptaose in DMF (please see following section for experimental details).

The characteristics of bottle-brush block copolymers are shown in Table 1, which indicate the formation of well-defined block copolymers with narrow size distribution.

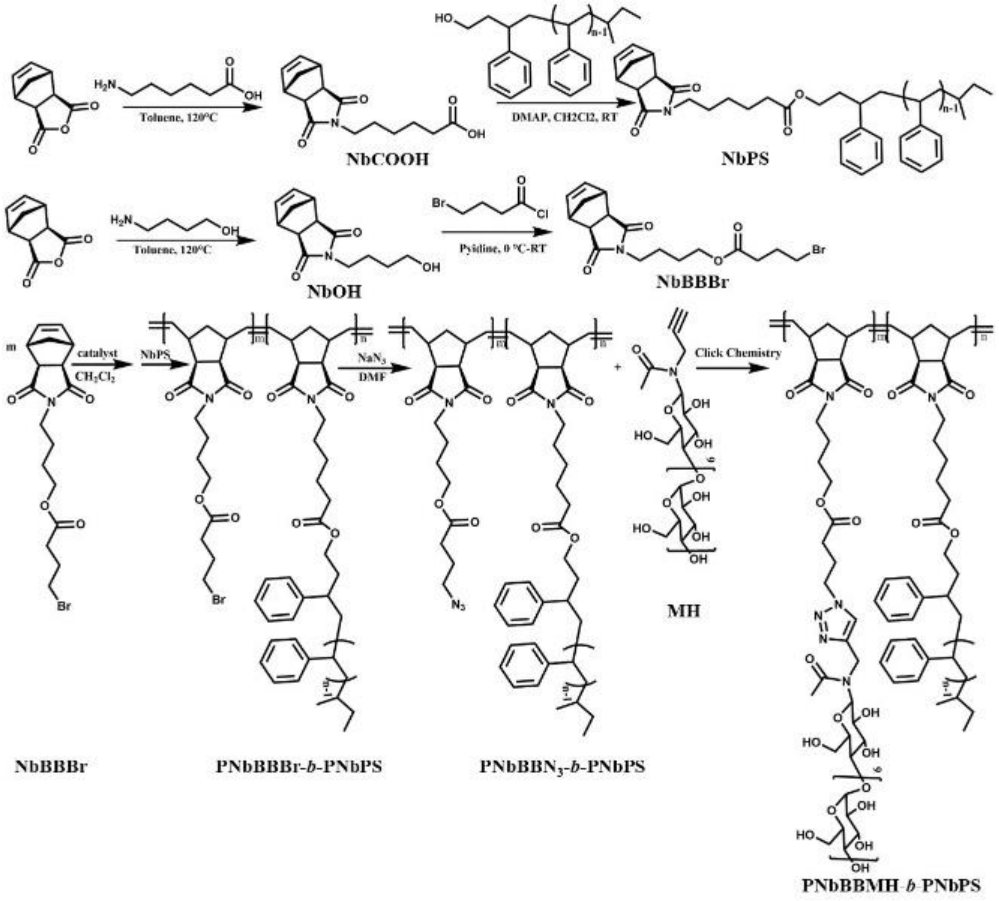

Scheme 1. Synthesis of oligosaccharide based bottle brush block copolymers.

The PNbBBMH-b-PNbHPS bottle-brush block copolymers and their precursors were characterized by proton nuclear magnetic resonance spectroscopy (^{1}H NMR), Fourier-transform infrared spectroscopy (FTIR) and size exclusion chromatography (SEC) (see Figure 11-31). The presence of peaks characteristics of both PNbBBBr and PNbHPS in ^{1}H NMR spectrum (Figure 15A), confirms formation of PNBBBr-b-PNbHPS block copolymers. The composition of PNBBBr-b-PNbHPS block copolymer was determined by relative integration of the peaks positioned at 4.03 ppm due to –

CH_2COO– of the PNbBBBr and 5.30-5.90 ppm dedicated to –*CH=CH*– of polynorbornene backbone. In addition, the absence of peak at 6.25 ppm due to norbornene moieties of the both monomers in ^{1}H NMR spectrum of PNbBBBr-b-PNbPS indicates their total conversion during polymerization. As it is shown in Table 1, the experimental molar composition of the PNbBBBr-b-PNbPS block copolymers are very close agreement to their initial feed ratio. The decrease in the peak intensity at 3.47 ppm due to *–NCH_2CH_2–* of the copolymer backbone and *–CH_2CH_2Br* of PNbBBBr and partial shifts towards ppm value (at 3.36 ppm due to *–CH_2–N_3* formation) and complete displacement of the peak at 2.51 ppm due to *–$OCOCH_2$–* of PNbBBBr block, in the ^{1}H NMR spectrum of PNbBBN_3-b-PNbPS (see Figure 15B), indicates quantitative azido functionalization. Finally, the appearance of additional peaks at 8.07-8.26 ppm and 3.30-6.10 ppm dedicated to triazole ring and maltoheptaose respectively in the ^{1}H NMR spectrum of PNbBBH-b-PNbHPS (Figure 15C) confirms the grafting of the maltoheptaose to the copolymer backbone. The composition of the final block copolymer was determined by the relative integration of the signals located at 5.16 ppm due to C1 protons of maltoheptaose and 6.30-7.35 ppm phenyl ring of polystyrene. Additionally, in the FTIR spectrum (Figure 16), the complete disappearance of the signal at ~2100 cm-1 in PNbBBH-b-PNbHPS in block copolymer sample, dedicated to azido group, suggested its total consumption during click reaction. Moreover, the SEC results revealed a clear shift of the elution peak upon the click reaction, which is good evidence for the successful formation of the desired block copolymers via the click reaction (Figure 17). However, the shift takes place towards the lower-molecular-weight rather than the higher-molecular-weight region, probably due to decrease in hydrodynamic volume of PNbBBH-b-PNbHPS upon maltoheptaose grafting.

Various samples of PNbBBH-b-PNbHPS with different molecular weight were prepared by changing the monomers to initiator ratio. The elution peaks in SEC spectra of PNbBBMH-b-PNbPS samples (Figure 18-21) shift towards higher molecular weights, upon increasing the monomer to initiator ratio, indicated nicely controlled polymerization process.

As it is clear from Table 1, composition of the most of the bottle-brush copolymer samples is close to the expected values (BR01-04 & BR07, Table 1) except for samples BR05 and BR06, where amount of carbohydrate block appeared to be roughly half with respect to the expected values, although the ^{1}H NMR of their precursors showed

complete conversion of –Br function in PNbBBBr-b-PNbPS to $–N_3$ in $PNbBBN_3$-b-PNbPS during azido functionalization (Figure 22-24) and FTIR spectra of the PNbBBMH-b-PNbPS samples showed full consumption of azido function during grafting of MH in click reaction (Figure 25-31). This decrease in carbohydrate part in these particular samples is probably due to a sort of micellization of PNbBBMH-b-PNbPS in deuterated DMF which partially hide the carbohydrate part and prevent its detection by ^{1}H NMR.

Table 1. Characteristics of bottle-brush block copolymers

Sample	NbBBBr/NbPS/ I Feed ratio	Molar mass of NbPS (^{1}H NMR) (g/mol)	[a]Experimental $f^{PNbBBBr}/f^{PNbPS}$ (mol/mol)	[b]Experimental $f^{PNbBBMH}/f^{PNbPS}$ (mol/mol)	[c]Molar mass of PNbBBMH-b-PNCs (SEC) kg/mol	Đ	[d]Experimental $f^{PNbBBMH}/f^{PNbPS}$ (v/v)
BR01	100/100/1	2200	0.55/0.45	0.53/0.47	823.5	1.10	0.39/0.61
BR02	150/150/1	2200	0.51/0.49	0.54/0.46	998.7	1.07	0.39/0.61
BR03	200/200/1	2200	0.50/0.50	0.52/0.48	1313.0	1.02	0.38/0.62
BR04	300/300/1	2200	0.50/0.50	0.52/0.48	1455.0	1.02	0.38/0.62
BR05	225/225/1	1930	0.53/0.47	0.26/0.74	2424.6	1.05	0.16/0.84
BR06	250/250/1	1930	0.49/0.51	0.25/0.75	3124.9	1.02	0.16/0.84
BR07	350/250/1	2200	0.67/0.33	0.65/0.25	5013.4	1.04	0.51/0.49

(a) Molar composition of PNbBBBr-b-PNbPS block copolymers was determined by the relative integration of the peaks positioned at 4.03 ppm due to – CH_2COO– of the PNbBBBr and 5.30-5.90 ppm dedicated to –CH=CH– of polynorbornene backbone.

(b) The molar composition of the PNbBBMH-b-PNbPS copolymer was determined by the relative integration of the signals located at 5.16 ppm due to C1 protons of maltoheptaose and 6.30-7.35 ppm phenyl ring of polystyrene.

(c) The molar mass of PNbBBMH-b-PNbPS was determined by SEC using light scattering putting dn/dc values for copolymers as 0.113 mL/g.

(d) The volume fraction of PNbBBMH-b-PNbPS was determined using polymer densities values of 1.05 and 1.36 for PS and MH respectively.

Table 2. Characteristics of PS-OH samples prepared via anionic polymerization of styrene monomer in toluene at 35 °C, followed by termination by ethylene oxide.

Sample	Mn (SEC) g/mol	Mn (^{1}H NMR) g/mol	Đ (Distribution of dispersity)
PS-OH-01	1780	1940	1.06
PS-OH-01	1400	1650	1.07

2.5 Experimental Section

This part was done by M. Mumtaz in our group.

2.5.1 Materials

6-aminohexanoic acid (≥98.5%), 4-(dimethyamino) pyridine (DMAP, regentPlus, ≥99%), *N,N′*-diisopropylcarbodiimide (99%), NaN_3 (regentPlus, ≥99.5%), trimethylamine (TEA, 99%), 4-bromobutyryl chloride (95%), 1,4-dioxane (anhydrous, 99.8%), and calcium hydride (CaH_2, 95%), magnesium sulfate (anhydrous, regentPlus, ≥99.5%), ethylene oxide solution (2.5-3.3M in THF), di-n-butylmagnesium solution (1.0 M in heptane) and sec-butyllithium solution (1.4 M in cylcohexane) were purchased from Sigma Aldrich and used as received. Prop-2-yn-1-amine (95%), cis-5-Norbornene-exo-2,3-dicarboxylic anhydride (96%), and Tricyclohexylphosphine[1,3-bis(2,4,6-trimethylphenyl)-4,5-dihydroimidazol-2-ylidene][benzylidene]Ru(IV) dichloride (95%) were purchased from ABCR and used without further purification. *N*-(4-hydroxybutyl)-cis-5-norbornene-exo-2,3-dicorboxiimide (NbBOH) ((*1*), *N*-(hexanoic acid)-cis-5-norbornene-exo-2,3-dicorboxiimide (NbCOOH) (*1*) and Grubbs 3rd generation catalyst (*2*) were prepared according to literature procedure.[40,41] Toluene (Biosolve) was first distilled over CaH_2 and then over polystyryllithium. Styrene (Sigma Aldrich, ReagentPlus, ≥99%) was first distilled over CaH_2 and then over di-n-dibutylmagnesium. CH_2Cl_2 (CP) stabilized by amylene and pyridine (extra dry) was obtained from Biosolve and distilled over CaH_2 at 35 °C prior to use. Maltoheptaose (MH) (Hayashibara Company) alkynyl group according to literature method (*3*) The Cu/CuO nanopowder (CuNP, 20-50 nm, 99.9 % metal basis) was purchased from Alfa Aesar. Tetrahydrofuran (THF), absolute methanol and absolute ethanol were bought from Biosolve. *N,N*-Dimethylformamide (DMF, Fisher scientific)

and 4-amino-1-butanol (>98%, TCI europe) were used as received. Milli-Q water was obtained by water purification to a resistivity of 18.2MΩ cm using a Millipore Ultrapure system. The deuterated solvents were purchased from Eurisotop. The cuprisorb resin was bought from Seachem.

2.5.2 Methods

2.5.2.1 General procedure for the synthesis of ω-hydroxyl terminated polystyrene (PS-OH)

Hydroxyl-terminated polystyrene was prepared by anionic polymerization of styrene accompanied by the termination with ethylene oxide. In a particular example PS-OH was prepared as fallow: Toluene (150 mL) was introduced in a 1 L flamed dried round bottom two necked flask equipped with magnetic stirrer and specially designed joint with roto-flow, under vacuum. Styrene (25 g, 27.6 mL) was then added and fill the flask with argon. Sec-butyllithium (~1.3 M in cyclohexane, 10 mmol, 9.61 mL) was then introduced in order to initiate the polymerization. The color of the reaction mixture turns red. The reaction flask was placed in an oil bath preheated at 35 °C for 3h. The polymerization reaction was finally terminated by the addition of ethylene oxide (5.0 mL, ~3M solution in THF) in the reaction mixture, accompanied by the addition of excess of degassed methanol. The solvent was removed under vacuum using rotary evaporator at 40°C. The polymer was redissolved in appropriate amount of THF and precipitated twice in methanol (1L). The white precipitated hydroxyl terminated polystyrene was filtered using sintered glass funnel under vacuum and dried in a vacuum oven at 40 °C for overnight. 24 g of solid product, 96% yield. The sample was characterized using ^{1}H NMR and SEC see Figure 11-12 and Table 2). M_n (^{1}H NMR) ~ 1940 g/mol, M_n (SEC, DMF) = 1780 g/mol.

2.5.2.2 General procedure for the synthesis of 2-polystyrylethyl-6-(cis-5-norbornene-exo-2,3-dicorboxiimide) hexanoate (NbPS)

Hydroxyl terminated PS (10 g), N-(hexanoic acid)-cis-5-norbornene-exo-2, 3-dicorboxiimide (1.80 g, 1.3 eq) and DMAP (1.60 g) was introduced in 250 mL round bottom flask equipped flask equipped with magnetic stirrer and roto-flow.

Dichloromethane (100 mL) was added and wait till all the solid disappeared. The reaction mixture was placed in an ice bath at 0 °C and DIPC (3eq vs acid 3.0 mL) was added dropwise and allowed the reaction mixture to warm at room temperature. The reaction mixture was allowed to react at room temperature for 72h. The solvent was removed by rotary evaporator under vacuum at 30 °C. The crude product was re-dissolved in appropriate amount of THF and precipitated twice in methanol, in order to remove all the traces of by products and excess of acid. The white solid was filtered and dried in a vacuum oven at 40 °C for overnight. 11 g of white solid. 96% yield, M_n = 2197 g/mol (^{1}H NMR).

2.5.2.3 General procedure for the synthesis of *N*-(4-bromobutanoate butyl)-cis-5-norbornene-exo-2, 3-dicorboxiimide (NbBBBr)

N-(4-hydroxybutyl)-cis-5-norbornene-exo-2,3-dicorboxiimide (4 g, 17 mmol) was introduced in 250 mL, flamed dried two necked round bottom flak equipped with magnetic stirrer, septum and a special joint to introduce solvent in inert atmosphere. CH_2Cl_2 (50 mL) was then added and wait till all the solid disappeared. Pyridine (4.95 mL, 61.2 mmol) was then introduced and put the flak in an ice bath at 0 °C. Finally, 4-bromobutyryl chloride (2.36 mL, 20.4 mmol) was introduced drop by drop through septum and allow the reaction mixture to warm at room temperature. The reaction mixture was allowed to react at this temperature for overnight. The reaction mixture was diluted with CH_2Cl_2 washed with water (3 x 100 mL) and brine. The organic layer was collected, dried over Na_2SO_4, and concentrated under vacuum, affording the product as a light brown viscous oil (6.2 g, 95% yield).

2.5.2.4 General procedure for the synthesis of Synthesis of PNbBBBr-b-PNbPS

Several examples of PNbBBBr-b-PNbPS block copolymers were prepared via metathesis ring opening polymerization, by sequential addition of monomers using Grubbs 3rd generation catalyst. In a particular example, PNbBBBr-b-PNbPS (BB-02, Table-01) was prepared as follow: To a two necked flask containing a stir bar, equipped with roto-flow, NbBBBr (350 mg) was dissolved in 5 mL of CH_2Cl_2. To another vial, a solution of Grubbs 3rd generation bispyridyl catalyst (5 mg/mL in CH_2Cl_2) was freshly

prepared. Appropriate volumes of the catalyst solution to achieve the desired degrees of polymerization (DP) were then added to the vial containing NbBBBr. The reaction mixture was allowed to stir for 3 h at room temperature. In another two necked flask NbPS (2 g) was dissolved in CH_2Cl_2 (8 mL) and transfer to the first flask and the reaction mixture was allowed to stirrer for another 3h at room temperature. To quench the polymerization, a few drops of ethyl vinyl ether were then added. The reaction mixture was diluted with THF and precipitated in methanol (400 mL). The white powder was filtered and dried in vacuum oven at 40 °C for overnight. 2.1 g of block copolymer was obtained in 88% yields.

2.5.2.5 Azido-functionalized of PNbBBBr-b-PNbPS bottle-brush block copolymers

PNbBBBr-b-PNbPS (2 g) was charged in a two necked round bottom flask containing DMF (60 mL) and equipped with magnetic stirrer. NaN_3 (0.55 g, ~10eq vs NbBBBr unit) was then added under stirring and placed the reaction mixture on preheated oil bath at 60°C for overnight. The system was then let to cooled down to room temperature, diluted with CH_2Cl_2 (200 mL) and transferred into separating funnel where it was washed repeatedly washed with water to remove the residual tosylate salt, excess of NaN_3 and DMF. The organic layer was then dried by adding anhydrous $MgSO_4$. CH_2Cl_2 was removed by evaporation using rotary evaporator. The polymer was redissolved in appropriate amount of THF and precipitated twice in methanol (300 mL). The white precipitated of azido functionalized PNBBN_3-b-PNBPS was filtered using sintered glass funnel under vacuum and dried in a vacuum oven at 40 °C for overnight. 1.7 g of solid product, ~86% yield. The sample was characterized by ^{1}H NMR.

2.5.2.6 General procedure for the synthesis of PNbBBMH-*b*-PNbPS bottle brush block copolymer

In a particular example, PNbBBH-b-PNbPS (BR02, Table 1)was prepared as follow: In a round bottom, one necked flask equipped with rotoflow and magnetic stirrer was charged with PNbBBN_3-b-PNbPS (0.8 g), propargyl-maltoheptaose (1.5 eq, 0.6 g, $3.36x10^{-4}$ moles), and DMF (40 mL) and degassed by three freeze-pump-thaw cycles

and then copper nanopowder (2 eq vs acetylene group, 64 mg, 1.0 mmol) was added to the solution under argon flow and subjected to another freeze-pump-thaw cycle. The solution was stirred under argon atmosphere at 65 °C for 3 days. At the end of the reaction, the crude heterogeneous solution was diluted with DMF and filtered through diatomaceous earth. The obtained filtrate was stirred with 5.0 g cuprisorb resin at 40 °C overnight. The solution was filtered to remove the cuprisorb resin and the solvent was removed by distillation using roto-evaporator. The crude product was redissolved in appropriate amount of DMF and precipitate in methanol to remove excess of maltoheptaose. The resulting half-white solid was dried in vacuum at 40°C for overnight and characterized by ^{1}H NMR and SEC. 1.2 g solid product, ~85% yield.

2.5.3 Characterization

^{1}H NMR spectra of polymer samples were recorded on a Bruker Avance 400 MHz spectrometer with a frequency of 400.13 MHz and calibrated with the signal of deuterated solvent. The size exclusion chromatography (SEC) was performed at 40 °C using an Agilent390 MDS system (290 LC pump injector, ProStar 510column oven, 390 MDS refractive index detector) equipped with Knauer Smartline UV detector 2500 and two Agilent Poly Pore PL1113-6500 columns (linear, 7.5 × 300 mm; particle size, 5 μm; exclusion limit, 200-2,000,000) and 1260 Infinity II GPC/SEC MDS Dual-Angle Light Scattering Detector (laser wavelength/ power 660 nm/50 mW; Rayleigh scattering angles 15° and 90°), in DMF containing lithium chloride (0.01 M) at the flow rate of 1.0 mL min^{-1}. FT-IR spectra were recorded using a PerkinElmer Spectrum RXI FT-IR spectrometer. Increment in refractive (dn/dc) index of PNbBBMH-b-PNbPS block copolymer was determined using WYATT Optilab rex refractometer in DMF at 40°C.

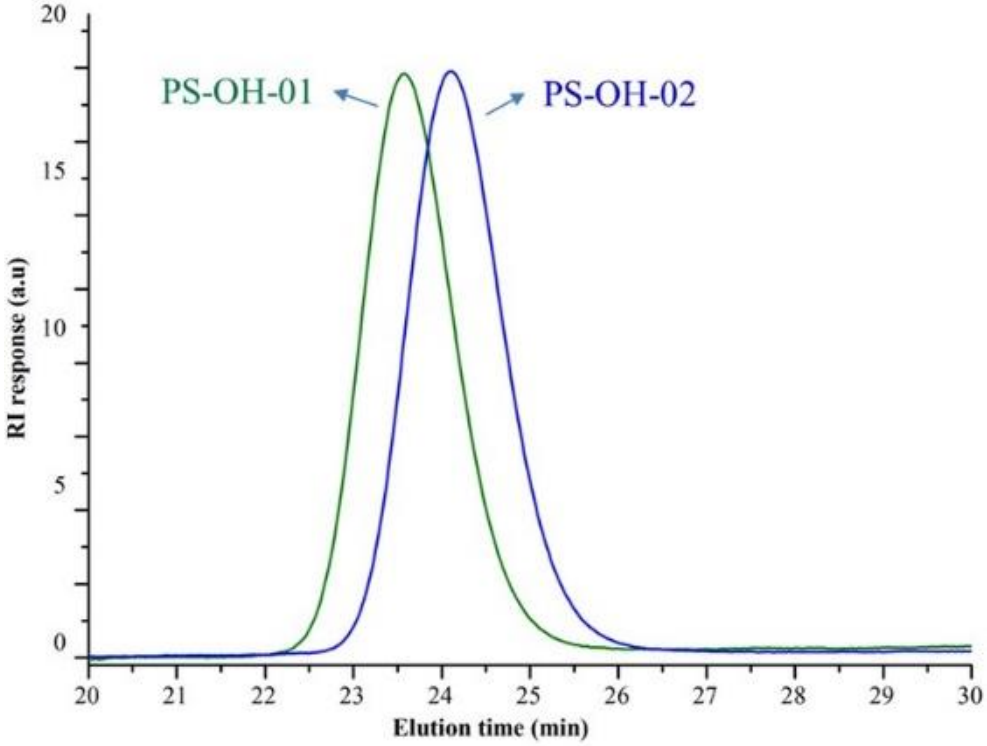

Figure 11. SEC traces of PS-OH-01 and PS-OH-02 using DMF as eluent and PS as calibration standard at 40°C (please see Table 1 for further details).

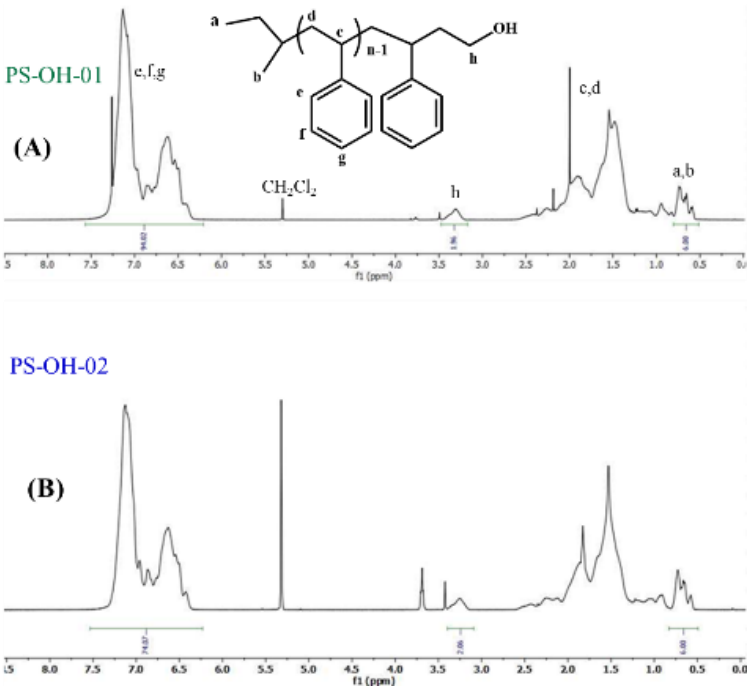

Figure 12. ^{1}H NMR Spectra of PS-OH-01 and PS-OH-02 in $CDCl_3$ at 25 °C (400 MHz) (please see Table 1 for further details)

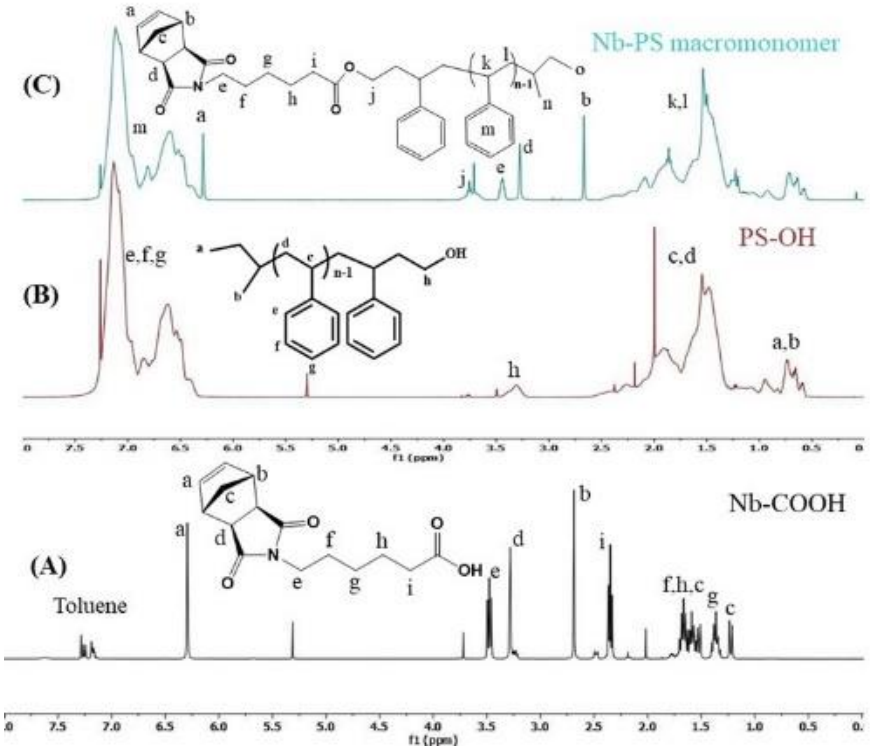

Figure 13. ^{1}H NMR spectra of (A) PNbCOOH (B) PS-OH and (C) NbPS in $CDCl_3$ at 25 °C (400 MHz)

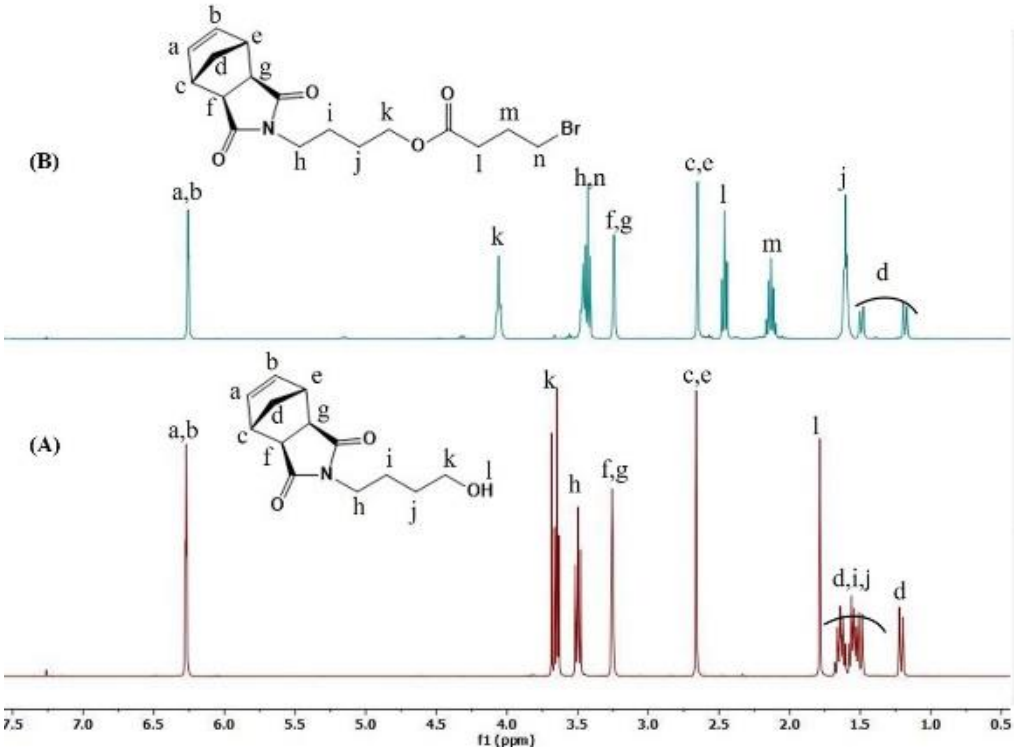

Figure 14. ^{1}H NMR spectra of (A) PNbBOH and (B) PNbBBBr in $CDCl_3$ at 25 °C (400 MHz)

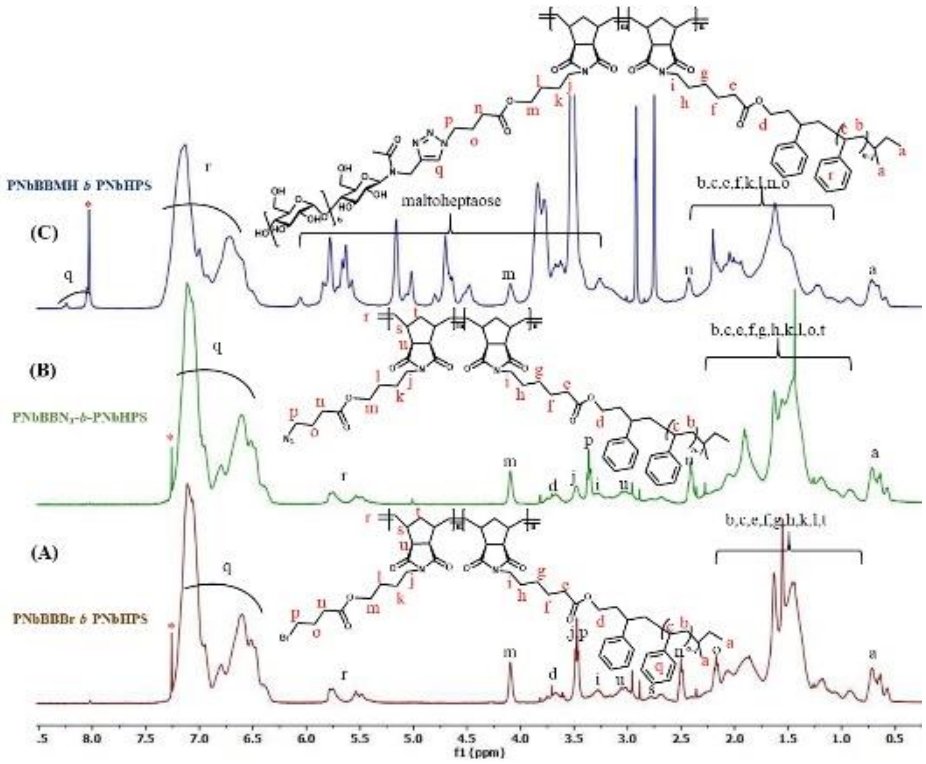

Figure 15. ^{1}H NMR of (A) PNbBBBr-b-PNbPS-02, in $CDCl_3$ (B) PNbBBN_3-b-PNbPS-02 in $CDCl_3$ and PNbBBMH-b-PNbPS in DMF-d_7 at 25 °C (BB02, table 1)

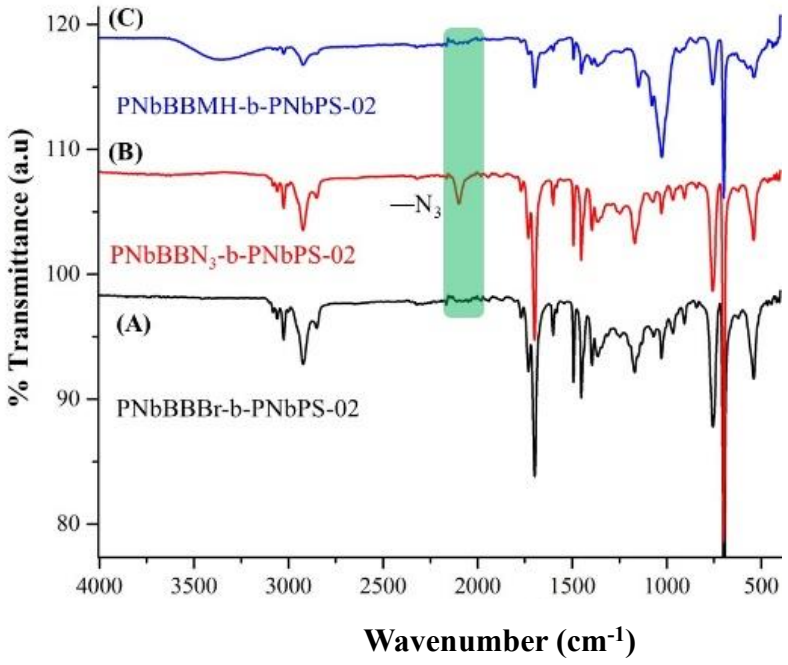

Figure 16. FTIR of (A) PNbBBMH-b-PNbPS-02, (B) PNbBBN_3-b-PNbPS-02 and (C) PNbBBBr-b-PNbPS-02 (Complete disappearance of peak at 2100 cm^{-1}indicates the total conversion of azido function during the click reaction.)

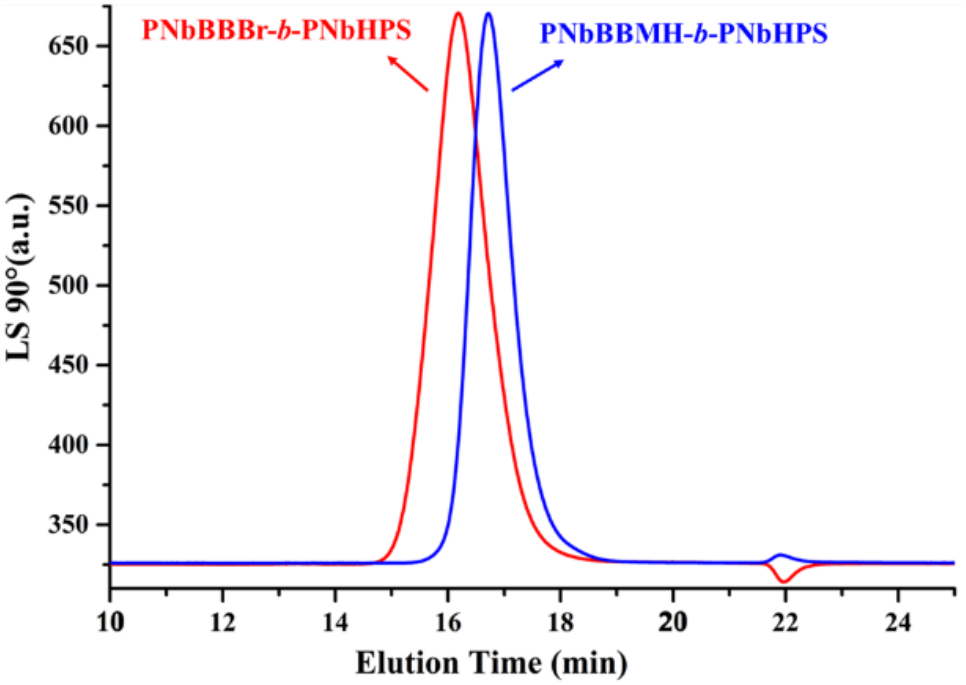

Figure 17. SEC traces of PNbBBBr-b-PNbPS and PNbBBMH-b-PNbPS (BR02, Table 1) using DMF as an eluent at 40 °C.

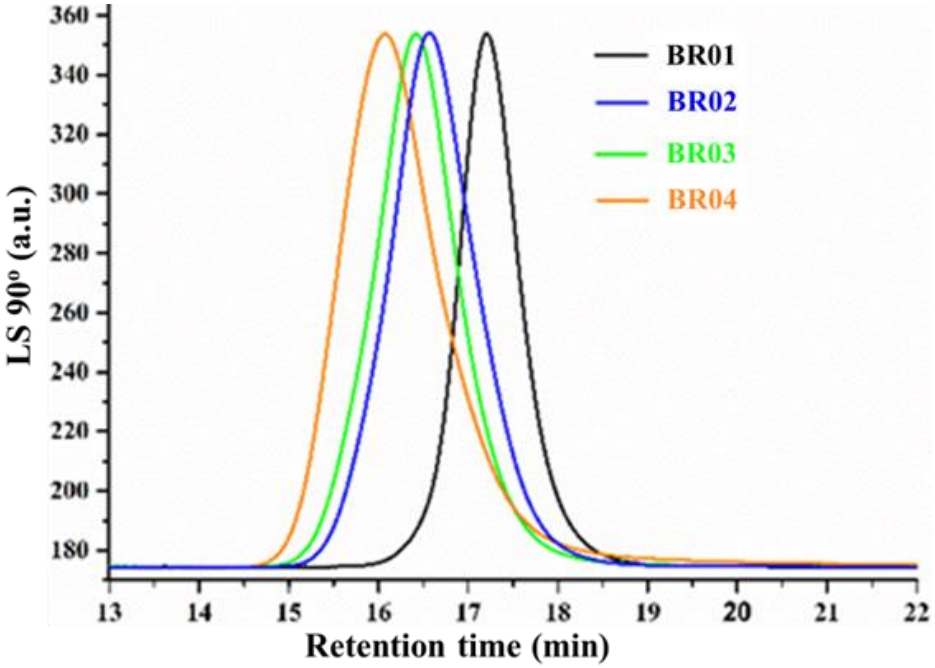

Figure 18. SEC traces of BR01-04 (Table 1) using DMF as an eluent at 40 °C.

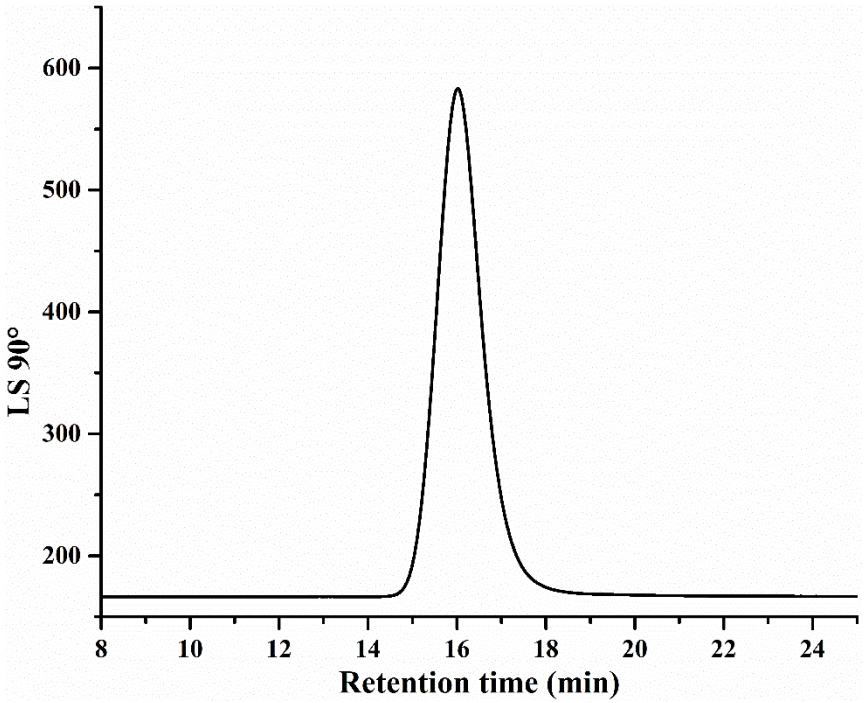

Figure 19. SEC traces of BR05 (Table 1) using DMF as an eluent at 40 °C.

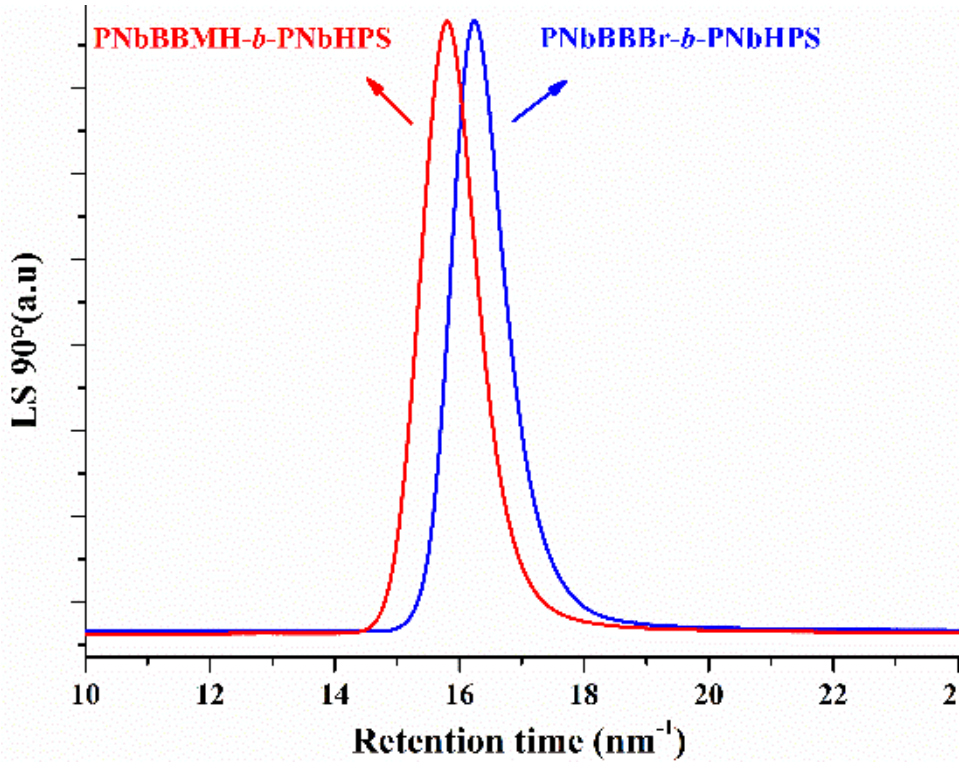

Figure 20. SEC traces of PNbBBBr-b-PNbPS and PNbBBMH-b-PNbPS (BR06, Table1) using DMF as an eluent at 40 °C.

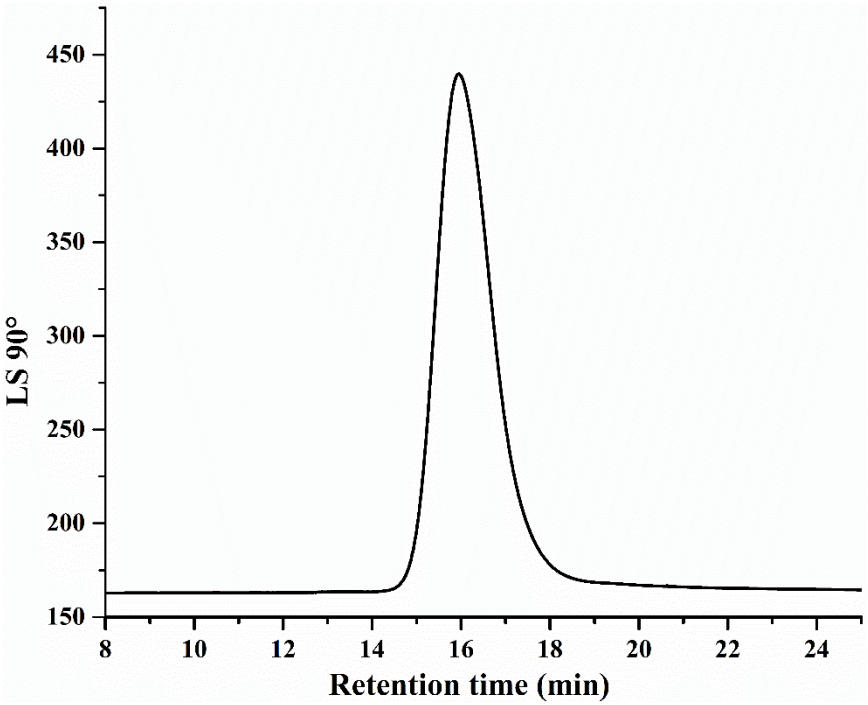

Figure 21. SEC traces of BR07 (Table 1) using DMF as an eluent at 40 °C.

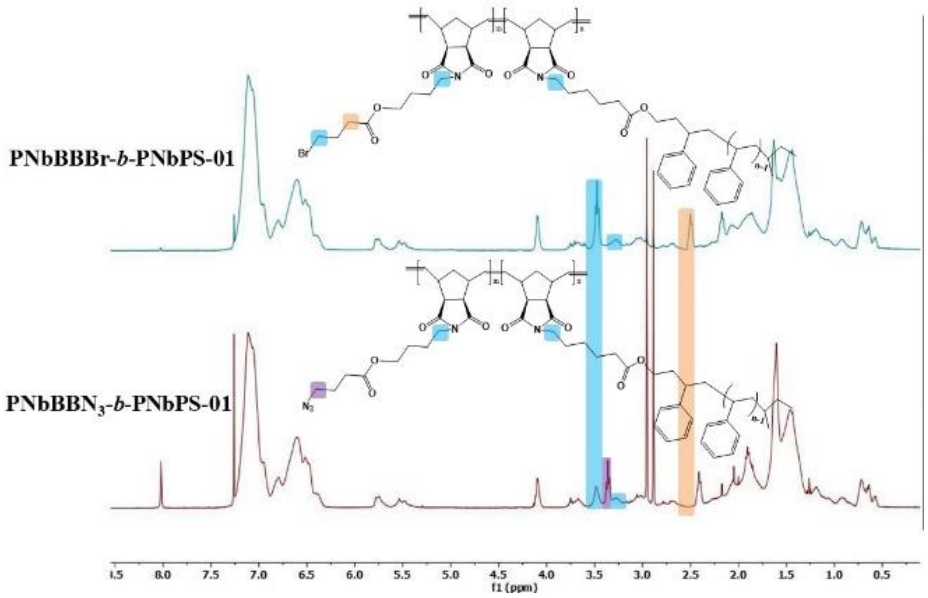

Figure 22. ^{1}H NMR of PNbBBBr-b-PNbPS-01and $PNbBBN_3$-b-PNbPS-01 in $CDCl_3$ at 25 °C (BR01, table 1)

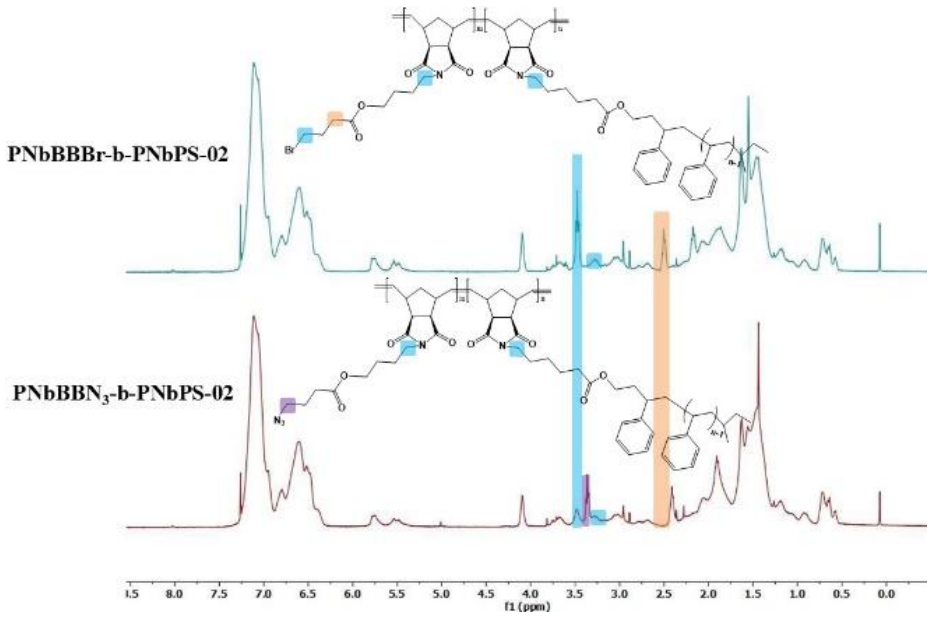

Figure 23. ^{1}H NMR of PNbBBBr-b-PNbPS-02 and PNbBBN$_3$-b-PNbPS-02 in $CDCl_3$ at 25 °C (BR02, table 1)

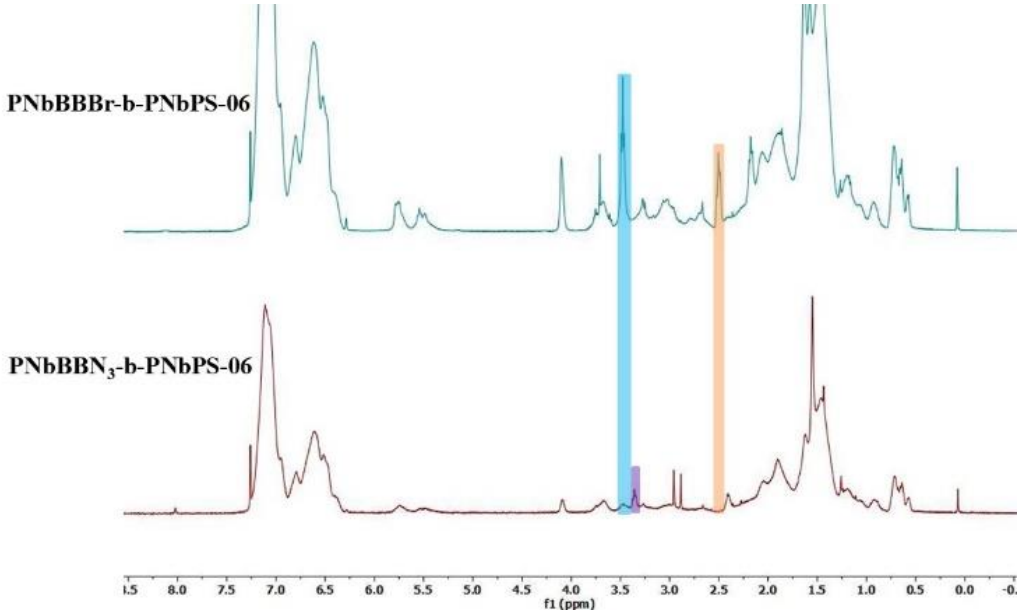

Figure 24. ^{1}H NMR of PNbBBBr-b-PNbPS-06 and PNbBBN$_3$-b-PNbPS-06 in $CDCl_3$ at 25 °C (BR05, Table 1)

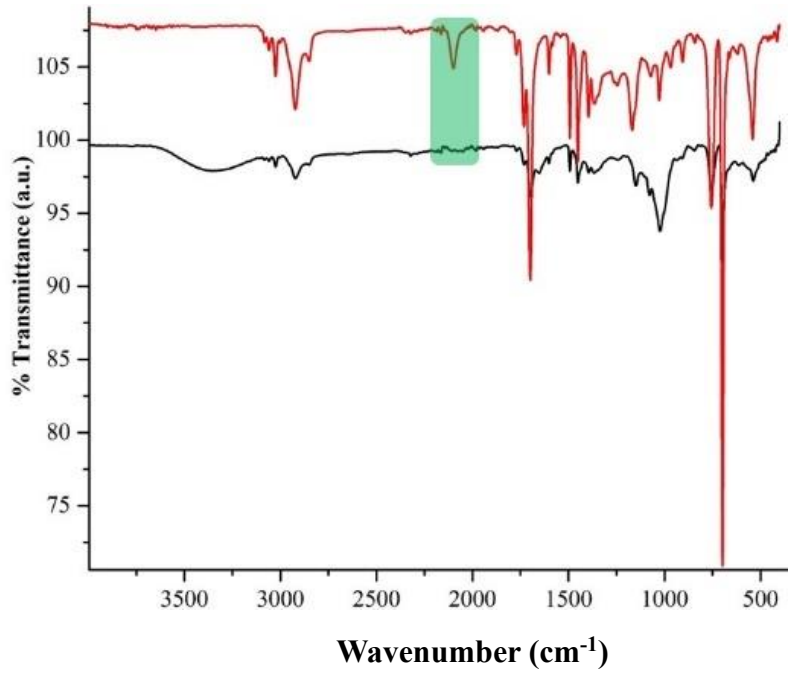

Figure 25. FTIR of $PNbBBN_3$-b-PNbPS-01 and PNbBBBr-b-PNbPS-01 (BR01, table 1) (Complete disappearance of peak at 2100 cm^{-1} indicates the total conversion of azido function during the click reaction)

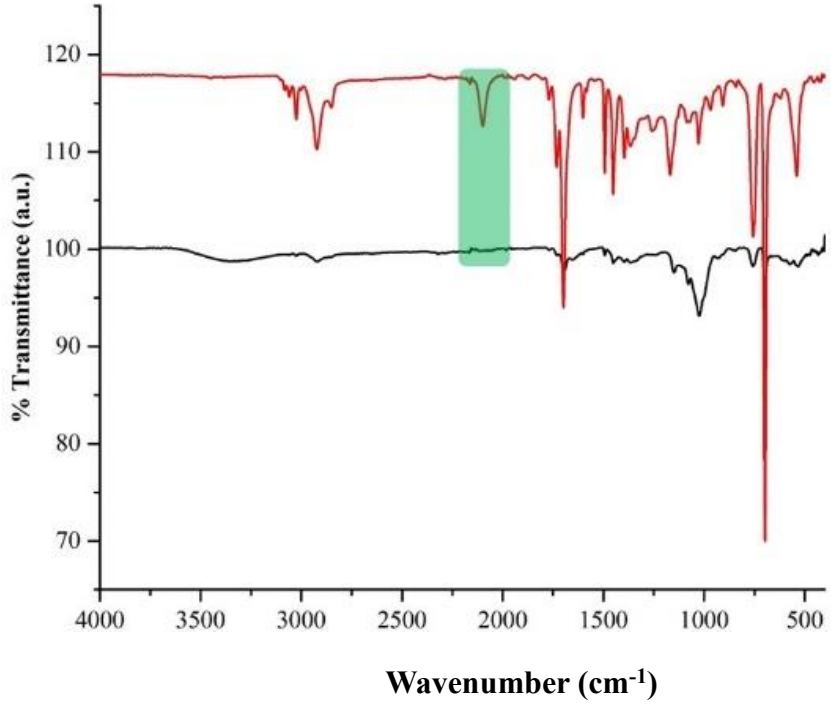

Figure 26. FTIR of $PNbBBN_3$-b-PNbPS-02 and PNbBBBr-b-PNbPS-02 (BR02, table 1) (Complete disappearance of peak at 2100 cm^{-1} indicates the total conversion of azido function during the click reaction)

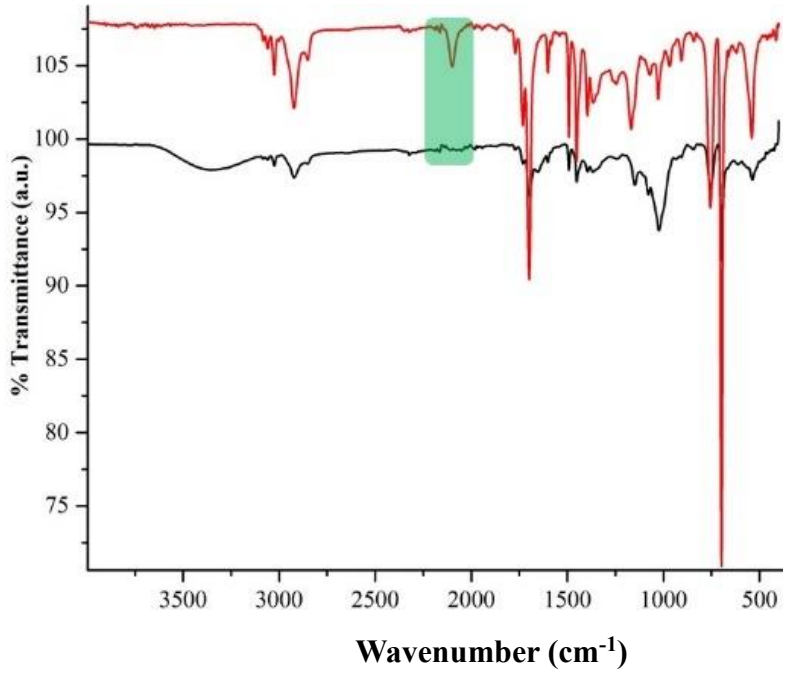

Figure 27. FTIR of PNbBBN$_3$-b-PNbPS-03 and PNbBBBr-b-PNbPS-03 (BR03, table 1) (Complete disappearance of peak at 2100 cm^{-1}indicates the total conversion of azido function during the click reaction)

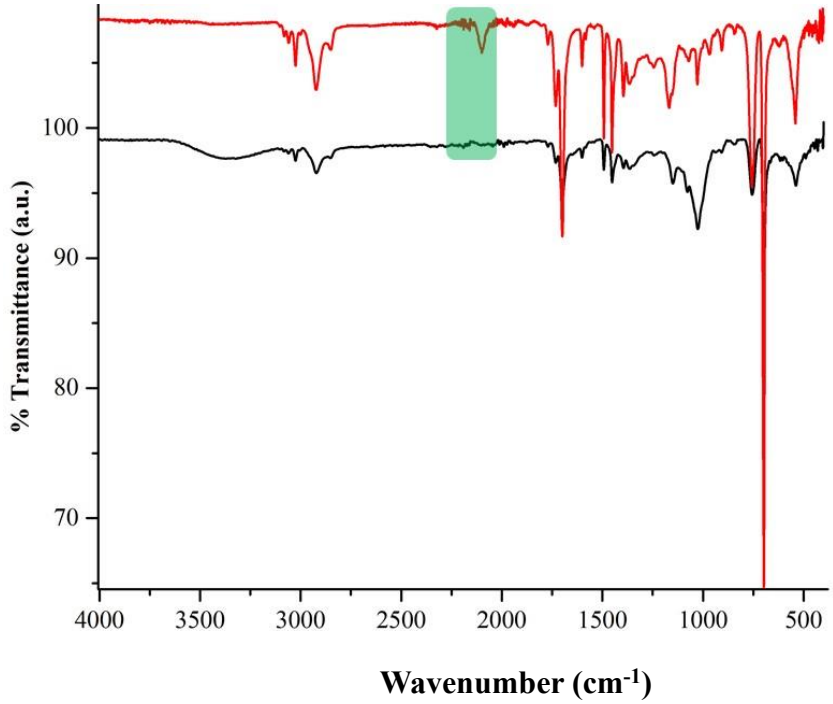

Figure 28. FTIR of PNbBBN$_3$-b-PNbPS-04 and PNbBBBr-b-PNbPS-04 (BR04, table 1) (Complete disappearance of peak at 2100 cm^{-1} indicates the total conversion of azido function during the click reaction)

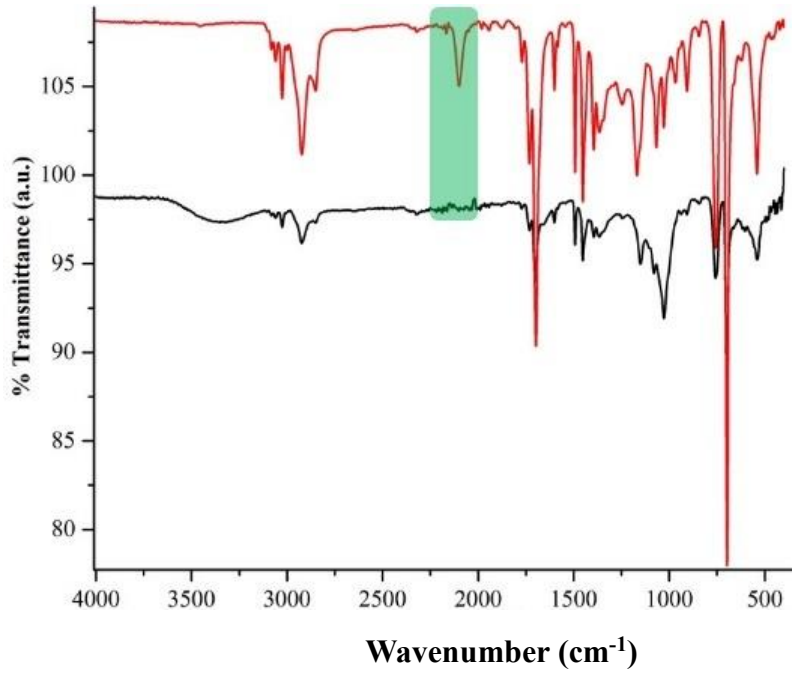

Figure 29. FTIR of $PNbBBN_3$-b-PNbPS-05 and PNbBBMH-b-PNbPS-05 (BR05, table 1) (Complete disappearance of peak at 2100 cm^{-1} indicates the total conversion of azido function during the click reaction)

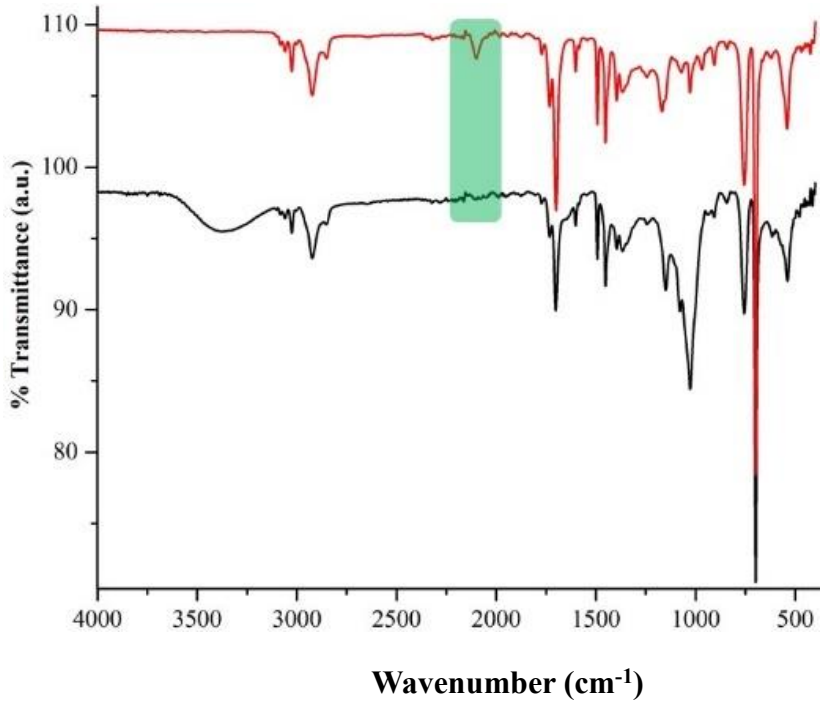

Figure 30. FTIR of $PNbBBN_3$-b-PNbPS-06 and PNbBBMH-b-PNbPS-06 (BR06, table 1) (Complete disappearance of peak at 2100 cm^{-1} indicates the total conversion of azido function during the click reaction)

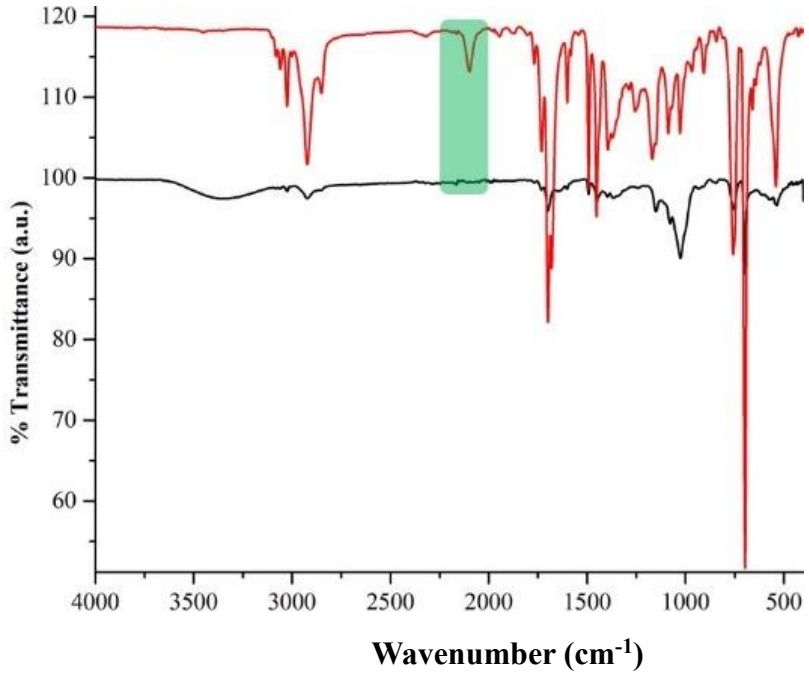

Figure 21. FTIR of $PNbBBN_3$-b-PNbPS-07 and PNbBBMH-b-PNbPS-07 (BR07, table 1) (Complete disappearance of peak at 2100 cm^{-1} indicates the total conversion of azido function during the click reaction).

2.6 Conclusion

Herein, a series of brush block copolymers (BR01-07) with various molecular weights at range of 823.5-5013.4 kg/mol, were successfully synthesized by the combination of ROMP grafting-from and grafting-to approaches. The dispersity value of BR01-07 at range of 1.02-1.10 showed the narrow dispersity property. One kind of side chain attached the polynorbornene backbone was the hydrophobic polystyrene (PS) as a soft block with two different weights (1930 g/mol for BR01-04 and BR07; 2200 g/mol for BR05 and BR06), the other side chain was the hydrophilic maltaoheptaose (1250 g/mol, MH) for BR01-07. Particularly, the ratio volume fraction between PS and MH side chains of BR07 bottlebrushes was the 0.51/0.49 determined by using polymer densities values of 1.05 and 1.36 for MH and PS respectively, which was much different from the other bottlebrushes (BR01-06). Moreover, these bottlebrushes and their precursors were characterized by FTIR, NMR and SEC.

References:

1. Verduzco, R.; Li, X.; Pesek, S. L.; Stein, G. E., Structure, function, self-assembly, and applications of bottlebrush copolymers. *Chem Soc Rev* **2015,** *44* (8), 2405.
2. Sheiko, S. S.; Sumerlin, B. S.; Matyjaszewski, K., Cylindrical molecular brushes: Synthesis, characterization, and properties. *Prog Polym Sci* **2008,** *33* (7), 759.
3. Liao, L.; Liu, J.; Dreaden, E. C.; Morton, S. W.; Shopsowitz, K. E.; Hammond, P. T.; Johnson, J. A., A convergent synthetic platform for single-nanoparticle combination cancer therapy: ratiometric loading and controlled release of cisplatin, doxorubicin, and camptothecin. *J Am Chem Soc* **2014,** *136* (16), 5896.
4. Azzaroni, O., Polymer brushes here, there, and everywhere: Recent advances in their practical applications and emerging opportunities in multiple research fields. *J Polym Sci Part A Polym Chem* **2012,** *50* (16), 3225.
5. Rempp, P.; Lutz, P.; Masson, P.; Franta, E., Macromonomers-a new class of polymeric intermediates in macromolecular synthesis. I-synthesis and characterization. *Makromol Chem* **1984,** *8* (S19841), 3.
6. Liberman-Martin, A. L.; Chu, C. K.; Grubbs, R. H., Application of bottlebrush block copolymers as photonic crystals. *Macromol Rapid Commun* **2017,** *38* (13), 1700058.
7. Tu, S.; Choudhury, C. K.; Luzinov, I.; Kuksenok, O., Recent advances towards applications of molecular bottlebrushes and their conjugates. *Cur Opin Solid State Mater Sci* **2019,** *23* (1), 50.
8. Lee, H. I.; Pietrasik, J.; Sheiko, S. S.; Matyjaszewski, K., Stimuli-responsive molecular brushes. *Prog Polym Sci* **2010,** *35* (1-2), 24.
9. Feng, C.; Li, Y.; Yang, D.; Hu, J.; Zhang, X.; Huang, X., Well-defined graft copolymers: from controlled synthesis to multipurpose applications. *Chem Soc Rev* **2011,** *40* (3), 1282.
10. Sun, H.; Yu, D. M.; Shi, S.; Yuan, Q.; Fujinami, S.; Sun, X.; Wang, D.; Russell, T. P., Configurationally constrained crystallization of brush polymers with poly(ethylene oxide) side chains. *Macromolecules* **2019,** *52* (2), 592.
11. Steponaviciute, M.; Klimkevicius, V.; Makuska, R., Synthesis and stability against oxidation of random brush copolymers carrying PEO side chains and catechol moieties. *Mater Today Commun* **2020,** *25*, 101262.
12. Wright, D. B.; Touve, M. A.; Adamiak, L.; Gianneschi, N. C., ROMPISA: ring-opening metathesis polymerization-induced self-assembly. *ACS Macro Lett* **2017,** *6* (9), 925.
13. Xu, B.; Qian, H.; Lin, S., Self-assembly and photoinduced spindle-toroid morphology transition of macromolecular double-brushes with azobenzene pendants. *ACS Macro Lett* **2020,** *9* (3), 404.
14. Karavolias, M. G.; Elder, J. B.; Ness, E. M.; Mahanthappa, M. K., Order-to-disorder transitions in lamellar melt self-assembled core-shell bottlebrush polymers. *ACS Macro Lett* **2019,** *8* (12), 1617.
15. Chen, K.; Hu, X.; Zhu, N.; Guo, K., Design, Synthesis, and self-assembly of janus bottlebrush polymers. *Macromol Rapid Commun* **2020,** *41* (20), 2000357.

16. Liao, Y.; Chen, W. C.; Borsali, R., Carbohydrate-based block copolymer thin films: ultrafast nano-organization with 7 nm resolution using microwave energy. *Adv Mater* **2017,** *29* (35), 1701645.
17. Neary, W. J.; Fultz, B. A.; Kennemur, J. G., Well-defined and precision-grafted bottlebrush polypentenamers from variable temperature ROMP and ATRP. *ACS Macro Lett* **2018,** *7* (9), 1080.
18. Wu, Y.; Zhang, L.; Zhang, M.; Liu, Z.; Zhu, W.; Zhang, K., Bottlebrush polymers with self-immolative side chains. *Polym Chem* **2018,** *9* (14), 1799.
19. Sukegawa, T.; Masuko, I.; Oyaizu, K.; Nishide, H., Expanding the dimensionality of polymers populated with organic robust radicals toward flow cell application: synthesis of TEMPO-crowded bottlebrush polymers using anionic polymerization and ROMP. *Macromolecules* **2014,** *47* (24), 8611.
20. Strover, L. T.; Malmstrom, J.; Travas-Sejdic, J., Graft copolymers with conducting polymer backbones: a versatile route to functional materials. *Chem Rec* **2016,** *16* (1), 393.
21. Rzayev, J., Molecular bottlebrushes: new opportunities in nanomaterials fabrication. *ACS Macro Lett* **2012,** *1* (9), 1146.
22. Gao, H.; Matyjaszewski, K., Synthesis of molecular brushes by "grafting onto" method: combination of ATRP and click reactions. *J Am Chem Soc* **2007,** *129* (20), 6633.
23. Lanson, D.; Ariura, F.; Schappacher, M.; Borsali, R.; Deffieux, A., Comb copolymers with polystyrene and polyisoprene branches: effect of block topology on film morphology. *Macromolecules* **2009,** *42* (12), 3942.
24. Ma, H.; Ha, S.; Jeong, J.; Wang, V.; Kim, K. T., Synthesis of discrete bottlebrush polymers via the iterative convergent growth technique and post-functionalization. *Polym Chem* **2022**, *13*, 3689.
25. Clauss, Z. S.; Wardzala, C. L.; Schlirf, A. E.; Wright, N. S.; Saini, S. S.; Onoa, B.; Bustamante, C.; Kramer, J. R., Tunable, biodegradable grafting-from glycopolypeptide bottlebrush polymers. *Nat Commun* **2021**, *12*, 6472.
26. Lee, N. J.; Kim, D.; Yoo, K.; Yu, Y.; Kim, B. S.; Kim, J. G., Divergent strategy for the synthesis of bottlebrush polymers via postpolymerization modification of macromonomer, *J Polym Sci* **2020**, *58*, 3237.
27. Heroguez, V.; Breunig, S.; Gnanou, Y.; Fontanille, M., Synthesis of r-norbornenylpoly(ethylene oxide) macromonomers and their ring-opening metathesis Polymerization. *Macromolecules* **1996**, *29*, 13.
28. Heroguez, V.; Gnanou, Y.; Fontanille, M., Novel amphiphilic architectures by ring-opening metathesis polymerization of macromonomers. *Macromolecules* **1997**, *30*, 17.
29. Grande, D.; Six, J. L.; Breunig, S.; Heroguez, V.; Fontanille, M.; Gnanou, Y., Polymers with novel topologies by ring-opening metathesis polymerization of macromonomers. *Polym Adv Technol* **1998**, *9*, 60l.
30. Varlas, S.; Lawrenson, S. B.; Arkinstall, L. A.; O'Reilly, R. K.; Foster, J. C., Self-assembled nanostructures from amphiphilic block copolymers prepared via ring-opening metathesis polymerization (ROMP). *Prog Polym Sci* **2020,** *107*, 101278.

31. Sowers, M. A.; McCombs, J. R.; Wang, Y.; Paletta, J. T.; Morton, S. W.; Dreaden, E. C.; Boska, M. D.; Ottaviani, M. F.; Hammond, P. T.; Rajca, A.; Johnson, J. A., Redox-responsive branched-bottlebrush polymers for in vivo MRI and fluorescence imaging. *Nat Commun* **2014,** *5*, 5460.
32. Sun, G.; Cho, S.; Clark, C.; Verkhoturov, S. V.; Eller, M. J.; Li, A.; Pavia-Jimenez, A.; Schweikert, E. A.; Thackeray, J. W.; Trefonas, P.; Wooley, K. L., Nanoscopic cylindrical dual concentric and lengthwise block brush terpolymers as covalent preassembled high-resolution and high-sensitivity negative-tone photoresist materials. *J Am Chem Soc* **2013,** *135* (11), 4203.
33. Sunday, D. F.; Dolejsi, M.; Chang, A. B.; Richter, L. J.; Li, R.; Kline, R. J.; Nealey, P. F.; Grubbs, R. H., Confinement and processing can alter the morphology and periodicity of bottlebrush block copolymers in thin films. *ACS Nano* **2020,** *14*(12), 17476.
34. Miyake, G. M.; Weitekamp, R. A.; Piunova, V. A.; Grubbs, R. H., Synthesis of isocyanate-based brush block copolymers and their rapid self-assembly to infrared-reflecting photonic crystals. *J Am Chem Soc* **2012,** *134* (34), 14249.
35. Gu, W.; Huh, J.; Hong, S. W.; Sveinbjornsson, B. R.; Park, C.; Grubbs, R. H.; Russell, T. P., Self-assembly of symmetric brush diblock copolymers. *ACS Nano* **2013,** *7* (3), 2551.
36. Fenyves, R.; Schmutz, M.; Horner, I. J.; Bright, F. V.; Rzayev, J., Aqueous self-assembly of giant bottlebrush block copolymer surfactants as shape-tunable building blocks. *J Am Chem Soc* **2014,** *136* (21), 7762.
37. Ma, H.; Kim, K. T., Self-assembly of bottlebrush block copolymers into triply periodic nanostructures in a dilute solution. *Macromolecules* **2020,** *53* (2), 711.
38. Li, Y.; Zou, J.; Das, B. P.; Tsianou, M.; Cheng, C., Well-defined amphiphilic double-brush copolymers and their performance as emulsion surfactants. *Macromolecules* **2012,** *45* (11), 4623.
39. Macfarlane, R. J.; Kim, B.; Lee, B.; Weitekamp, R. A.; Bates, C. M.; Lee, S. F.; Chang, A. B.; Delaney, K. T.; Fredrickson, G. H.; Atwater, H. A.; Grubbs, R. H., Improving brush polymer infrared one-dimensional photonic crystals via linear polymer additives. *J Am Chem Soc* **2014,** *136* (50), 17374.
40. Camm, K. D.; Castro, N. M.; Liu, Y.; Czechura, P.; Snelgrove, J. L.; Fogg, D. E., Tandem ROMP-hydrogenation with a third-generation Grubbs catalyst. *J Am Chem Soc* **2007,** *129* (14), 4168.
41. Kang, E. H.; Yu, S. Y.; Lee, I. S.; Park, S. E.; Choi, T. L., Strategies to enhance cyclopolymerization using third-generation Grubbs catalyst. *J Am Chem Soc* **2014,** *136* (29), 10508.

Chapter 3: Carbohydrate-based Bottlebrushes and Their Self-assembly: Tunable Full-Color Reflective to Photonic Crystals

3.1 Introduction

In nature, structural colors of diverse creatures such as tropical fishes (Neon tetra),[1] longhorn beetles,[2] peacock feathers,[3] and butterfly wings [4] so on, embellish the colorful world owning to their intrinsic photonic structures.[5] These photonic structures are made of periodic nanostructures in which two components or more with varying refractive indices arranges periodically in geometry.[6-9] When the domain of periodicity in photonic structures is comparable to the wavelength of light, this light cannot propagate through these nanostructures and then are able to be reflected with the specific wavelength, generating a photonic band gap (PBG)[10, 11] The wavelength of reflected light dominated by PBG is mainly related to the combination of the refractive index, domain size, and nanostructure morphology.[12] Interestingly, responsive coloration in some creatures exposed to the external stimuli,[1,2,5,12] commonly occurs in reproductive behavior, social communication and camouflage,[13-15] acting as an essential part of nature. Inspired by the active-nature photonic structures, it is opportune to design the artificial architecture of materials with the responsive and reversible coloration property, particularly in tunable one-dimensional photonic crystals (1D-PCs).[14]

As for the simplest 1D-PCs, the wavelength of reflected light is proportional to the refractive index of alternated layers and domain sizes.[16, 17] Therefore, researchers have manipulated these two factors to construct the structural color by using top-down and bottom-up strategies.[14] Various preparation approach brings about the different architecture and physicochemical property. In comparison with the top-down method, the bottom-up method usually requires the self-assembly of polymers or nanoparticles into PCs and arouses researchers particular of interest due to its relative inexpensiveness, fast and simple procedure.[18, 19] Unfortunately, the formation of colloid photonic crystals from the self-assembly of nanoparticles are frequently accompanied with the face-centered cubic or hexagonal closely packed morphology,[20, 21] limiting geometric diversities and responsive applications on structural coloration. In contrast,

the self-assembly of polymers including linear and brush block copolymers have come to fore as a versatile and flexible candidate for fabricating the tunable 1D-PCs controlled by the responsiveness and reversibility of domain sizes, exhibiting similar structural coloration in nature.[12,22-27] Based on these polymers fabricated into 1D-PCs, brush polymers have several superior advantages over other polymers due to their unique architecture: (1) highly dense and regularly spaced side chains attached to the backbone. [28-30] (2) extended wormlike or cylindrical backbone conformations.[31-33] (3) reduced chain entanglement compared to their linear block polymers.[34, 35] In addition, the optical properties of 1D-PCs can be further enhanced and diversified by introducing additives (namely polymers,[36] nanoparticles[37] and solvents[12]) to fulfill multifunctional performances such as responsiveness and reversibility. Therefore, it is advantageous to fabricate the responsive photonic crystals from the brush block polymer via self-assembly. In the continued development of photonics, structures and components of brush polymers will play an increasingly critical role, and it is therefore timely for designing a precisely and well-defined brush polymers in fabrication and application of photonic crystals.

Inspired by such distinctive properties of the carbohydrate molecules due to their natural abundance, good biocompatibility and renewable availability,[38-40] the combination of synthetic polymers with the carbohydrate molecules, leading to a variety of liner block copolymers, has been explored.[41-46] However, to date, little attention has been paid to the development of carbohydrate-decorated brush block copolymers (BRs). In previous studies of our group, the self-assemblies of a number of carbohydrate-based liner block copolymers that consisted of various hydrophobic synthetic polymers with oligo- or polysaccharides involving amylose, maltotriose (MT) and maltoheptaose (MH), were adequately and systematically investigated the desired nano-organized thin films and nanoparticles[43, 47-54]. With this useful information in hand, we are currently attempting to design a novel carbohydrate-decorated brush block copolymer to prepare the tunable photonic crystals. Based on the above consideration including well-studied on the assembly of linear PS-block-MH and UV cross-linking

capability of PS,[55-57] a series of bottlebrush block copolymers with polystyrene (PS) and maltoheptaose (MH) as side chains attached the backbone polynorbornene, were successfully synthesized with different molecular weight (from 823.5 KDa to 1455.0 KDa, detail information in the supporting information, BR01-04) tuned by backbone degree of polymerization in our group.

Subsequently, a simple and low-cost method to fabricate 1D-PCs from BR01-04 can be firstly carried out by different preparation techniques. Under vacuum at 60 ℃ for 24 h on the polydimethylsiloxane (PDMS) substrate, the color of the 1D-PCs prepared from BR01-04, colorless (BR01), blue (BR02), green (BR03) and orange (BR04) was clearly observed under the naked eyes, and an obvious red-shift phenomena for BR04 1D-PCs from orange, through red, to grey is easily shown to us by adding a small carbohydrate (sorbitol), finally the color covering the UV-vis. spectral range can be obtained from colorless to grey. Impressively, the color of the 1D-PCs prepared from BR01 or BR02 can be changed from blue, green, yellow, orange to pink, through the whole visible spectral range, by simply controlling preparation techniques and solvent annealing, independently or simultaneously, showing the tunability, responsiveness , and reversibility of BR01 and BR02 1D-PCs. To my best knowledge, reversible 1D-PCs throughout the whole visible spectral range from a single carbohydrate-based bottlebrush without extreme conditions, have rarely been reported so far,[58-60] opening up the light to a facile way for self-assembled responsive and tunable photonic structures from carbohydrate-based bottlebrushes.

3.2 Results and Discussion

3.2.1 Self-assembly and 1D-PCs properties of bottlebrushes (BR01-04): The maltoheptaose (MH, Mn=1250 g/mol) and polystyrene (PS, Mn=2200 g/mol, NMR, PDI=1.07) having similar MWs and narrow molecular weight distributions (NMWDs) are employed for side chains to attach the backbone composed of norbornene by using click chemistry and esterification rection respectively. Thanks to the advantageous characteristics of ruthenium-mediated ring opening metathesis polymerization, the obtained brush block copolymers (BR01-BR04) in high yields maintained the high NMWDs (PDI=1.02-1.10) at range of $8.24x10^5$-$1.46x10^6$ g/mol molecular weight. In this chapter, the near equal molar/weight ratios of MH and PS block is targeted to achieve the goal of lamellar nanostructures. (Please see Table 1 for details)

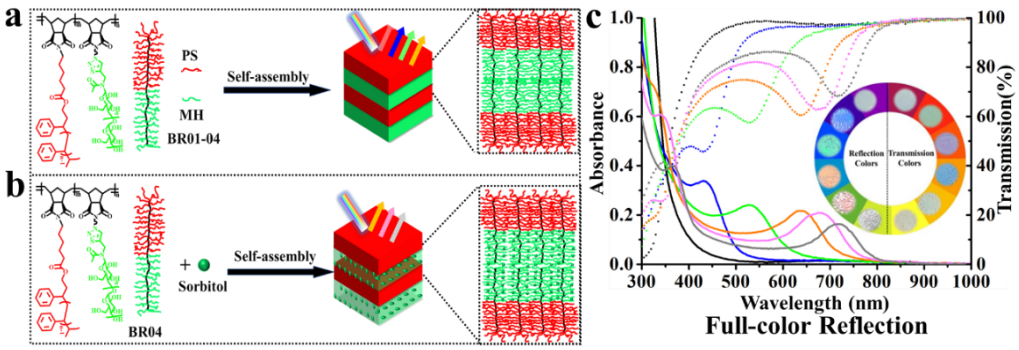

Figure 1. (a) The structure and scheme of brush block copolymers (BR01-04) attached with polystyrene (PS) and maltoheptaose (MH) as side chains and their self-assembly toward one-dimensional photonic crystals (1D-PCs). (b) Blending small carbohydrates (sorbitol) swells MH domain spacing. c) Absorbance (solid lines), transmission spectra (dash lines), and photograph of 1D-PCs obtained from a and b exhibits reflection colors on the left of the dash line and transmission colors on the right of the dash line.

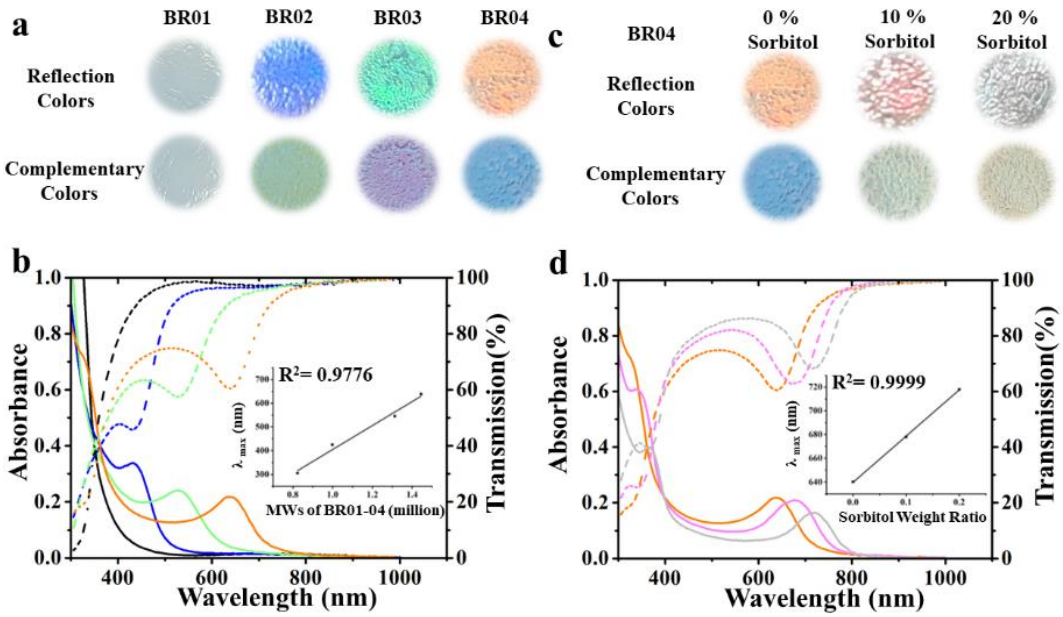

Figure 2. (a) Photographs of reflection and complementary colors for one-dimensional photonic crystals (1D-PCs) by self-assembly of BR01-04. (b) Plot of absorbance (solid lines) and transmission (dash lines) spectra as a function of wavelength for BR01-4 films with Mw=823.5 kDa (colorless), Mw=998.7 (blue), Mw=1313.0 kDa (green) and Mw=1455.0 kDa (orange). Insert image is the plot of the primary absorbance peak λ_{max} as a function of MWs of BR01-04. (c) Photographs of reflection and transmission colors for one-dimensional photonic crystals by self-assembly of BR04 with 0, 10% and 20 wt% sorbitol. (d) Plot of absorbance as a function of wavelength for BR04 1D-PCs with added sorbitol. Insert image is the plot of the primary absorbance peak λ_{max} as a function of sorbitol weight ratio.

With the hand of a series of well-defined bottlebrushes BR01-04 with a narrow/broad range of MWs, a simple self-assembly method to prepare one-dimensional photonic crystals (1D-PCs) is applied from these bottlebrushes (BR01-04, 4%, 100 μL) stock solution in DMF by drop casting on the PDMS under vacuum at 60℃ for 3h. To investigate the optical properties of the fabricated one-dimensional photonic crystals (1D-PCs), as shown in Figure 2, four examples of our polymers (BR01-04) from colorless, blue, green, to orange are presented by reflected light, which is respectively consistent with the complementary color from colorless, yellow, red to cyan when viewed with light transmitted through these four polymeric films. Sequentially, the absorbance and transmission spectrum of four colored 1D-PCs is measured by a

commercial spectrometer. For reference, the colored films are easily peeled off from the PDMS and easy to operate them by tapping the edge of films to do UV-Vis spectra. The primary absorbance peaks and pronounced transmittance dips are visible for BR01-04 at range of 308-640 nm, which shifts red and gets weaker along with the molecular weight of these bottlebrushes. The strong absorbance and striking transmittance dip at 430-640 nm originates from the photonic band gap of BR02-04.[61]As the MW of the BRs is increased, an obvious red shift from 430 nm to 640 nm can be clearly observed along with decreased absorbance intensity and transmittance dip intensity. For the red shit phenomena, it is understood that the wavelength of reflectance light is proportional to the domain space of 1D-PCs, which in turn is in regard to the MW of these BRs. Notably, the intensity of reflectance is directly related to the number of layers in the 1D-PCs. Therefore, as the thickness of the film was not strictly controlled, a variation in percent reflectance was observed.[62] When the polymer MW is increased further, unordered morphologies lacking any well-defined domains are observed in the SEM analysis (Figure 3a-d). Interestingly, a linear dependence (R^2=0.9776, Figure 2b, inserted image) between the MW and the λ_{max} of the primary absorbance peak of carbohydrate-decorated bottlebrushes shows a big difference in comparison to linear carbohydrate-based block polymers, where the domain size is theoretically proportional $MW^{2/3}$. [63] The unique behavior of carbohydrate-decorated bottlebrushes demonstrates a reduced chain entanglement to a certain degree due to the rigid architecture. Consequently, the large domain spacing of 1D-PCs ranged from 89-220 nm calculated from SEM measurements can be achieved by self-assembly of BR01-04 (Figure 3a-d).[16] Moreover, a linear relationship (R^2=0.9607) between the MW and domain spacing of BR01-4 is plotted in the Figure 3g, which in turn can be in concord with the insert image in Figure 2b. We remark here that for the sake of simplicity we give the optical response of the system in absorbance, rather than reflectance, although the visible peak of the photonic bandgap is not actually due to absorption. Absorbance however, takes into account all processes occurring in the sample due to absorption and reflection.[64] Specifically, the measured absorbance and transmittance are obviously wide because

of the surface roughness of these films at a range of 33-58 μm thickness as shown in Figure 3i-n.[65] The intensity of absorbance and transmittance is decreased with the MW of these bottlebrushes which may be ascribe to the layer thickness of lamella decreased with the MW of BR01-04 due to the increasing disorder along with the increasing MW during the self-assembly processes.[16, 62]

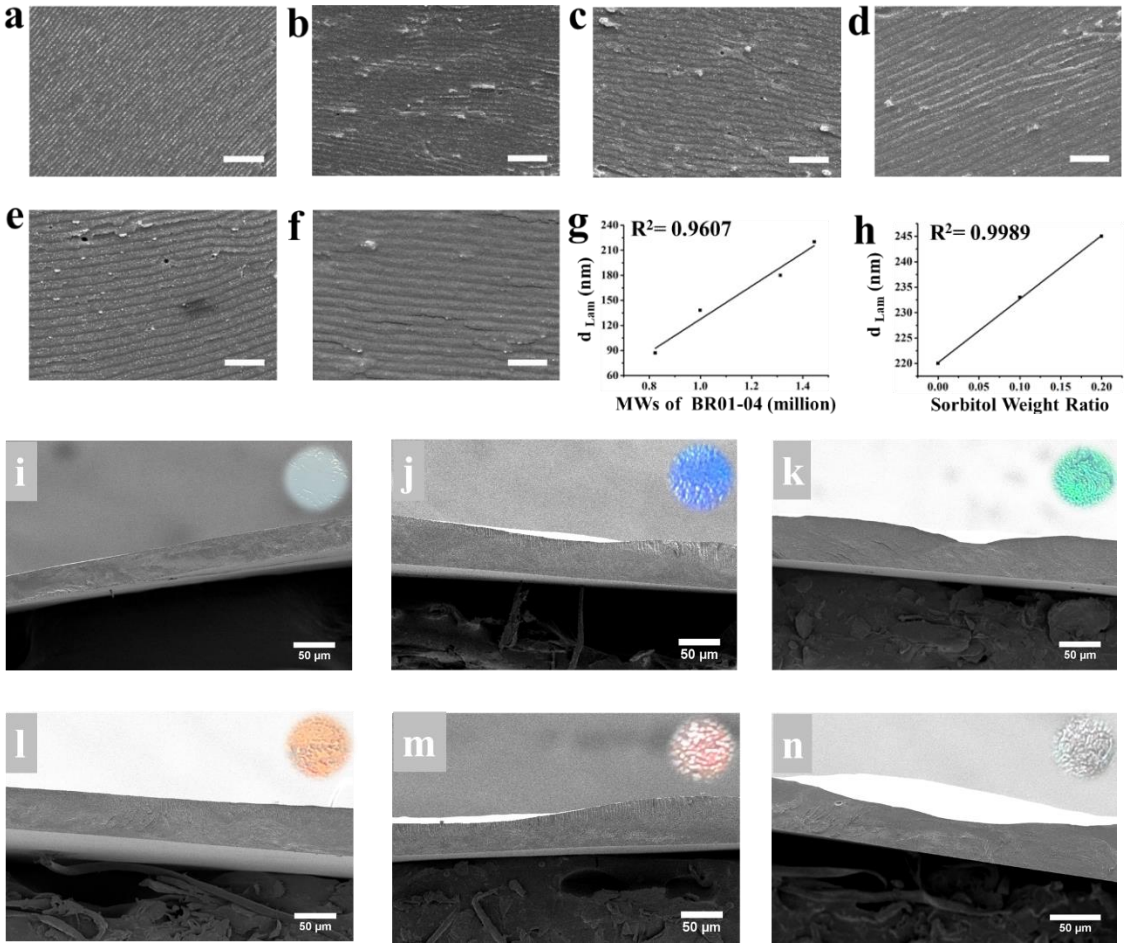

Figure 3. SEM cross section images of carbohydrate-based bottlebrushes BR01-04 with (a) Mw=823.5 kDa, (b) Mw=998.7 kDa, (c) Mw=1313.0 kDa, (d) Mw=1455.0 kDa. (e) blending 10 wt% sorbitol with BR04, and (f) blending 20% sorbitol with BR04. Scan bar is 1000 nm. (g) Plot of the BR04 domain spacings d_{Lam} (nm) as function of MWs of BR01-04. (h) Plot of the BR04 domain spacings d_{Lam} (nm) as function of sorbitol weight ratio. (i-n) SEM cross-section images of films from (a-f) are correspond to the colored films in the inserted up-right images.

Inspired by blending linear polymer additives to tune the domain sizes of 1D-PCs, we firstly try to blend some sorbitol (sugar alcohol, a type of carbohydrate) with the BR04

to manipulate its assembly.[66] As we expect, blending short commercial sorbitol with BR04 prior to casting a polymer film allows one to control the lamellar array periodicity from 220 nm to 245 nm, tune the photonic band gaps from the orange to grey. By varying the weight-percent ratio of the linear polymer analogs sorbitol from 0% to 20% at 10% intervals in the BR04 solution, two different colored films were prepared compared the film from the single BR04 solution. The λ_{max} of four photonic crystal films at the primary absorbance and transmission dip peak are increased with increasing incorporation of D-sorbitol. Impressively, a good linear relationship (R^2=0.9989) in increasing the primary absorbance peak λ_{max} as a function of increasing percentage of sorbitol can be obtained, thus achieving the 1D-PCs that reflect all wavelengths of light across the whole UV-Visible spectrum. These two blended samples can be even well-organized enough to observe second harmonic absorbance peaks,[66, 67] indicating a degree of ordering with the materials as well as the previously non-blended BR04 1D-PCs, which is consistence with SEM results that incorporating small carbohydrates (sorbitol, 20 wt%) can swell the MH domain while remains good periodicity of the BR04 stack lamellar structure with the linear relationship between periodicity and sorbitol weight ratio (Figure 3e-g). Based on the above results, the addition of short linear polymers to the carbohydrate-based bottlebrush offers a facile way of obtainnig tunable and tailorable films without synthesizing new brush polymer. In the end, the self-assembly of these BR01-04 can provide 1D-PCs nanostructured materials capable of reflecting light across UV-visible spectrum. The highly ordered 1D-PCs in this size regime have not been previously obtained via the self-assembly of linear polymer analogs.

3.2.2 Solvent responsive properties of BR01 photonic crystals

Since the color reflected from a thin film depends on the periodicity of the lamellae which can be swollen/shrunk by solvents, the color of thin films should be responsive to swelling in specific solvents. [12, 68, 69] As shown in Figure 4a, upon drop-casting a few microdrops (20 μL) of pure solvents (water, ethyl acetate, tetrahydrofuran, and

chloroform) and mixture solvents (THF/H_2O ratio increasing from 0% to 100% at 25% interval), the

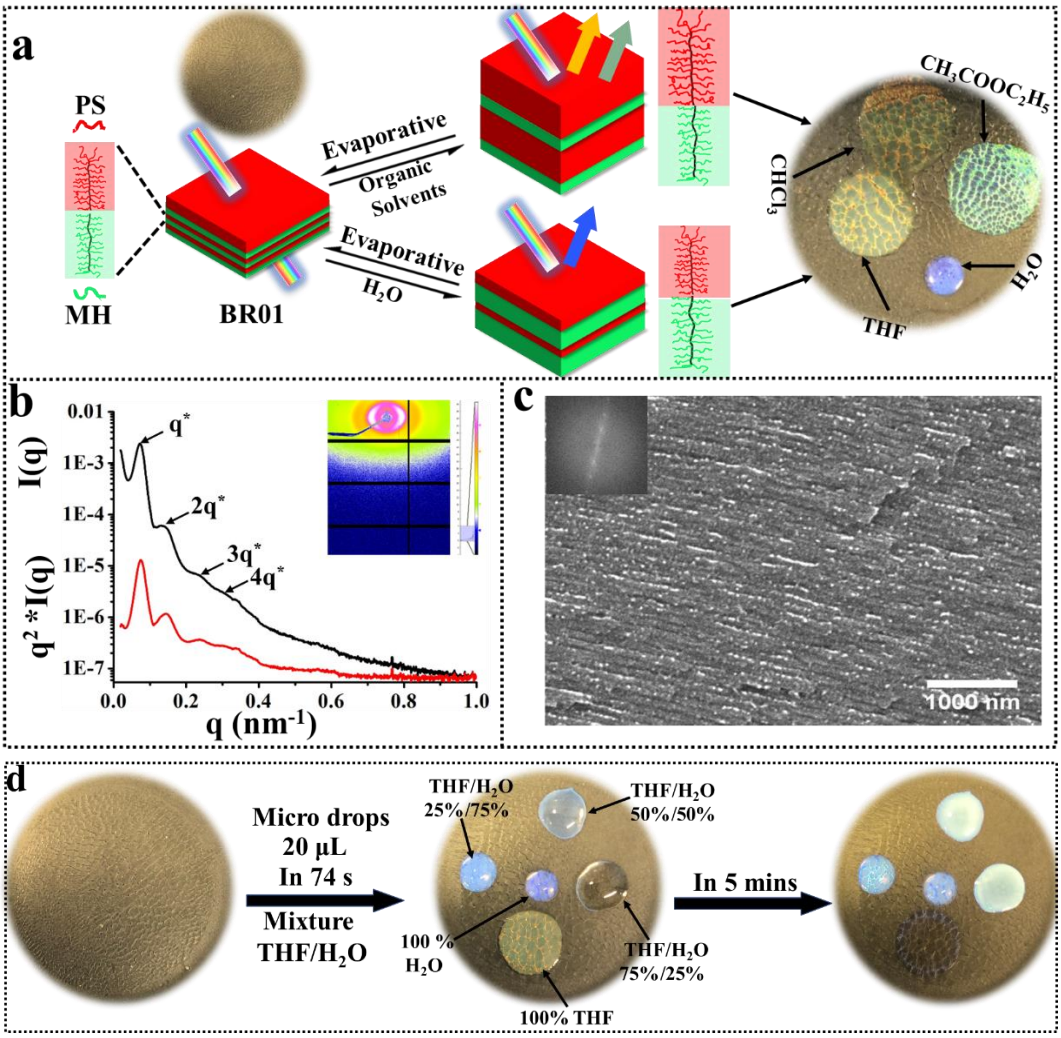

Figure 4. (a) Schematic illustrations and photographs of the BR01 film in a petridish prepared from 4 % volume concentrations in DMF (2 mL) at 60 ℃ under vacuum for 12h before and after drop-casting solvents H_2O, THF, ethyl acetate ($CH_3COOC_2H_5$) and choloroform ($CHCl_3$) at room temperature. (b) SAXS profiles for the BR01 film prepared from 4 % volume fraction in DMF (0.2 mL) in the capillary at 60 ℃ under vacuum for 12h. Inset image is the 2D SAXS pattern. (c) SEM section images of the BR01 film prepared from 4 % volume fraction in DMF (0.2 mL) on the glass slide at 60 ℃ under vacuum for 12h with its 2D Fourier power spectra (upper right inset). Scan bar is 1000 nm. (d) photographs of BR01 film prepared from (a) and before and after adding sequentialy mixture solvents (THF/H_2O ratio increasing from 0% to 100% at 25% interval) on the film for 5 mins.

colors of thin films prepared from BR01 show a dramatically red-shift from colorless to purple-blue-green-yellow-orange under naked eyes. For the BR01 bottlebrush composed of MH and PS as side chains, the upper layer on the film suface is the PS block because of its higher surface tension which is furtherly conformed by the fact that the ethyl acetate, THF and chloroform wet the surface and water droplets form on the surface (Figure 4a). The solvent swelling mechanism is qualitatively monitored by the film response time. In Movie 1, the colorless self-assembled BR01 film turns blue within 30 s on the addition of water while adding ethyl acetate, THF and chloroform can make the colorless film turn into immediately green, yellow and orange respectively,because it takes a longer time for water to penetrate the film surface into MH domains through surface defects, further diffuse through MH domain by the help of hole, grain boundaries, disclinations and disloctions[70, 71] occured in lamellar-forming photonic crystals (SEM images, Figure 5), while THF can diffuse through PS, MH damain and the interface quickly and asymetrically swell PS domain largly and MH domain slightly; ethyl acetate and chloroform mainly swell the PS due to the immiscibility between them and MH. Subsequently, a significantly blue-shift phenomena can be clearly observed after evaporation of solvents in 4 minutes (ethyl acetate, THF and chloroform), indicating that the reflected color is rapidly reversible which may be ascribe to the combination effect of the change refractive index contrast, increase/decrease in the self-assembly domain spacing and solvent quality[12, 22, 68] as the illustrated representation in Figure 4a. Notably, the asymmetry of the water-swollen lamellar structure indicates that only MH domain was prominently swollen by water due to the incompatibility between MH and PS chains. By swelling MH, PS domains or both of them with THF/H_2O mixture solvents, a bathochromic-shift is also observed from intial colorless to purple, blue, cyan, cyan and yellow along with the incrasing THF proportion at 25% interval from 0% to 100%. Specifically, the chromogenic time and spraying-out area are increased along with the increasing THF percentage at range of 25-75%, which may be acribe to the mixture solvent quality. The work mechism is not clear and further need to explore.(Figure 4d, Movie 2) Based on the obave results,

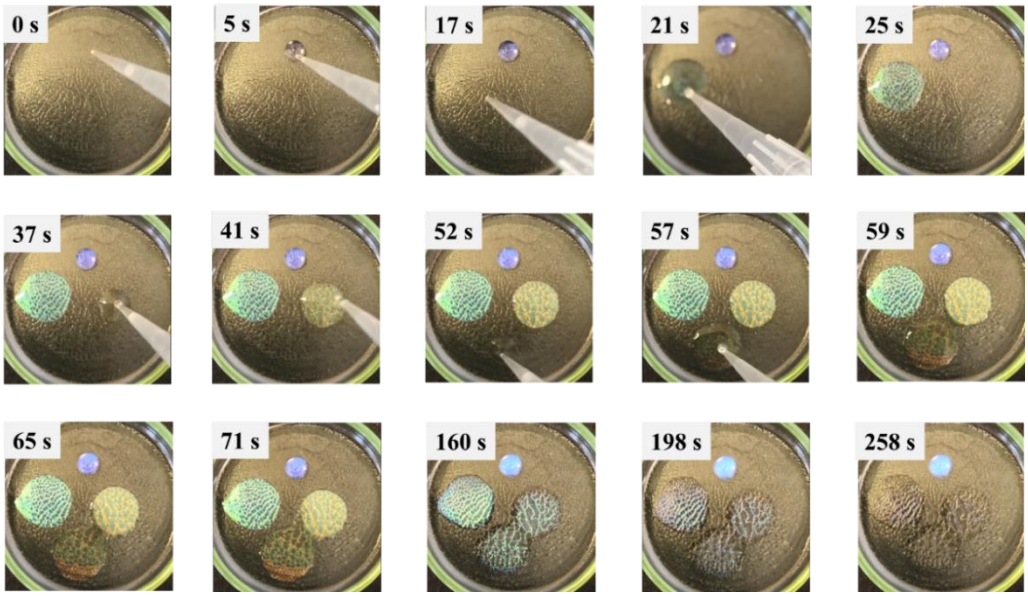

Movie1: Real-time photographes records of the BR01 film in a petridish prepared from 4 % volume concentrations in DMF (2 mL) at 60 ℃ under vacuum for 12h before and after drop-casting solvents H_2O, THF, ethyl acetate ($CH_3COOC_2H_5$) and choloroform ($CHCl_3$) at room temperature.

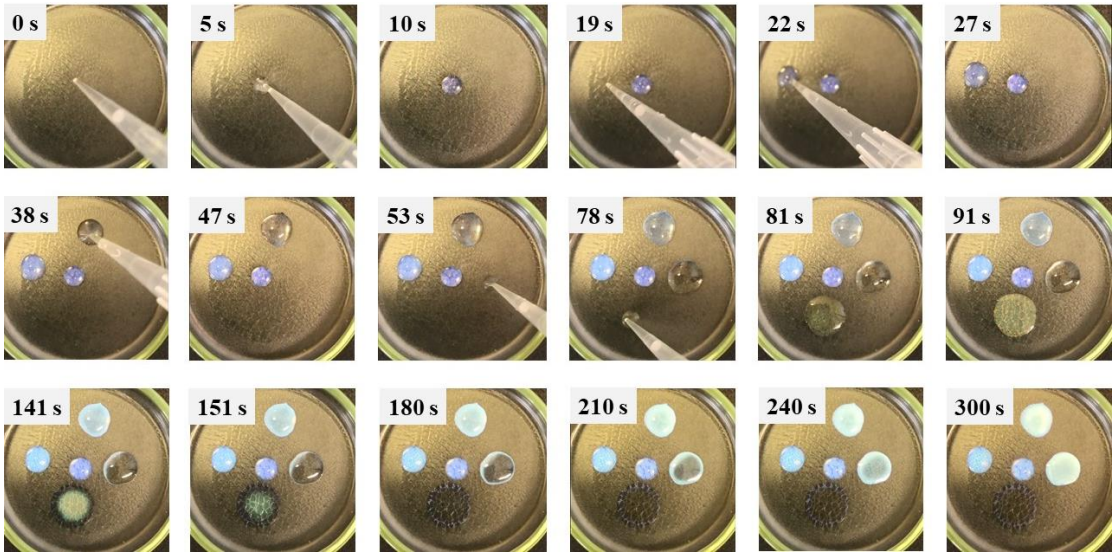

Movie2: Real-time photographes records of the BR01 film in a petridish prepared from 4 % volume concentrations in DMF (2 mL) at 60 ℃ under vacuum for 12h before and after drop-casting mixture solvents H_2O/THF with the incrasing THF proportion at 25% interval from 0% to 100% at room temperature.

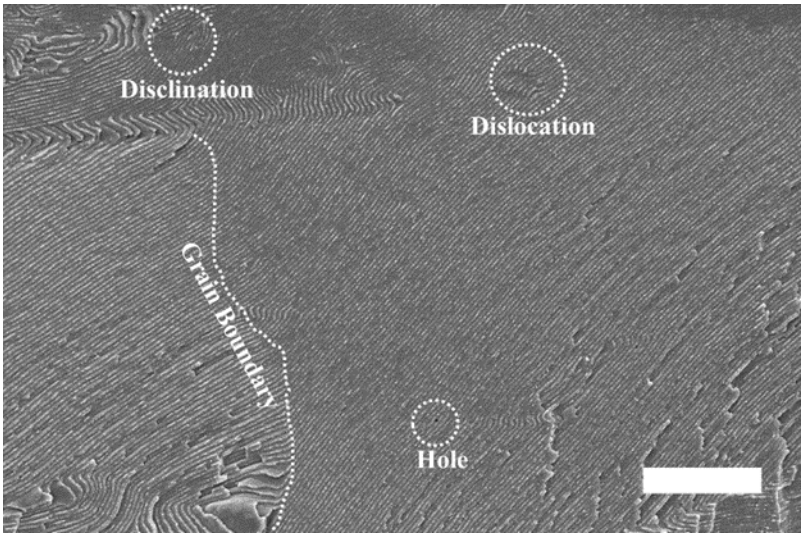

Figure 5. SEM cross sectional images of the BR01 film prepared from 4 % volume fraction in DMF (0.2 mL) on the glass slide at 60 ℃ under vacuum for 12h. Scan bar is 3000 nm.

the films fabricated from BR01 are rapidly responsive and reversible to slective solvents accompanied with structural coloration, showing a potential application as chemical sensors or color displays.

To investigate the hierarchical structure of BR01 films, small-angle X-ray scattering (SAXS) was used to identify the lattice types and spacings of the BR01 films, complemented by scanning electronic microscope (SEM). According to the SAXS profile (Figure 4b), the corresponding BR01 film shows strong scattering peaks at relative peak position ratios of 1: 2: 3: 4, which correspond to a pattern for a microphase separated lamellar structure. From the first order peak position ($q^* = 0.07464$ nm^{-1}, where q is the scattering wave vector), the long period spacing of the lamellar structure is found to be equal to 84 nm, which is consistance with SEM results that the well-organized lamellar morphology with similar domain space 89 nm is confirmed with its 2D Fourier Power spectra (Figure 4c, upper left insert). In the Figure 4b presented here, SAXS intensities for BR01 exhibiting the lamellar phase are multiplied through by q^2, as a first-order correction for the impact of the form factor of lamellae on the observed scattering intensity I(q). Thus, the peak positions in $q^2*I(q)$ correspond more closely and clearly to the peaks in the lattice's structure factor, from which the interdomain spacing d is extracted.[72] 2D SAXS presents several pairs of diffraction arc orientated

lamellae originating from the layer structure indicating well orientated lamellae (Figure 4b, inserted image).

3.2.3 Self-Assembly of BR02 into 1D-PCs and its solvent responsive properties

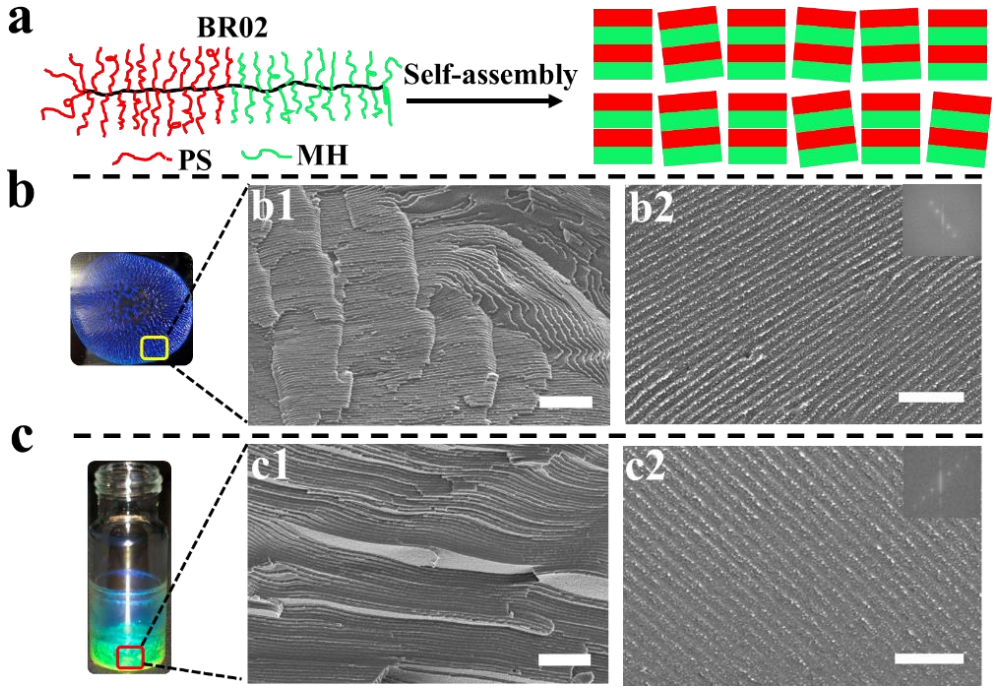

Figure 6. (a) A schematic illustration of the brush block copolymer (BR02) architecture with PS and MH as pendants attached to a polynorbornene backbone and its self-assembly to one-dimensional photonic crystals. (b) Cross-sectional SEM micrographs showed well-aligned (anisotropic) structures with their 2D Fourier power spectra (Upper right inset) and control over the self-assembled nanostructures and optical appearances at normal incident light by vacuum drying BR02 solution (4%, 1 mL in DMF) in a watch glass (Diameter: 4.5 cm) at 60 °C for 2 h; (C) in a vial (4 mL) at 60 °C for 24 h. Scan bar is 3000 nm (b1 and c1) and 1000 nm (b2 and c2) respectively from left to right.

As shown in Figure 6, a simply self-assembly method to one-dimensional photonic crystals (1D-PCs) is carried out by controlling evaporation from dimethylformamide (DMF) solution at 60 °C for 24 h in a vial or on a watch glass. The drastic difference in color is most starkly visualized by a single brush BR02 (Mn = 998.7 kg/mol) depending on different substrates, which appears blue on a watch glass while green color at the bottom of the vial are observed when vacuum drying in a vial (Figure 6b and 6c). These

results bring forth to the question why the same preparation method provided the markedly altered reflection colors. Scanning electron micrograph (SEM) provides insight into the self-assembly of 1D-PCs in a vial and watch glass, clearly visualizing domain spaces and morphologies of BR02 1D-PCs. As shown in Figure 6b and 6c, both of them shows the expected stacked lamellar morphology in which well-ordered lamellar structures can be clearly identified with a different domain spacings. The domain spacing from the blue color on the watch glass is calculated to around 140 nm comparison to 178 nm roughly domain spacing from the green color at bottom of the vial. Based on the above the results, we hypothesize that the slower evaporation rate of the solvent in the vial maybe facilitate the self-assembled 1D-PCs which in turn provide a solvent annealing atmosphere during the slower self-assembled process in a vial.[73] However, the distribution of the lamellae orientation is not perfectly uniform throughout the depth of 1D-PCs, and different orientations of the layered structure can be identified in the center part of the 1D-PCs which is due to reduced interfacial effects, while highly aligned layered structure is observed parallel to the 1D-PCs surface near the top surface of the 1D-PCs, indicating that the system achieves a thermodynamically preferred orientation parallel to the 1D-PCs surface.[74] (Figure 7)

To obtain thin 1D-PCs of uniform thickness, thin the polymer (BR02, 4%, 1mL) is prepared through controlled evaporation from DMF at room temperature under vacuum with a cold trap device for 9 h. Expectedly, the uniformly bright blue and green color can be clearly observed under naked eyes in comparison with Figure 8b and 8c. Upon the change of incident light angle (Figure 8b and 8c), less angular dependent optical appearance of 1D-PCs can be observed compared to that in Figure 9 in which blue and purple color can be clearly observed under different light incident angle due to the parallel stacked lamellar architecture in the fiber-like colored area. To investigate the internal structure of the obtained 1D-PCs, SEM measurements are performed on the 1D-PCs section. Figure 8b and 8c show the isotropic lamellar morphology in which less aligned layers are present and the orientation distribution of the lamellae is random thought out the section. Consequently, the predominant color is similar from every

observe direction in which the incident light can be possibility perpendicular to the lamellar structure. Impressively, the color of BR02 thin 1D-PCs is also responsive to swelling in specific solvents. As shown in Figure 8d, upon annealing in THF for 2h, mixture solvent (THF/H_2O, 1:1) for 12 h, and water for 12 h, the colors of thin 1D-PCs prepared from BR02 show a dramatically red-shift. Among them, a good mixture solvent (THF/H_2O, 1/1) for both PS and MH domains resulted in a dramatic increase in the domain spacing, and consequently, a distinct red-shift of the reflective light to pink from an original green. For selective solvent annealing such as tetrahydrofuran and

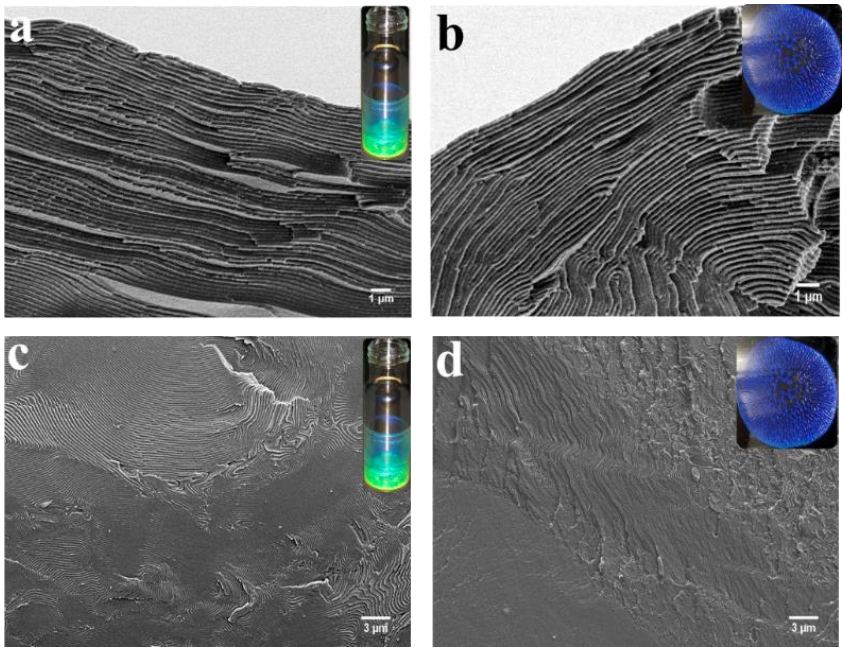

Figure 7 Cross-sectional SEM micrographs of BR02 1D-PCs in different positions: (a, b) near top surface part (c, d) center part. Different orientations of the layered structure can be identified in the center part of the film, while highly aligned layered structure was observed parallel to the film surface near the top surface of the film. (a, b) Scan bar is 1 μm. (c, d) Scan bar is 3 μm.

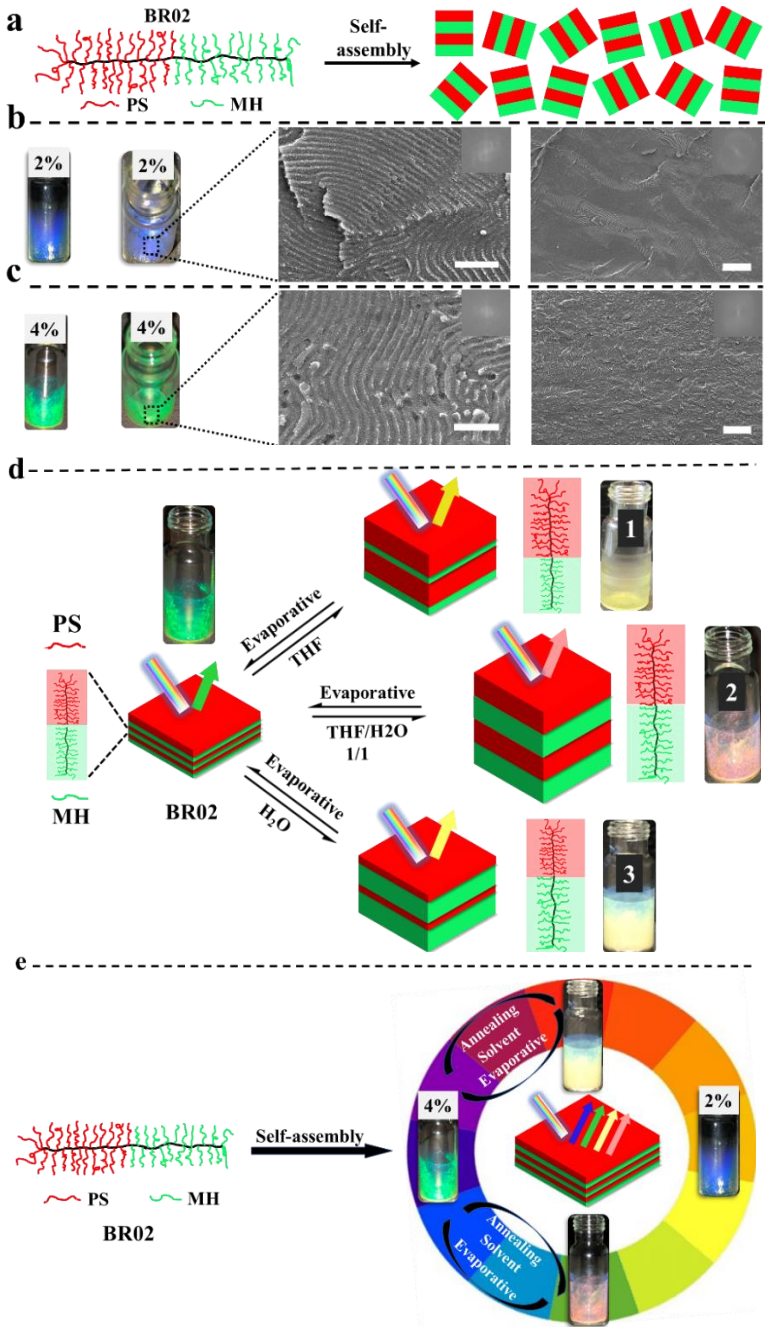

Figure 8. (a) A schematic illustration of the brush block copolymer (BR02) architecture with PS and MH as pendants attached to a polynorbornene backbone and its self-assembly to one-dimensional photonic crystals (1D-PCs). (b, c) Photograph of BR02 1D-PCs (2% and 4% in DMF) with the change of incident light angle from left to right, through evaporation from DMF under vacuum with a cold trap device for 9 h at room temperature. Cross-sectional SEM micrographs of BR02 1D-PCs (2% and 4% in DMF) showed the isotropic lamellar morphology with their 2D Fourier power spectra (upper left inset). Scan bar is 1000 nm and 5000 nm respectively from left to right. (d) Photographs of thin BR02 1D-PCs prepared from 4% BR02 in DMF at room temperature under vacuum with a cold trap device for 9h before and after selective solvents annealing (1) THF, 2h (2) (THF/H_2O,1/1), 12h (2) H_2O for 12 h at room temperature, then vacuum at room temperature for 48h. (e) The schematic illustration of the carbohydrate-based brush block copolymer (BR02) architecture with PS and MH side chains and its self-assembly to one-dimensional photonic crystals (1D-PCs) reflecting blue, green, yellow and pink colors.

water, the domain spacing and refractive index contrast of PS or MH domain are asymmetrically changed, resulting in a light yellow and bright yellow respectively. It is understood that, as for the selcctive THF, the THF difusion in both PS and MH domains can reduce the refractive index contrast and the effective refractive indices of two domains are simultaneously decreased. In comparison, as for water swelling film, the reflective intensity is increased due to an incrase in the refractive index contrast between the polymers domains. As for mixtue solvent (THF/H_2O, 1;1), an increase in both PS and MH domains plays an significant role while the influcence of refractive index contrast between the two domains could be ignored.[12] In total, the red-shifted reflective color should ascribe to increase independently and synergistically the corresponding domain spacing by selective solvents due to the large chemical incompatibility between PS and MH domains with a high-χ value 0.59.[75] (Figure 8d). Subsequently, upon vacuum at room temperature– for 48 h, a significantly blue-shift phenomena can be clearly observed after evaporation of solvents, suggesting that the structural coloration on swelling with solvents leading to changes in the reflected wavelength and intensity are found to be reversible on the evaporation of solvents, enabling cyclic swelling and deswelling of the nanostructure.[76, 77] Furthermore, in accordance with the Bragg equation for one-dimensional photonic crystals (1D-PCs),[78] the spectral position of the fundamental Bragg peaks can be tuned by manipulating the geometric or optical thicknesses of the layers constituting the 1D photonic lattice. The thicknesses of the layers can be controlled by manipulating the concentration of the polymer solution. As shown in Figure 8b and 8c, upon increasing volume concentration from 2 % to 4 %, the colors of BR02 1D-PCs display the red shift phenomena from blue (2 %) to green (4 %), which is consistence with domain spacings obtained from the SEM results (average domain spacing 137 nm for blue, Figure 8b; average domain spacing 174 nm for green, Figure 8c). It may be interpretated that, as the polymer concentration increase, the system is more kinetically arrested due to the reduced polymer chain mobility before the system achieving a thermodynamically preferred orientation parallel to the 1D-PCs surface, thus the orientation of the stacked lamellar

structure is more random. However, the slower evaporation rate of the solvent in the higher concentration (4%) may facilitate the self-assembled 1D-PCs in shorter range with larger domain spacing in comparison with that in the lower concentration (2%). Finally, the reflective color can be easily switchable across the entire visible spectrum by the various polymer concentrations and selective solvent swelling/deswelling on the domain spaces of 1D-PCs as illustrated presentation in Figure 8e. To our best knowledge, there are little to no articles about carbohydrate-based brush block copolymers toward the self-assembly of 1D-PCs capable of reversibility and turnability reflecting the entire visible spectrum only from a single carbohydrate-based brush block copolymer.

Meanwhile, in order to determine whether blending with sorbitol also work on BR02 bottlebrushes on the glass substrate, adding 20 wt % percent sorbitol into 4% BR02 DMF solution is performed and suquential evaporation from DMF under vacuum for 2h at 60 ℃ by dropping casting on the glass slide (1.5 cm x1.5 cm). As shown in Figure 10, there is a similar red-shift trendency happened to BR02, that is, blending sorbitol with BR02 prior to casting a polymer film allows one to control the domain spacing of parallel stacked lamellar structure in the colored fiber-like area from 140 nm to 173 nm, tune the structure color from the blue to green due to the increasing interspacing between PS and MH domains compared to the non-blended one. Microscopy photographs show the yellow and red color complementary with reflection color blue and green, respectively. Moreover, SEM images with their corresponding 2D Fourier power spectra (upper left inset) confirm that this blended sample also show highly ordered lamellar architecture as well as the the previously non-blended BR02 in the colored fiber-like area on the glass. To investigate the concentration effect of BR02 (12%, 0.3 mL in DMF) by drop-casting on the glass for 2h at 60 ℃ under vaccum, it is found that the thicker film is able to reflect the brigther blue with less angular independence compared to Figure 9a due to the random orientation of lamellar struture absorved in the cross-section of this flim with average domain space 135 nm (Figure 9d). Furtherly, by manipulating the high MW of BR04 solution (4%, 0.3 mL in DMF)

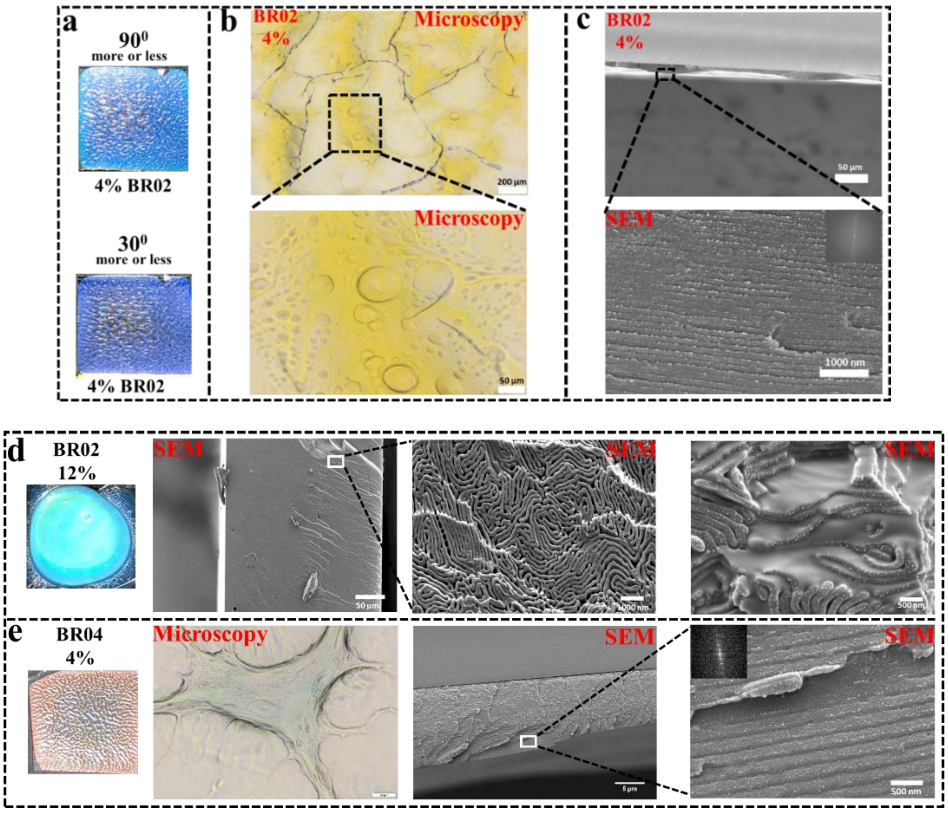

Figure 9. (a) Photograph for BR02 1D-PCs (0.3 mL, 4% volume fraction in DMF) reflected blue to purple with the change of incident light angle from up and down, through evaporation from DMF under vacuum for 2h at 60 ℃ by dropping casting on the glass slide (1.5 cm x 1.5cm). (b) Microscopies for BR02 1D-PCs obtained from (a) showing the yellow color complementary with reflection color blue. Scan bar is 200 µm and 50 µm respectively from up and down. (c) Cross-sectional SEM images of BR02 1D-PCs obtained from (a) showed the parallel stacked lamellar morphology with their 2D Fourier power spectra (upper left inset). Scan bar is 100 µm and 1000 nm respectively from up and down. (d) Photographes and SEM images for BR02 1D-PCs (0.3 mL, 12% volume fraction in DMF) from left and right, through evaporation from DMF under vacuum for 2h at 60 ℃ by dropping casting on the glass slide (1.5 cm x 1.5cm). (e) Photographes, Microscopies and SEM images for BR04 1D-PCs (0.3 mL, 4% volume fraction in DMF) from left and right, through evaporation from DMF under vacuum for 2h at 60 ℃ by dropping casting on the glass slide (1.5 cm x 1.5cm). (d) Scan bar is 50 µm, 1000 nm and 500 nm respectively from left and right. (e) Scan bar is 50 µm, 5 µm nm and 500 nm respectively from left and right.

in the same way, red-orange color can be observed in the colered fiber-like area on the glass (Figure 9e), which is consistence with the complementary blue-green color in the microscopy photograph. The SEM cross-section of colored fibre-like region shows the stacked parallel lamellar structure with average domain space 210 nm. In a word, the structure color properties of films prepared form the BRs system can indeed be influenced by their concentration, MW and additives.

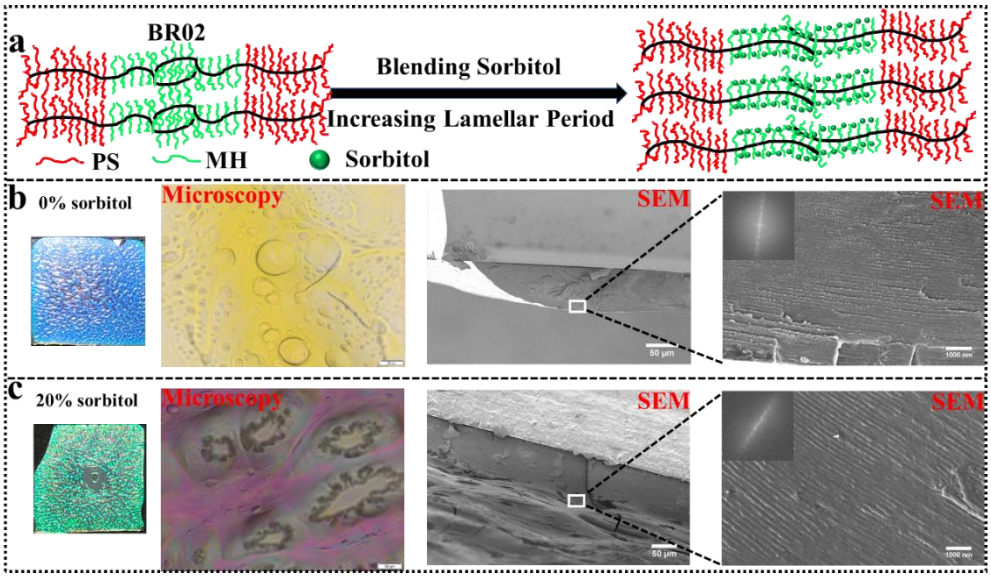

Figure 10. (a) Schematic illustraion for BR02 1D-PCs (0.3 mL, 4% volume fraction in DMF) reflecting color from blue to green before and after blending with 20 wt% sorbitol. (b) Photographes, Microscopies and SEM with their 2D Fourier power spectra (upper left inset) for BR02 1D-PCs from left and right, through evaporation from DMF under vacuum for 2h at 60 ℃ by dropping casting on the glass slide (1.5 cm x 1.5cm). (c) Photographes, Microscopies and SEM with their 2D Fourier power spectra (upper left inset) for BR02 1D-PCs blended with 20 wt% sorbitol from left and right, through evaporation from DMF under vacuum for 2h at 60 ℃ by dropping casting on the glass slide (1.5 cm x 1.5cm). (b,c) Scan bar is 50 μm, 50 μm and 1000 nm respectively from left and right.

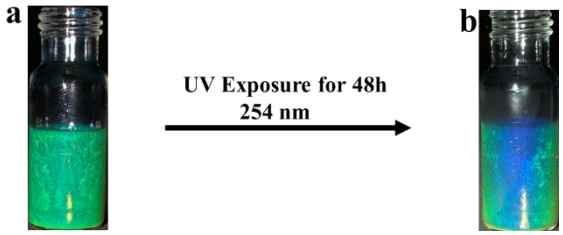

Figure 11. (a) Photographes for BR02 1D-PCs (1.0 mL, 4% volume fraction in DMF), through evaporation from DMF under vacuum for 7h at room temperature with a cold trap, before and after UV light (254 nm) exposure for 48h.

Table 1. Characteristics of bottle-brush block copolymers

Sample	NbBBBr/NbPS/I Feed ratio	Molar mass of NbPS (^{1}H NMR) [g/mol]	Experimental $f^{PNbBBBr}/f^{PNbPS}$ [mol/mol][a)]	Experimental $f^{PNbBBMH}/f^{PNbPS}$ [mol/mol][b)]	Molar mass of PNbBBMH-b-PnPS [Kg/mol][c)]	Đ	Experimental $f^{PNbBBMH}/f^{PNbPS}$ [v/v][d)]
BR01	100/100/1	2200	0.55/0.45	0.53/0.47	823.5	1.10	0.39/0.61
BR02	150/150/1	2200	0.51/0.49	0.54/0.46	998.7	1.07	0.39/0.61
BR03	200/200/1	2200	0.50/0.50	0.52/0.48	1313.0	1.02	0.38/0.62
BR04	300/300/1	2200	0.50/0.50	0.52/0.48	1455.0	1.02	0.38/0.62

[a)] Molar composition of PNbBBBr-b-PNbPS block copolymers was determined by the relative integration of the peaks positioned at 4.03 ppm due to –CH_2COO– of the PNbBBBr and 5.30-5.90 ppm dedicated to –*CH=CH*– of polynorbornene backbone;

[b)] The molar composition of the PNbBBMH-b-PNbPS copolymer was determined by the relative integration of the signals located at 5.16 ppm due to C1 protons of maltoheptaose and 6.30-7.35 ppm phenyl ring of polystyrene;

[c)] The molar mass of PNbBBMH-b-PNbPS was determined by SEC using light scattering putting dn/dc values for copolymers as 0.113 mL/g; [d)] The volume fraction of PNbBBMH-b-PNbPS was determined using polymer densities values of 1.05 and 1.36 for PS and MH respectively.

As aforementioned UV cross-linking capability of PS, we also firstly try to alter the structure color of BR02 1D-PCs upon exposure to UV light (6 w, 50-60Hz). As shown in Figure 11, a blue-shift color from green to blue can be clearly observed pendicular to the colored vial under UV light (254 nm) for 48h, suggesting that BR02 1D-PCs are also responsive to UV light. Based on the above results, multi-responsiveness such as solvents and UV light and flexible tairobility by additives can promote their practical use as a toolbox.

3.3 Experimental Section

UV Equipment: UV spectra were recorded on a Cary 50 Bio UV/vis spectrophotometer (Varian) from 200 to 1000 nm.

Scanning Electron Microscope (SEM): Samples were fractured, pasted on metallic stub with double sided carbon tape and sputter-coated with Au/Pd. Secondary electron images were recorded with an FEI Quanta 250 scanning electron microscope equipped with a field emission gun and operating at 2.5 kV.

Small-angle X-ray Scattering (SAXS): SAXS measurements were performed using the CRG-BM02 beamline at the European Synchrotron Radiation Facility. A silver behenate sample was used for calibrating the q scale. Bulk samples were prepared by filling the BR01 4% 200 uL into glass capillaries with 1.5mm in diameter and then put into a oven at 60 ℃ for 12 h under vacuum, finally transferred into sample holder for SAXS experiments. The SAXS experiments were performed using 15keV X-rays and scattering intensities were recorded on a charge-coupled device detector placed about 780mm behind the sample after 10 s exposures. All these data were collected at ambient pressure. The scattering intensities were corrected for grid distortion, the detector response, dark current, and sample transmission.

3.4 Conclusion

In conclusion, a series of well-defined carbohydrate-based bottlebrushes BR01-04 (PDI=1.02-1.10) was successfully synthesized at range of $0.82x10^6$-$1.3x10^6$ g/mol molecular weight. The self-assembly of these bottlebrushes into one-dimensional photonic crystals are capable of reflecting light through the whole UV-Vis spectra with

domain spacing ranged from 89-245 nm (SEM results). The well-organized nanostructures in the size regime have not been previously reported from the carbohydrate-based linear block polymers. Impressively, a robust and effective way to prepare 1D-PCs, capable of full-color reflection, is developed by a single carbohydrate-based brush block copolymer (BR01 or BR02) self-assembly. Compared to the BR02 molecular brush, the lower molecular weight improve the side chain mobilty of BR01.Consequently, the BR01 1D-PCs exhibits the rapidly responsive and reversible strutural coloration exposed to the solvents stimuli in seconds. By using the different preparation method of BR02 1D-PCs, the expected stacking lamellae of SEM images are clearly observed with the anisotropic and isotropic orientation in which the optical appearance is the angular-dependent and near-perfect angular independent respectively. Simple tuning the concentration of BR02 solution in DMF from vacuuming drying at room temperature with a cold trap afforded the formation of blue (2%) and green colors (4%), and the reflective green color is readily tunable across the entire visible spectrum by the combination effect of solvent swelling domains of lamellar morphology and the changes of refractive index contrast between the two blocks (PS and MH), providing the promising potential applications as color displays, chemical sensors or indicators.

References:

1. Yoshioka, S.; Matsuhana, B.; Tanaka, S.; Inouye, Y.; Oshima, N.; Kinoshita, S., Mechanism of variable structural colour in the neon tetra: quantitative evaluation of the Venetian blind model. *J R Soc Interface* **2011,** *8* (54), 56.
2. Liu, F.; Dong, B. Q.; Liu, X. H.; Zheng, Y. M.; Zi, J., Structural color change in longhorn beetles Tmesisternus isabellae. *Opt Express* **2009,** *17* (18), 16183.
3. Vukusic, P.; Sambles, J. R.; Lawrence, C. R.; Wootton, R. J., Structural colour. Now you see it-now you don't. *Nature* **2001,** *410* (6824), 36.
4. Zi, J.; Yu, X.; Li, Y.; Hu, X.; Xu, C.; Wang, X.; Liu, X.; Fu, R., Coloration strategies in peacock feathers. *Proc Natl Acad Sci U S A* **2003,** *100* (22), 12576.
5. Kinoshita, S.; Yoshioka, S., Structural colors in nature: the role of regularity and irregularity in the structure. *Chemphyschem* **2005,** *6* (8), 1442.
6. Ge, J.; Yin, Y., Responsive photonic crystals. *Angew Chem Int Ed Engl* **2011,** *50* (7), 1492.
7. Lv, J.; Ding, D.; Yang, X.; Hou, K.; Miao, X.; Wang, D.; Kou, B.; Huang, L.; Tang, Z., Biomimetic chiral photonic crystals. *Angew Chem Int Ed Engl* **2019,** *58* (23), 7783.
8. Li, W.; Wang, Y.; Li, M.; Garbarini, L. P.; Omenetto, F. G., Inkjet printing of patterned, multispectral, and biocompatible photonic crystals. *Adv Mater* **2019,** *31* (36), 1901036.
9. Cersonsky, R. K.; Antonaglia, J.; Dice, B. D.; Glotzer, S. C., The diversity of three-dimensional photonic crystals. *Nat Commun* **2021,** *12* (1), 2543.
10. Aguirre, C. I.; Reguera, E.; Stein, A., Tunable colors in opals and inverse opal photonic crystals. *Adv Funct Mater* **2010,** *20* (16), 2565.
11. Galisteo-Lopez, J. F.; Ibisate, M.; Sapienza, R.; Froufe-Perez, L. S.; Blanco, A.; Lopez, C., Self-assembled photonic structures. *Adv Mater* **2011,** *23* (1), 30.
12. Xu, Y.; Hickey, R. J., Solvent-responsive and reversible structural coloration in nanostructured block polymer films. *Macromolecules* **2020,** *53* (14), 5711.
13. Stuart-Fox, D.; Moussalli, A., Camouflage, communication and thermoregulation: lessons from colour changing organisms. *Philos Trans R Soc Lond B Biol Sci* **2009,** *364* (1516), 463.
14. Yue, Y.; Gong, J. P., Tunable one-dimensional photonic crystals from soft materials. *J Photochem Photobiol CPhotochem Rev* **2015,** *23*, 45.
15. Sweeney, A.; Jiggins, C.; Johnsen, S., Insect communication: polarized light as a butterfly mating signal. *Nature* **2003,** *423* (6935), 31.
16. Piunova, V. A.; Miyake, G. M.; Daeffler, C. S.; Weitekamp, R. A.; Grubbs, R. H., Highly ordered dielectric mirrors via the self-assembly of dendronized block copolymers. *J Am Chem Soc* **2013,** *135* (41), 15609.
17. Xu, D.; Yu, H.; Xu, Q.; Xu, G.; Wang, K., Thermoresponsive photonic crystal: synergistic effect of poly(N-isopropylacrylamide)-co-acrylic acid and morpho butterfly wing. *ACS Appl Mater Interfaces* **2015,** *7* (16), 8750.
18. von Freymann, G.; Kitaev, V.; Lotsch, B. V.; Ozin, G. A., Bottom-up assembly of photonic crystals. *Chem Soc Rev* **2013,** *42* (7), 2528.

19. Liberman-Martin, A. L.; Chu, C. K.; Grubbs, R. H., Application of bottlebrush block copolymers as photonic crystals. *Macromol Rapid Commun* **2017,** *38* (13), 1700058.
20. Gao, Y.; Zhou, Y.; Xu, X.; Chen, C.; Xiong, B.; Zhu, J., Fabrication of oriented colloidal crystals from capillary assembly of polymer-tethered gold nanoparticles. *Small* **2022,** *18* (13), 2106880.
21. Bo, A.; Liu, Y.; Kuttich, B.; Kraus, T.; Widmer-Cooper, A.; de Jonge, N., Nanoscale faceting and ligand shell structure dominate the self-assembly of nonpolar nanoparticles into superlattices. *Adv Mater* **2022,** *34* (20), 2109093.
22. Song, D. P.; Jacucci, G.; Dundar, F.; Naik, A.; Fei, H. F.; Vignolini, S.; Watkins, J. J., Photonic resins: designing optical appearance via block copolymer self-assembly. *Macromolecules* **2018,** *51* (6), 2395.
23. Wang, Z.; Chan, C. L. C.; Zhao, T. H.; Parker, R. M.; Vignolini, S., Recent advances in block copolymer self-assembly for the fabrication of photonic films and pigments. *Adv Opt Mater* **2021,** *9* (21), 2100519.
24. Guo, T.; Yu, X.; Zhao, Y.; Yuan, X.; Li, J.; Ren, L., Structure memory photonic crystals prepared by hierarchical self-assembly of semicrystalline bottlebrush block copolymers. *Macromolecules* **2020,** *53* (9), 3602.
25. Zhang, T.; Yang, J.; Yu, X.; Li, Y.; Yuan, X.; Zhao, Y.; Lyu, D.; Men, Y.; Zhang, K.; Ren, L., Handwritable one-dimensional photonic crystals prepared from dendronized brush block copolymers. *Polym Chem* **2019,** *10* (12), 1519.
26. Yu, Y. G.; Seo, C.; Chae, C. G.; Seo, H. B.; Kim, M. J.; Kang, Y.; Lee, J. S., Hydrogen bonding-mediated phase transition of polystyrene and polyhydroxystyrene bottlebrush block copolymers with polyethylene glycol. *Macromolecules* **2019,** *52* (11), 4349.
27. Yu, Y. G.; Chae, C. G.; Kim, M. J.; Seo, H. B.; Grubbs, R. H.; Lee, J. S., Precise synthesis of bottlebrush block copolymers from ω-end-norbornyl polystyrene and poly(4-tert-butoxystyrene) via living anionic polymerization and ring-opening metathesis polymerization. *Macromolecules* **2018,** *51* (2), 447.
28. Xia, Y.; Olsen, B. D.; Kornfield, J. A.; Grubbs, R. H., Efficient synthesis of narrowly dispersed brush copolymers and study of their assemblies: the importance of side chain arrangement. *J Am Chem Soc* **2009,** *131* (51), 18525.
29. Hadjichristidis, N.; Pitsikalis, M.; Pispas, S.; Iatrou, H., Polymers with complex architecture by living anionic polymerization. *Chem Rev* **2001,** *101* (12), 3747.
30. Zhang, M.; Müller, A. H. E., Cylindrical polymer brushes. *J Polym Sci Part A Polym Chem* **2005,** *43* (16), 3461.
31. Wintermantel, M.; Gerle, M.; Fischer, K.; Schmidt, M.; Wataoka, I.; Urakawa, H.; Kajiwara, K.; Tsukahara, Y., Molecular bottlebrushes. *Macromolecules* **1996,** *29* (3), 978.
32. Sheiko, S. S.; Moller, M., Visualization of macromolecules-a first step to manipulation and controlled response. *Chem Rev* **2001,** *101* (12), 4099.
33. Henn, D. M.; Fu, W.; Mei, S.; Li, C. Y.; Zhao, B., Temperature-induced shape changing of thermosensitive binary heterografted linear molecular brushes

between extended wormlike and stable globular conformations. *Macromolecules* **2017,** *50* (4), 1645.
34. Sveinbjornsson, B. R.; Weitekamp, R. A.; Miyake, G. M.; Xia, Y.; Atwater, H. A.; Grubbs, R. H., Rapid self-assembly of brush block copolymers to photonic crystals. *Proc Natl Acad Sci U S A* **2012,** *109* (36), 14332.
35. Liang, H.; Grest, G. S.; Dobrynin, A. V., Brush-like polymers and entanglements: from linear chains to filaments. *ACS Macro Lett* **2019,** *8* (10), 1328.
36. Miyake, G. M.; Piunova, V. A.; Weitekamp, R. A.; Grubbs, R. H., Precisely tunable photonic crystals from rapidly self-assembling brush block copolymer blends. *Angew Chem Int Ed Engl* **2012,** *51* (45), 11246.
37. Song, D. P.; Li, C.; Colella, N. S.; Lu, X.; Lee, J. H.; Watkins, J. J., Thermally tunable metallodielectric photonic crystals from the self-assembly of brush block copolymers and gold Nanoparticles. *Adv Opt Mater* **2015,** *3* (9), 1169.
38. Morris, J.; Bietsch, J.; Bashaw, K.; Wang, G., Recently developed carbohydrate based gelators and their applications. *Gels* **2021,** *7* (1), 24.
39. Solanki, A.; Das, M.; Thakore, S., A review on carbohydrate embedded polyurethanes: an emerging area in the scope of biomedical applications. *Carbohydr Polym* **2018,** *181*, 1003.
40. Vankar, Y. D.; Schmidt, R. R., Chemistry of glycosphingolipids-carbohydrate molecules of biological significance. *Chem Soc Rev* **2000,** *29* (3), 201.
41. Hung, C. C.; Nakahira, S.; Chiu, Y. C.; Isono, T.; Wu, H. C.; Watanabe, K.; Chiang, Y. C.; Takashima, S.; Borsali, R.; Tung, S. H.; Satoh, T.; Chen, W. C., Control over molecular architectures of carbohydrate-based block copolymers for stretchable electrical memory devices. *Macromolecules* **2018,** *51* (13), 4966.
42. Kumar, S.; Maiti, B.; De, P., Carbohydrate-conjugated amino acid-based fluorescent block copolymers: their self-assembly, pH responsiveness, and/or lectin recognition. *Langmuir* **2015,** *31* (34), 9422.
43. Isono, T.; Kawakami, N.; Watanabe, K.; Yoshida, K.; Otsuka, I.; Mamiya, H.; Ito, H.; Yamamoto, T.; Tajima, K.; Borsali, R.; Satoh, T., Microphase separation of carbohydrate-based star-block copolymers with sub-10 nm periodicity. *Polym Chem* **2019,** *10* (9), 1119.
44. Stenzel, M. H.; Davis, T. P.; Fane, A. G., Honeycomb structured porous films prepared from carbohydrate based polymers synthesized via the RAFT process. *J Mater Chem* **2003,** *13* (9), 2090.
45. Chen, G., The past ten years of carbohydrate polymers in ACS Macro Letters. *ACS Macro Lett* **2021,** *10* (9), 1145.
46. Chen, J.; Kamitakahara, H.; Edgar, K. J., Synthesis of polysaccharide-based block copolymers via olefin cross-metathesis. *Carbohydr Polym* **2020,** *229*, 115530.
47. Otsuka, I.; Tallegas, S.; Sakai, Y.; Rochas, C.; Halila, S.; Fort, S.; Bsiesy, A.; Baron, T.; Borsali, R., Control of 10 nm scale cylinder orientation in self-organized sugar-based block copolymer thin films. *Nanoscale* **2013,** *5* (7), 2637.
48. Liao, Y.; Chen, W. C.; Borsali, R., Carbohydrate-based block copolymer thin films: ultrafast nano-organization with 7 nm resolution using microwave energy. *Adv Mater* **2017,** *29* (35), 1701645.

49. Isono, T.; Miyachi, K.; Satoh, Y.; Nakamura, R.; Zhang, Y.; Otsuka, I.; Tajima, K.; Kakuchi, T.; Borsali, R.; Satoh, T., Self-assembly of maltoheptaose-block-polycaprolactone copolymers: carbohydrate-decorated nanoparticles with tunable morphology and size in aqueous media. *Macromolecules* **2016,** *49* (11), 4178.
50. Zepon, K. M.; Otsuka, I.; Bouilhac, C.; Muniz, E. C.; Soldi, V.; Borsali, R., Glyco-nanoparticles made from self-assembly of maltoheptaose-block-poly(methyl methacrylate): micelle, reverse Micelle, and encapsulation. *Biomacromolecules* **2015,** *16* (7), 2012.
51. Hung, C. C.; Lin, Y. C.; Chuang, T. H.; Chiang, Y. C.; Chiu, Y. C.; Mumtaz, M.; Borsali, R.; Chen, W. C., Harnessing of spatially confined perovskite nanocrystals using polysaccharide-based block copolymer systems. *ACS Appl Mater Interfaces* **2022**, *14*(26), 30279.
52. Liao, Y.; Goujon, L. J.; Reynaud, E.; Halila, S.; Gibaud, A.; Wei, B.; Borsali, R., Self-assembly of copper-free maltoheptaose-block-polystyrene nanostructured thin films in real and reciprocal space. *Carbohydr Polym* **2019,** *212*, 222.
53. Liao, Y.; Liu, K.; Chen, W. C.; Wei, B.; Borsali, R., Robust sub-10 nm pattern of standing sugar cylinders via rapid "microwave cooking". *Macromolecules* **2019,** *52* (22), 8751.
54. Gross, A. J.; Chen, X.; Giroud, F.; Travelet, C.; Borsali, R.; Cosnier, S., Redox-active glyconanoparticles as electron shuttles for mediated electron transfer with bilirubin oxidase in solution. *J Am Chem Soc* **2017,** *139* (45), 16076.
55. Li, L.; Zhong, Y.; Li, J.; Chen, C.; Zhang, A.; Xu, J.; Ma, Z., Thermally stable and solvent resistant honeycomb structured polystyrene films via photochemical cross-linking. *J Mater Chem* **2009,** *19* (39), 7222.
56. Yaseen, A. A.; Al-Tikrity, E. T. B.; Yousif, E.; Ahmed, D. S.; Kariuki, B. M.; El-Hiti, G. A., Effect of ultraviolet irradiation on polystyrene containing cephalexin schiff bases. *Polymers (Basel)* **2021,** *13* (17), 2982.
57. Friess, F. V.; Hu, Q.; Mayer, J.; Gemmer, L.; Presser, V.; Balzer, B. N.; Gallei, M., Nanoporous block copolymer membranes with enhanced solvent resistance via UV-mediated cross-linking strategies. *Macromol Rapid Commun* **2022,** *43* (3), 2100632.
58. Sakai-Otsuka, Y.; Nishiyama, Y.; Putaux, J. L.; Brinkmann, M.; Satoh, T.; Chen, W. C.; Borsali, R., Competing molecular packing of blocks in a lamella-forming carbohydrate-block-poly(3-hexylthiophene) copolymer. *Macromolecules* **2020,** *53* (20), 9054.
59. Ribeiro, J. P. M.; Mendonça, P. V.; Coelho, J. F. J.; Matyjaszewski, K.; Serra, A. C., Glycopolymer brushes by reversible deactivation radical polymerization: preparation, applications, and future challenges. *Polymers (Basel)* **2020,** *12* (6), 1268.
60. Clauss, Z. S.; Wardzala, C. L.; Schlirf, A. E.; Wright, N. S.; Saini, S. S.; Onoa, B.; Bustamante, C.; Kramer, J. R., Tunable, biodegradable grafting-from glycopolypeptide bottlebrush polymers. *Nat Commun* **2021,** *12* (1), 6472.
61. Hermatschweiler, M.; Ledermann, A.; Ozin, G. A.; Wegener, M.; von Freymann, G., Fabrication of silicon inverse woodpile photonic crystals. *Adv Funct Mater* **2007,** *17* (14), 2273.

62. Miyake, G. M.; Weitekamp, R. A.; Piunova, V. A.; Grubbs, R. H., Synthesis of isocyanate-based brush block copolymers and their rapid self-assembly to infrared-reflecting photonic crystals. *J Am Chem Soc* **2012,** *134* (34), 14249.
63. Matsen, M. W.; Bates, F. S., Conformationally asymmetric block copolymers. *J Polym Sci Part B Polym Phys* **1997,** *35* (6), 945.
64. Paterno, G. M.; Iseppon, C.; D'Altri, A.; Fasanotti, C.; Merati, G.; Randi, M.; Desii, A.; Pogna, E. A. A.; Viola, D.; Cerullo, G.; Scotognella, F.; Kriegel, I., Solution processable and optically switchable 1D photonic structures. *Sci Rep* **2018,** *8* (1), 3517.
65. Sakellari, I.; Kabouraki, E.; Karanikolopoulos, D.; Droulias, S.; Farsari, M.; Loukakos, P.; Vamvakaki, M.; Gray, D., Quantum dot based 3D printed woodpile photonic crystals tuned for the visible. *Nanoscale Adv* **2019,** *1* (9), 3413.
66. Macfarlane, R. J.; Kim, B.; Lee, B.; Weitekamp, R. A.; Bates, C. M.; Lee, S. F.; Chang, A. B.; Delaney, K. T.; Fredrickson, G. H.; Atwater, H. A.; Grubbs, R. H., Improving brush polymer infrared one-dimensional photonic crystals via linear polymer additives. *J Am Chem Soc* **2014,** *136* (50), 17374.
67. Martorell, J.; Vilaseca, R.; Corbalán, R., Second harmonic generation in a photonic crystal. *Appl Phys Lett* **1997,** *70* (6), 702.
68. Matsushita, A.; Okamoto, S., Tunable photonic crystals: control of the domain spacings in lamellar-forming diblock copolymers by swelling with immiscible selective solvents and a neutral solvent. *Macromolecules* **2014,** *47* (20), 7169.
69. Wang, H.; Zhang, K. Q., Photonic crystal structures with tunable structure color as colorimetric sensors. *Sensors (Basel)* **2013,** *13* (4), 4192.
70. Hu, H.; Gopinadhan, M.; Osuji, C. O., Directed self-assembly of block copolymers: a tutorial review of strategies for enabling nanotechnology with soft matter. *Soft Matter* **2014,** *10* (22), 3867.
71. Fan, Y.; Tang, S.; Thomas, E. L.; Olsen, B. D., Responsive block copolymer photonics triggered by protein-polyelectrolyte coacervation. *ACS Nano* **2014,** *8* (11), 11467.
72. Bendejacq, D.; Ponsinet, V.; Joanicot, M.; Loo, Y. L.; Register, R. A., Well-ordered microdomain structures in polydisperse poly(styrene)-poly(acrylic acid) diblock copolymers from controlled radical polymerization. *Macromolecules* **2002,** *35* (17), 6645.
73. Howard, M. P.; Reinhart, W. F.; Sanyal, T.; Shell, M. S.; Nikoubashman, A.; Panagiotopoulos, A. Z., Evaporation-induced assembly of colloidal crystals. *J Chem Phys* **2018,** *149* (9), 094901.
74. Parker, R. M.; Frka-Petesic, B.; Guidetti, G.; Kamita, G.; Consani, G.; Abell, C.; Vignolini, S., Hierarchical self-assembly of cellulose nanocrystals in a confined geometry. *ACS Nano* **2016,** *10* (9), 8443.
75. Sinturel, C.; Bates, F. S.; Hillmyer, M. A., High χ-low N block polymers: how far can we go? *ACS Macro Lett* **2015,** *4* (9), 1044.
76. Liu, S.; Yang, Y.; Zhang, L.; Xu, J.; Zhu, J., Recent progress in responsive photonic crystals of block copolymers. *J Mater Chem C* **2020,** *8* (47), 16633.

77. Fan, Y.; Walish, J. J.; Tang, S.; Olsen, B. D.; Thomas, E. L., Defects, solvent quality, and photonic response in lamellar block copolymer gels. *Macromolecules* **2014,** *47* (3), 1130.
78. Joannopoulos, J. D.; Johnson, S. G.; Winn, J. N.; Meade, R. D., Photonic crystals: Molding the Flow of Light, 2nd ed., Princeton University Press: Princeton, NJ, **2008**

Chapter 4: Self-assembly of Carbohydrate-based Brush Block Copolymers into Photonic Particles

4.1 Introduction

Brush block copolymers (BRs), as a versatile building block to construct the photonic materials, have received considerable attentions due to their tunable parameters such as the grafting density, composition and length of side chains or the structure of backbone.[1-4] To date, a large number of articles reported on the self-assembly of BRs into photonic crystals in thin films or bulk state, have been extensively investigated by researchers.[3, 5-9] As aforementioned in the chapter 3, angular dependence of structure coloration is usually observed in the photonic crystal films based on the Bragg diffraction equation,[10, 11] probably impeding the robustness of structural colors.[12] Recently, the self-assembly of brush block copolymers in solutions have increasingly aroused researchers interests because it provides a promising pathway for fabricating the angular-independent photonic materials with diverse architectures, resulting in their potential applications as versatile photonic devices, color displays, cosmetics and coatings.[13-19]

In 2020, a series of dendronized brush block copolymers at range of molecular weight (477-1144 kDa) were successfully synthesized by Swager and coworkers and their confined self-assembly into the photonic ellipsoidal particles were able to reflect full-colors via solvent evaporation in emulsion. Near-perfect axially stacked lamellar multilayers can be observed in elongated ellipsoidal particles at range of domain spacing from 153 nm to 298 nm. Furtherly, Fe_3O_4-functionalized photonic ellipsoidal particles exhibited the off/on switchable color rapidly by the assistance of magnetic field.[18] Meanwhile, Parker and coworkers reported that an amphiphilic brush block copolymer anchored polystyrene and polyethylene oxide as side chains, can be easily used to fabricate the porous microparticles via self-assembly within an emulsified droplet by the controlling swelling micelles. Those estimated pore size in microparticles in the range 133-193 nm were realized by controlling the permeated water into microparticles, leading to isotropic photonic pigments reflecting color from blue to red

across the entire visible spectrum. Such angular independent optical properties of photonic pigments were attributed to the coherent scattering occurring in pores with the short-range distribution, showing high color purity with ignored iridescence.[17] Coincidentally, in 2022, Song and colleagues[19] also demonstrated that angular independent photonic pigments with a similar porous microparticles can be successfully achieved by blending with two various molecule weight of BRs (high and low) within multiple emulsified droplets and sequential solidification, resulting in the reflecting colors from various blue, through green, yellow to different red. Notably, when the percentage between high weight and low weight BRs was less than two, the well-controlled water/oil interface with extremely bending improved the tunable structural coloration efficiently only by changing the molecule weight a little bit, avoiding the time-consuming complex procedures of synthesis and high cost of photonic pigments. According to recent tendency of photonic particles, it is found that three-dimensional architectures with tunable internal structure, shape and sizes, can be successfully realized via the confined self-assembly of BRs within the emulsification droplets, enable them having structural colorations covering the whole UV-vis spectrum.

In this context, I also attempt to fabricate the angular independent 3D photonic crystals via the confined self-assembly of BRs in the emulsified water according to the reported method.[17] Unfortunately, only blue color from BRs can be observed under different conditions including as molecular weight, surfactants, concentrations, homogenizer speed and time, which may be ascribe to Reyleigh sccatering form the formation of nanoparticles in solutions due to the only solubility of BR06-07 in non-volatile DMF. Surprisingly, highly homogenous core-shell glyconanoparticles can be easily obtained via the self-assembly of carbohydrate-based BR06-07 anchoring polystyrene (PS) and maltoheptaose (MH) as side chains under the water vapor environment. The diameter of core-shell glyconanoparticles with precisely position and highly density of MH composed of shell, can be adjustable by manipulating the molecular weight of BRs, providing promising candidates for the biomedical field. Specifically, AFM images showed that the surface morphology of the sphere

glyconanoparticles from a single BRs (BR06) on the hydrophilic-modified silicon can be tunable into uniform cubic and donut structure after thermal annealing treatments, which may put forward new insight into the design and synthesis of functional materials with unique structures, properties, and applications by using post-treatments of the glyconanoparticles.

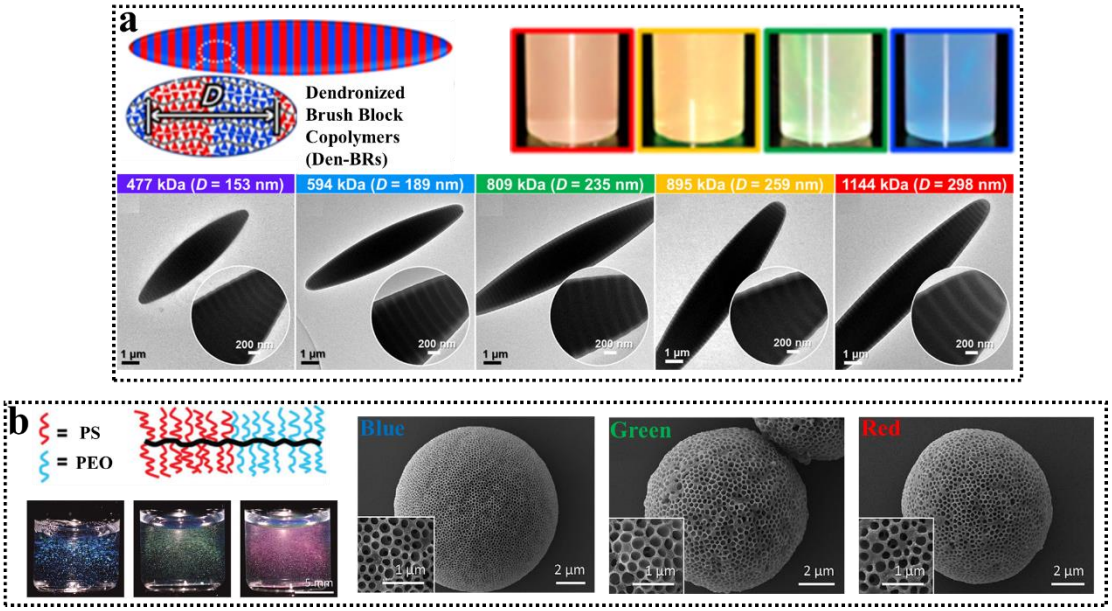

Figure 1. Scheme representation, photographs and TEM images for photonic ellipsoidal particles (a)[18] and photonic porous particles (b)[17] prepared from the Den-BRs and BRs via self-assembly, respectively.

4.2 Results and Discussion

The controllable synthesis of glycopolymer brushes with precisely position and density are still desired and challenging due to their promising candidates for the biomedical field. In this work, an effective strategy has been applied to exert control over the position and density of maltoheptaose (MH) and polystyrene (PS) by the combination of the ruthenium-catalyzed ring-opening metathesis polymerization (ROMP) grafting-though and click chemistry grafting-to approach. Within hands of BR01-07, BR01-04 are firstly used to fabricate the photonic particles in the emulsified solution according to the reported method by Parker group.[17] In those initial experiments as shown in Figure 2, only blue color is observed under different conditions including as molecular weight, surfactants, concentrations, homogenizer speed and time. This blue color may

be ascribed to the formation of core-shell particles with an isotropic short-range structure in the emulsified water via self-assembly of BRs.[20] Green, yellow and red are still desirable but not realized until now from our group. More techniques will be explored under way.

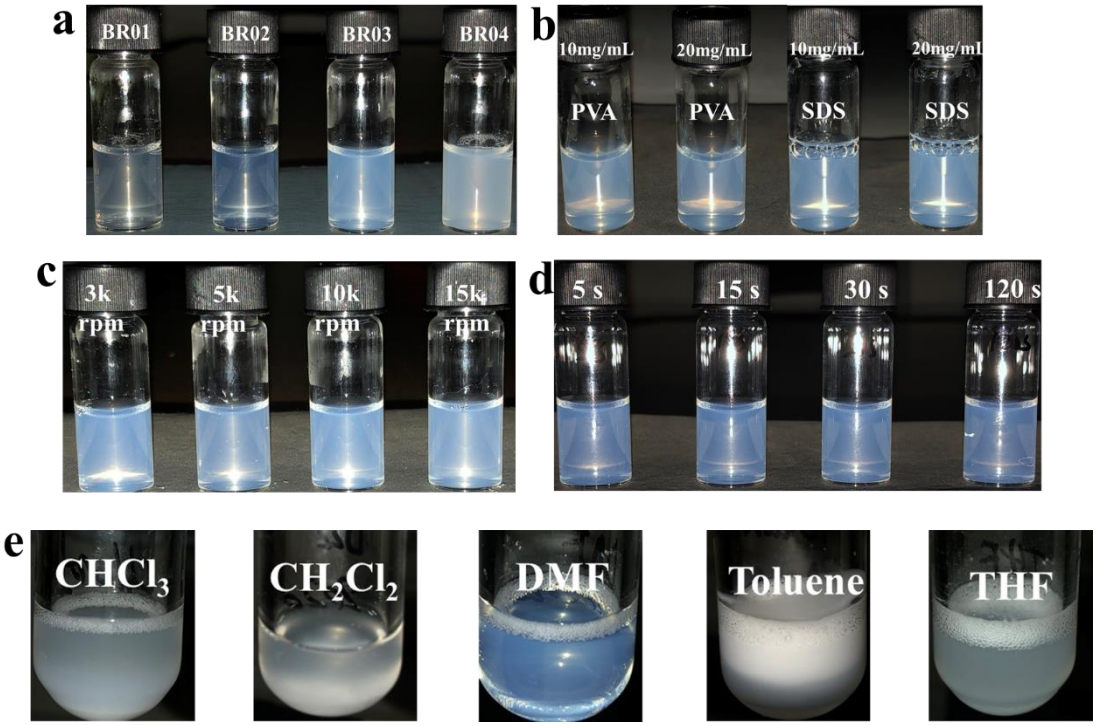

Figure 2. Photographs for the preparation of brush block copolymers (BR01-04) emulsions by using a rotor-stator homogenizer (detail information in the following experimental section) under various conditions (a) different molecular weight BR01-04 (20 mg/mL, 500 µL in DMF) in rang of 0.824-1.455 kDa at 10 k rpm for 80 s in the polyvinyl achohol (PVA) emulfisied water (20 mg/mL, 5 mL) (b) BR03 suspensions (20 mg/mL, 500 µL in DMF) at different concentration (10 mg/mL, 20 mg/mL) of different surfactants (PVA and sodium dodecyl sulfate termed as SDS). (c) BR03 suspensions (20 mg/mL, 500 µL in DMF) at different homogenizer speed from 3k to 15k for 80 s in PVA emulfisied water (20 mg/mL, 5 mL). (d) BR03 suspensions (20 mg/mL, 500 µL in DMF) at different time from 5s to 120s at 10k in PVA emulfisied water (20 mg/mL, 5 mL). (e) BR03 stock solution (20 mg/mL) in different solvents ($CHCl_3$, CH_2Cl_2, DMF, Toluene, THF) at 10 k for 80 s in PVA emulfisied water (20 mg/mL, 5 mL). All those photographs are taken under dark environment.

Interestingly, the resultant unique brush-like BRs can be engineered to form homogenous nanoparticles by using solvent diffusion-evaporation-mediated self-assembly (SDEMS).[21] The self-assembly process is investigated detailly by dynamic light scattering (DLS) and NMR spectroscopy and the core-shell glyconanoparticles was further confirmed by TEM. Surprisingly, the homogenous core-shell GNCs from the polymer-based amorphous BR06 can be tunable into diverse morphologies such as uniform cubes and donuts on the hydrophilic-modified silicon substrates. The detail information will be represented in the following section.

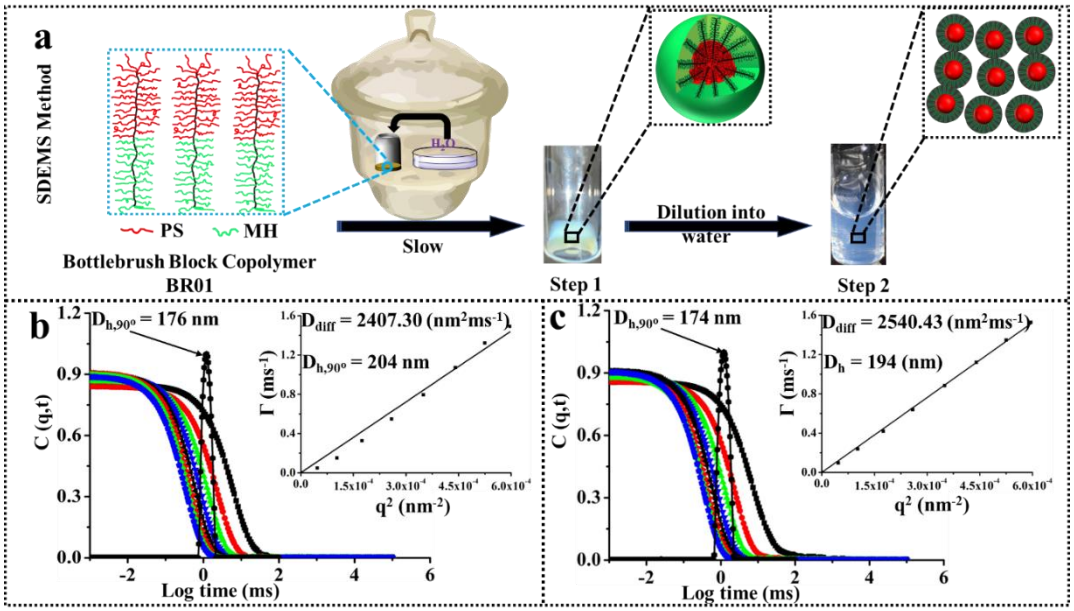

Figure 3. (a) Photographs and schematics of the bottlebrush block copolymer BR06 solution (80 mg/mL, 400 µL DMF) and their self-assembly into glyconanoparticles (69 mg/mL, 14% volume fraction H_20, step 1) by using H_2O solvent diffusion-evaporation-mediated self-assembly (SDEMS)[21] for 24 h, then furtherly diluted 100 times into deionized water to obtain the blueish suspension (0.69 mg/mL, 1% volume fraction DMF in deionized water, step 2). DLS results for BR06 nanoparticles prepared from step 1 and 2 by diluting solution into deionized water (b) 0.069 mg/mL and (c) 0.69 mg/mL. Autocorrelation function C(q,t) measured at scattering angles of 30°-135° by step of typically 15° and relaxation time distribution A(t) at 90°. The corresponding insert image is dependence of relaxation frequency (Γ) on the square of the wavevector (q2) from b and c respectively.

4.2.1 Glyconanoparticles preparation from the BR06

The preparation of glyconanoparticles (GNCs) from a carbohydrate-based bottlebrush block copolymer BR06 is following two key steps: (1) the BR06 is firstly dissoved in DMF, (2) formation of homogeneous core-shell GNCs under H_2O annealing for 24 h in a sealed container. These two steps are summarized in Figure 3a. Carbohydrate-block copolymer brush specifics are given in Table 1 of chapter 2. Initially, the carbohydrate-based bottlebrush block copolymer, poly(norbornene)-graft-(poly(styrene)$_{250}$)-block-(poly-(norbornene))-graft-maltoheptaose$_{250}$ (abbrev. BR06), is dissolved (80 mg/mL) in a *N,N*-dimethylformamide (DMF) which is common solvent for both blocks (PS and MH). The brush-like copolymer solution was under H_2O annealing for 24 h in a sealed container and then the GNCs is formed (Figure 3, step 1). H_2O is selected for PS and induced self-assembly into homogenous core-shell GNCs with a PS core and MH shell (TEM, Figure 5, step 2). To calculate the weight of solvents (H_2O) absorbed by BR06 solution (80 mg/mL, 0.4 mL DMF) as a function of time, a series of data was recorded as shown in Figure 4. A linear relationships is fitted by H_2O annealing in range time of 48 h. As a result, for H_2O annealing in 24h, the BR06 solution concentration is slightly decreased to 69 mg/mL. To investigate the hydrodynamic radius (R_h) and size distribution of the resulted nanoparticles by diluting 100 and 1000 times of suspension in step 1 into deionized water, dynamic light scattering (DLS) measurements are carried out on these two dilution nanoparticle dispersions (0.069 mg/mL and 0.69 mL). Figure 3b shows the relaxation time functions at scattering angles at 90° and the autocorrelation functions at the scattering angles of 30°-135° at interval 15°. A monomodal relaxation time distribution (PD.I.=0.0511) can be observed for the nanoparticles from the BR06 in deionized water, which indicates the well-defined nanoparticles (NCs) with the diameter values of 176 nm (abbrev. $D_{h,90°}$ =176 nm). By the Stokes-Einstein relation from the diffusion coefficient values (D_{diff}: 2407.30 nm^2ms^{-1}) that is obtained by the linear relationship between the relaxation frequency ($\Gamma = 1/\tau$) and the square of the wavevector (q^2), the D_h is calculated to be 204 nm (Figure 3b). Upon increasing the concentration of the nanoparticles from 0.069 mg/mL to 0.69

mg/mL in deionized water, the similarity on the particle size can be obtained from DLS measurements (Figure 3b and 3c), which indicates that BR06 nanoparticles remain the high stability.

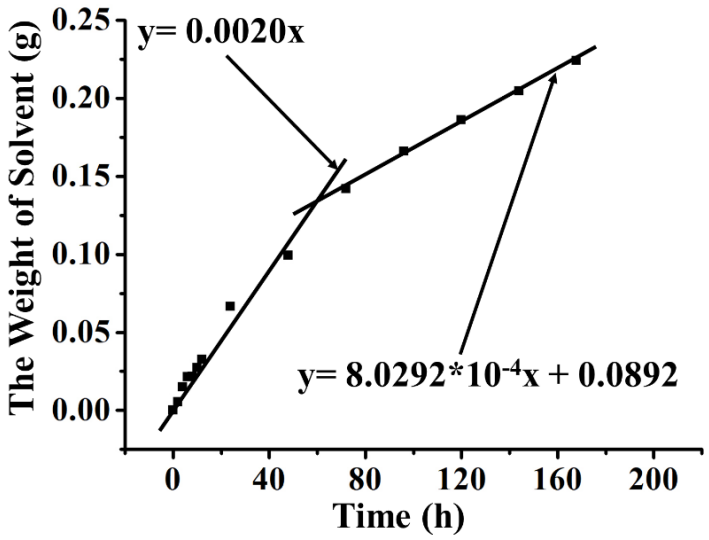

Figure 4. The weight of H_2O solvent absorbed by BR06 solution (80 mg/mL, 0.4 mL DMF) as a function of time.

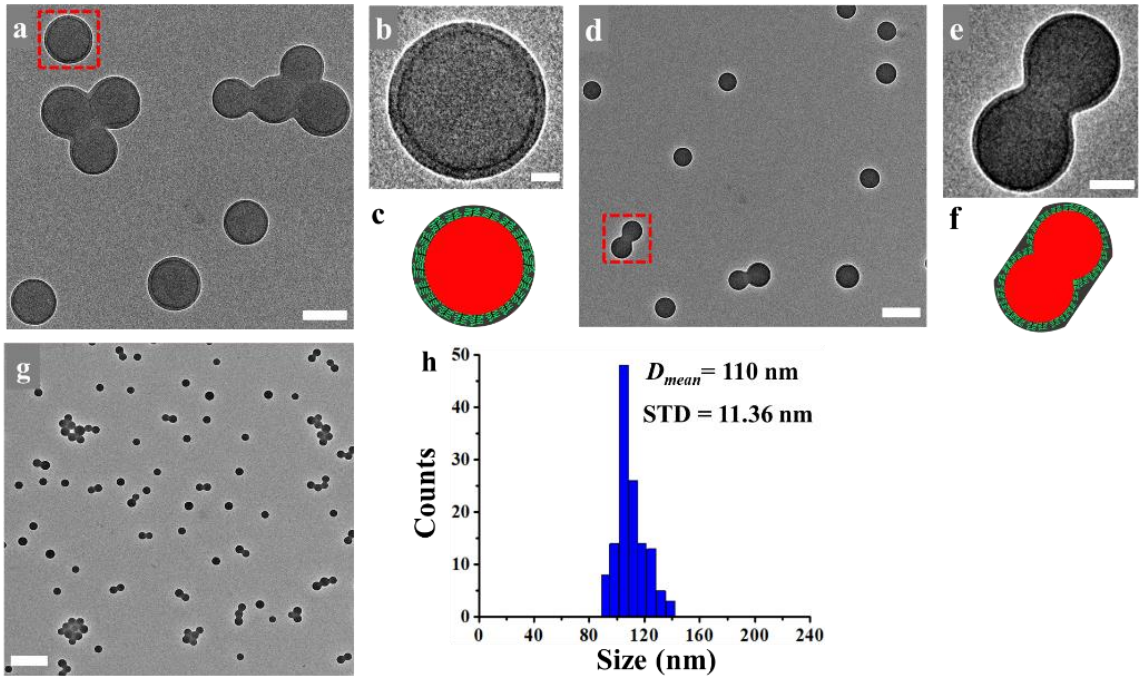

Figure 5. TEM images of the nanoparticles prepared from BR06 suspension (Figure 3, step 2) with different scale size a) scale bar for 100 nm b) scale bar for 20 nm d) scale bar for 200 nm, e) scale bar for 50 nm, g) scale bar for 500 nm and (h) the diameter distribution collected from g). c) and f) are schematic diagrams of b) and d) respectively, green: MH; red: polystyrene.

The structures of GNCs are also characterized by transmission electron microscopy (TEM), atomic force microscopy (AFM). Figure 5 shows the TEM images for nanoparticles prepared from BR06 suspension under different scan sizes. Individual spherical nanoparticles with thin shell and domain core, are clearly observed in Figure 5a and 2b. Figure 5d and 5e shows the nanoparticles formed fusional structure of two or several individual nanoparticles without clear boundaries. Figure 5c and 5f are schematic diagrams of core-shell and fusional structure nanoparticles respectively. It can be interpreted that the movement of individual nanoparticles can result in more chance to encounter, tangle and cross mutually during drying solvent.[22] The narrow size distribution observed in the TEM analysis (Figure 5h) is consistent with the sharp and monomodal relaxation time distribution of the nanoparticle dispersion obtained from DLS. The average diameter value of the nanoparticles is calculated to be 110 nm based on TEM analysis.

Meanwhile, AFM height images is preformed to investigate the surface morphology of BR06 by dropping casting BR06 suspension (0.069 mg/mL in deionized water,10 drops, Figure 3a, step 2) on the hydrophilic modified silicon substrate for 24h at room temperature. As shown in Figure 6, it shows us the presence of single spherical nanoparticles (diameter: 140 nm height: 107 nm) and a set of nanoparticles together (diameter: 125 nm height: 102 nm). Furthermore, the nanoparticles from step 1 (69 mg/mL, Figure 3) and step 2 suspension (0.69 mg/mL, Figure 3) can arrange spontaneously with ambient drying so that the nanoparticles pack together to form a hexagonal arrangement in short range as shown in Figure 6a and 6d respectively, which ascribes to the association of GNCs shell among neighboring particles leading to facilitate the formation of a hexagonal pattern of GNCs with few defects.[23] The 2D Fourier transform of the left bottom portion of the image (Figure 6b and 6e) shows the six intensity peaks denoting periodicity and hexagonal structure of the nanoparticles with a periodicity of approximately 133 nm and 127 nm (corresponding to the measured averaged interparticle core distance), indicating that the BR06 nanoparticles are preferentially incorporated into the 2D structure. The narrow size distribution observed

in the AFM analysis (Figure 6f) is consistent with the sharp and monomodal relaxation time distribution of the nanoparticle dispersion obtained from DLS. The average diameter value of the nanoparticles is calculated to be 126 nm based on AFM analysis, which confirms that the particle diameter of BR06 nanoparticles is larger than those observed by TEM analysis, which may be attributed to be so-called "pancake deformation" due to the interaction between the nanoparticles and the hydrophilic surface.[24] In comparison to the BR06 particles prepared from the traditional precipitation method (Figure 7),[25] obvious aggregates and highly polydispersity in size and shape of particles can be confirmed by the AFM height and phase images of Figure 6g-h and two broad population of DLS results with a PD.I. value 0.393 in Figure 6i.

To investigate the mechanism of the GNCs formation, dynamic light scattering (DLS) is applied to trace the size and size distribution of BR06 solution in DMF as a function of time under H_2O annealling. As shown in Figure 8, the distribution curve appeares wide monodisperse ($R_{h,90}^{o}$ = 20 nm) with low intensity around 0.3 for initial solution due to the volume of individual macromolecular. After H_2O annealing for 16h, a bimodal size distribution is exhibited in the measurement. The major intensity sharp distribution peak at 127 nm corresponds to the formation of core-shell NCs (core: PS, shell: MH) due to the hydrophobic force while the small weak intensity distribution peak around 20 nm ascribe to some existing individual macromolecules. With increasing the H_2O annealing time to 24h, the distribution analysis reveals only a single sharp and narrow peak around 125 nm, indicating all the individual macromolecular self-assemble into core-shell NCs. Moreover, the intensity of DLS and Tyndall effect is increasing with the H_2O annealing time, which is consistent with our interception as shown in the schemes in Figure 8a. Additionally, NMR spectrum allow us to monitor the formation of NCs generated from 20 mg/mL BR06 million solution in deuterium DMF under the H_2O annealing. As shown in Figure 8c, the gradual decrease and further disappearance of the signal corresponding to PS part (red rectangle shadow marked area) at range of 7-8 ppm can be clearly observed along with the H_2O annealing time while there was still weak signal belong to MH at range of 5-6 ppm in the end (zoom

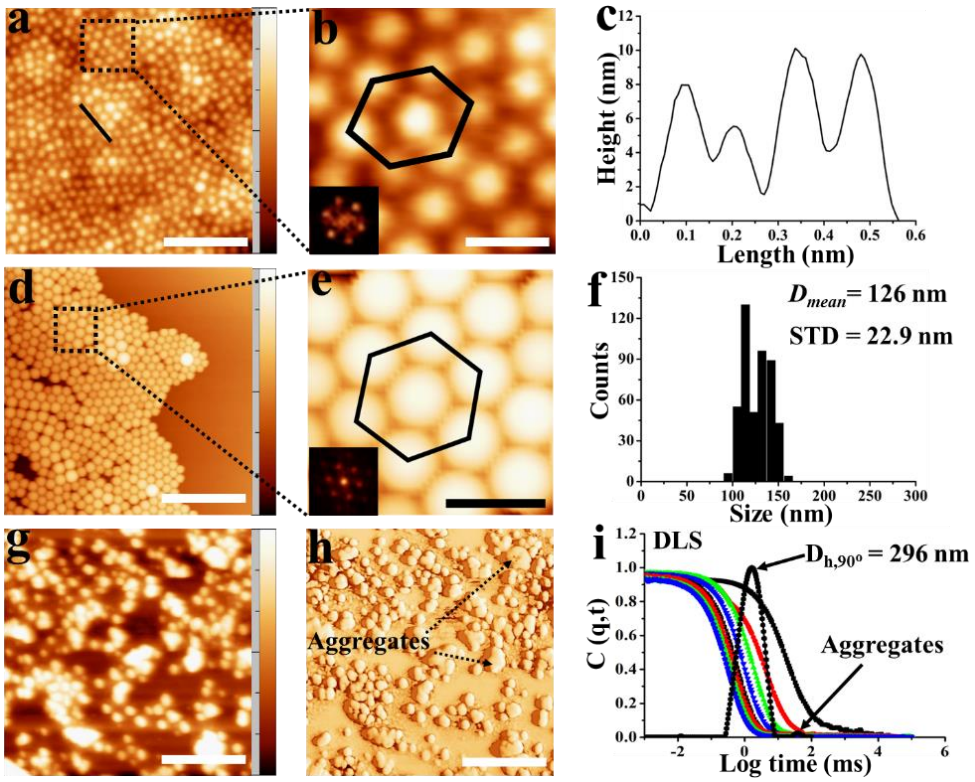

Figure 6. (a-b) AFM height images of the BR06 NCs from step 1 (Figure 3, 20 µL, 69 mg/mL in the mixtue solvent DMF/H_2O) and (d-e) step 2 suspension (Figure 3, 200 µL, 0.69 mg/mL in deionized water) dropped casting on a silicon slide with ambient drying for 12h. (c) the corresponding section analysis of the height image a by the black line. (f) the diameter distribution collected from a. Left bottom insert images are the corresponding 2D Fourier-transformed image in the zoom image (b and e) respectively. Hexagon is formed by the selected six nanoparticles in zoom image b and e respectively. (g and h) AFM height and phase images of the BR06 GNCs (0.5 mg/mL in the deionized water) prepared from the traditional precipitation method.[25] (i) DLS results for BR06 GNCs (0.5 mg/mL in the deionized water) prepared from the traditional precipitation method. Autocorrelation function C(q,t) measured at scattering angles of 30°-135° by step of typically 15° and relaxation time distribution A(t) at 90°.(a, d, g and h) scale bar for 1000 nm.(b, e) scale bar for 200 nm.

image of Figure 8c), which is ascribe to the hydrophobic PS core surrounded by the hydrophilic MH shell leading to the disappearance of the ^{1}H-NMR signals from core components while weak signals associated with outer shell is still observed due to the partly dissolved MH in DMF.[26] The appearance of the NMR tube is changed from the

initial transparence, through turbid to milky along with the H_2O annealing time. Upon laser pointer through the tube, Tyndall effect is obviously observed after the H_2O annealing for 48-96h, indicating the formation of NCs. Combined with the above NMR, DLS, AFM, and TEM results, the reasonable conjecture is schemed in Figure 8a.

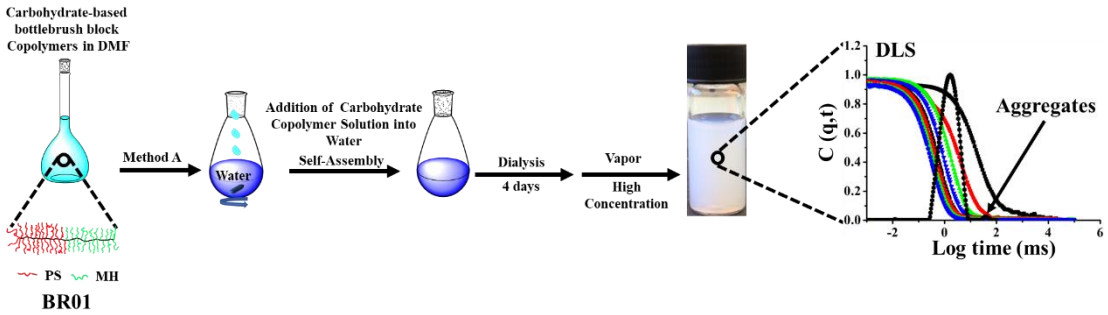

Figure 7. Schematic illustration of the self-assembly procedure of BR06 by the traditional precipitation mathod A.

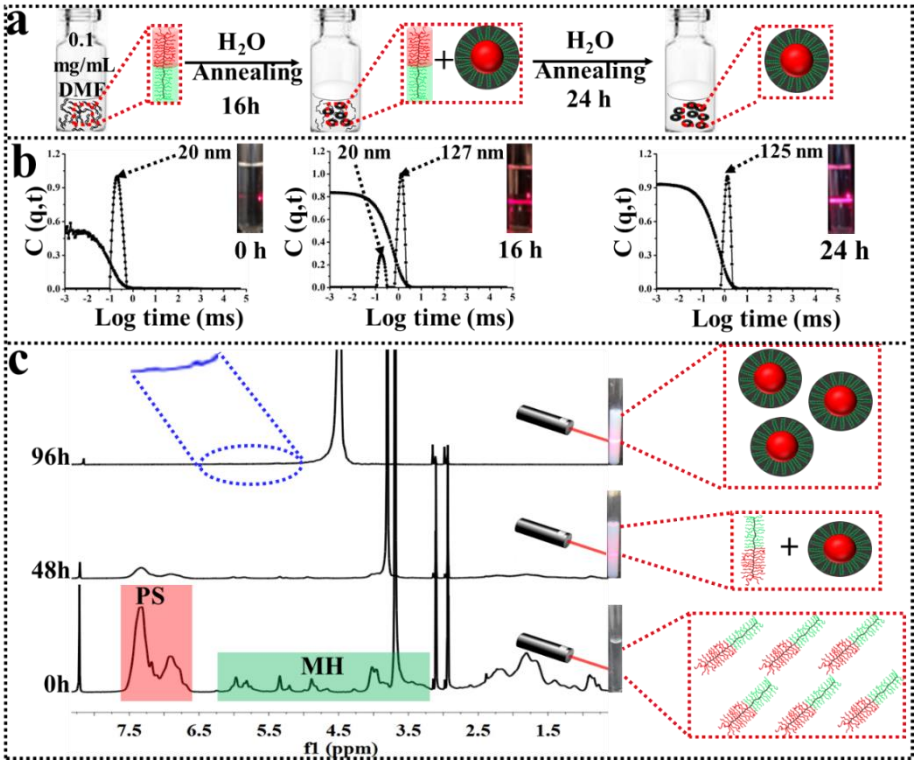

Figure 8. (a) Schemes and (b) DLS trace of the BR06 GNCs formation process (0.1 mg/mL in DMF) and (c) NMR spectrum trace of the BR06 GNCs formation process (20 mg/mL in DMF) as a function of time under H_2O annealing. Inset images are the photographs of samples passed through by laser as a function of time.

4.2.2 Temperature effect on surface morphology of BR06 GNCs

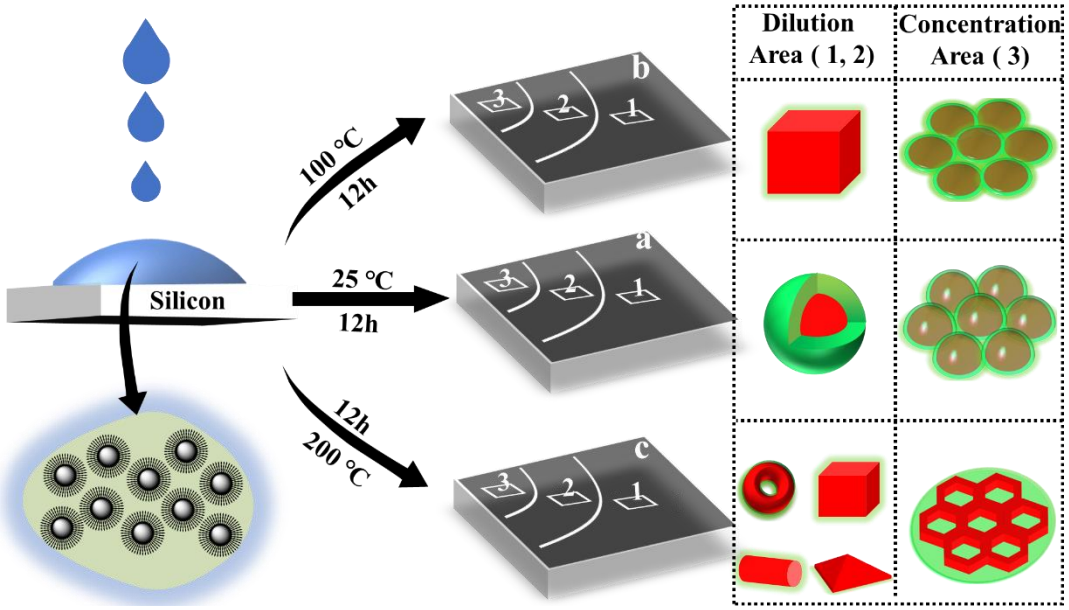

Figure 9. Schematic illustrations of BR06 GNCs morphology at different temperature for 12 h after drop casting on the hydrophilic-modified silicon sunstrates.

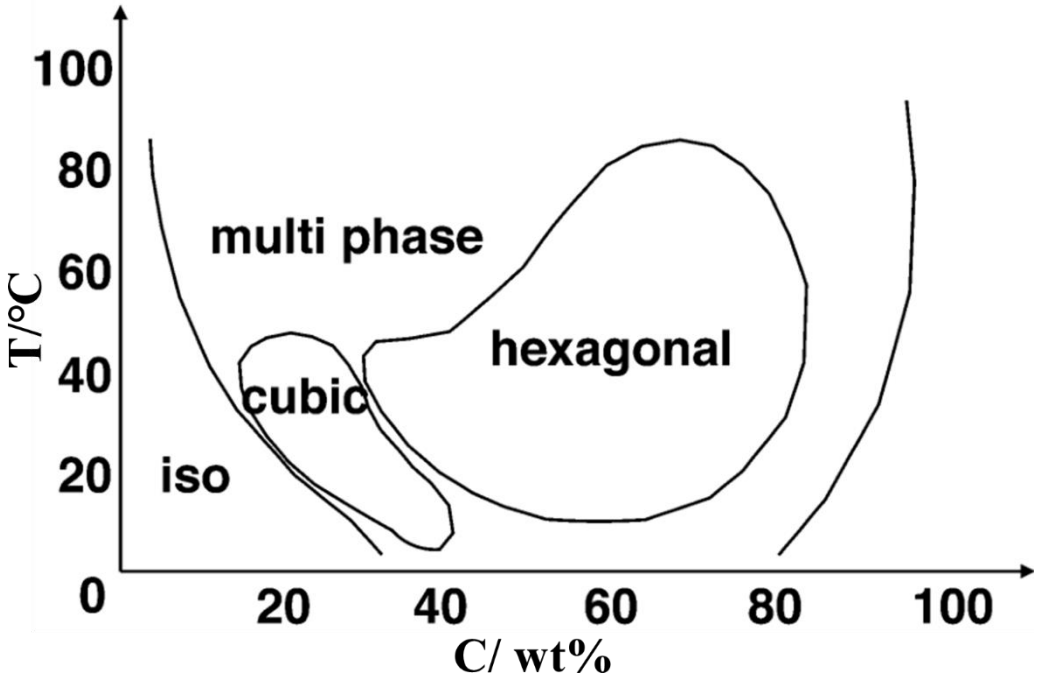

Figure 10. The experimental phase digram of a linear triblock copolymer P123 in water.[27]

The morphology evolution of GNCs (0.069 mg/mL in deionized water, 400 μL) from a single amorphous asymmertry BR06 on the hydrophilic modified silicon substrate is demonstrated in Figure 9 by drop casting on a silicon slide at various annealing

temperatures. As a results, a rich diversity of achitectures including as sphere, cubic, donut, rod, triangle, and hexagon, can be exhibited from polymeric-based GNCs upon the evaporation of water solvent. The temperature and concentration of BR06 play a vital important role in dominating the final structures via self-assembly which refers to the aggregation behavior and phase diagrams of the linear triblock copolymers in Figure 10.[27] Generally, the region of low concentration of BR06 GNCs deposited in the hydrophilic substrates (Figure 9, Marked 1, 2) shows that the formation of sphere at room temperature, cubic at intermediate temperature, multiple morphologies including as doughnut, irregular cubic, rod and triangle at high temperature is dipicted in the schematic illustration. As for the high concentration of region marked 3 in Figure 9, the short-range order of hexagonal structure at 25 ℃, slightly melted hexagonal structure at 100 ℃ and honeycomb structure at 200 ℃ can be clearly observed after the evaporation of water on the hydrophilic-modified silicon substrate. Specifically, the AFM height images, line-profiles and surface roughness can be taken advantage of investigating the gradual morphology evolution of BR06 nanoparticles at the different temperatures. Initially, the BR06 nanoparticles solution (0.069 mg/mL in deionized water, 400 μL) is dropped casting on the hydrophilic modified silicon substrate with ambient drying for 12h as shown in Figure 11a1.

As for low concentration area (1 and 2 in Figure 9), the height and diameter (height: 107 nm; diameter: 198 nm) of the individual nanoparticles are clearly plotted by the cross-sectional line-profile in Figure 11a3 in which the diameter is much larger than that calculated from Figure 6d possibly due to the combination effect of an extending isolated nanoparticle avoiding crowding with other nanoparticles and “pancake deformation”.[24] Interestingly, as shown in Figure 11b, 12a and 12b, by evaporating BR06 GNCs solution at 100 ℃ for 12h on the hydrophilic modified silicon substrate and then reducing temperature down to room temperature, homogenous well-shaped nanocubes and irregular stacked nanocubes are clearly observed on the hydrophilic modified silicon substrate, in which the height of the nanocubic (height: 35 nm; diameter: 98 nm) and stacked nanocubic (height: 50 nm; diameter: 200 nm) are smaller

in comparison to that of the initial spherical GNCs as shown in Figure 11a. These symmetrical nanocubes should be ascribe to the formation of the crystalline structure via self-assembly of these agglomerates when reaching the critical volume fraction.[28] The formation process of the crystalline structure are possible following three steps: (1) BR06 GNCs docomposes into small spherical nanoparticles, (2) rod-like shape nanostructures can be formed via the coalescence of these small uints, (3) these rods are able to transform themselves to nanocubes by spraying-out way.[29] So far, such uniform nanocubes from a single amorphous asymmetrical brush-like copolymer have never been achieved via self-assembly upon evaporation-induced crystallization of BR06 suspension.[30] Furtherly, upon thermal annealling at 200 ℃ for 12h, the morphology of BR06 GNCs changes drastically which may be due to the degradation of core-shell GNCs as well as enhanced diffusion.[31] As shown in Figure 11c and 12e, such thermal treatment on the BR06 GNCs solution can result in homogenous toroids propably due to the growth and necleation mechanism,[32] that is, homogenous GNCs degrade firstly into small nanoparticles, then these small nanoparticles can grow into diskes, sequential a hole necleates in the middle of disks, finally the formation of rings evolved from these holes.[32] Meanwhile, irregular cubes, rods and triangles can be also observed Figure 12d, which may be due to the intro or inter-nanoparticles coalescnece.[33]

The diameter of the toroid is calculated to be 113 nm from the peak to peak distance (Figure 11c3), and the average width and height of the toroidal ring is 54 nm and 4.5 nm respectively which is much smaller than that of nano cubic and sphere. This differences in height and the width of sphere, cubic and donut can be presented at different temperature, probably because the hydrophilic MH shell part and hydrophobic PS core part of NCs can decompose into sub-nanoparticles and them grow by merging the nearby corresponding components at elevated temperature in order to minimize the surface and interface energy.[31] These toroidals show the same contrast in the outside and inside of rings in the AFM image which indicates that this structure is different from the collapsed vesicle with a darker periphery and a lighter center in the AFM. [32]

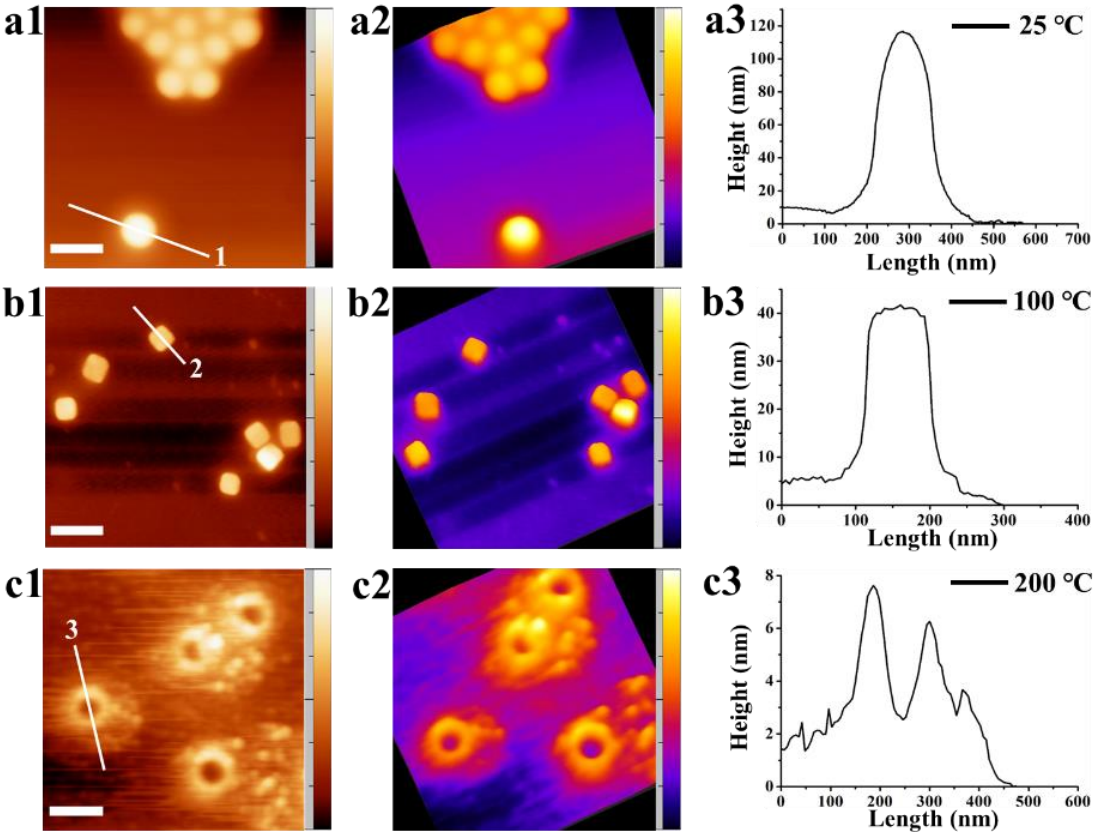

Figure 11. AFM Images of the BR06 nanoparticles (0.069 mg/mL in deionized water, Figure 3, step 2 suspension) dropped casting on a silicon slide at various annealing temperatures for 12 h for the low concentration area of the silicon substration. (a1) 25 ℃ for 12h, 0.00-163.31 nm for height. (b1) 100 ℃ for 12h, 0.00-66.18 nm for height. (c1) 200 ℃ for 12h, 0.00-11.29 nm for height. (a2-d2) the corresponding AFM 3D height of a1-c1. (a3-d3) the corresponding section analysis of the height images by the lines. Scan bar in a1-c1 is 200 nm.

As for high concentration area shown in Figure 13, at 25 ℃ for 12h, AFM height images exhibit that the GNCs can order a hexagonal structure in short range by drop casting on the hydrophilic substrate. Sequentially, the GNCs begin to melt sligtly and connect the neighboring one at 100 ℃ for 12h. Eventually, the GNCs can be decomposed and futherly segregate and self-assemble into honeycomb structure with cavities (average diameter:70 nm) when performing a thermal annealing at 200 ℃ for 12h (Figure 13c),

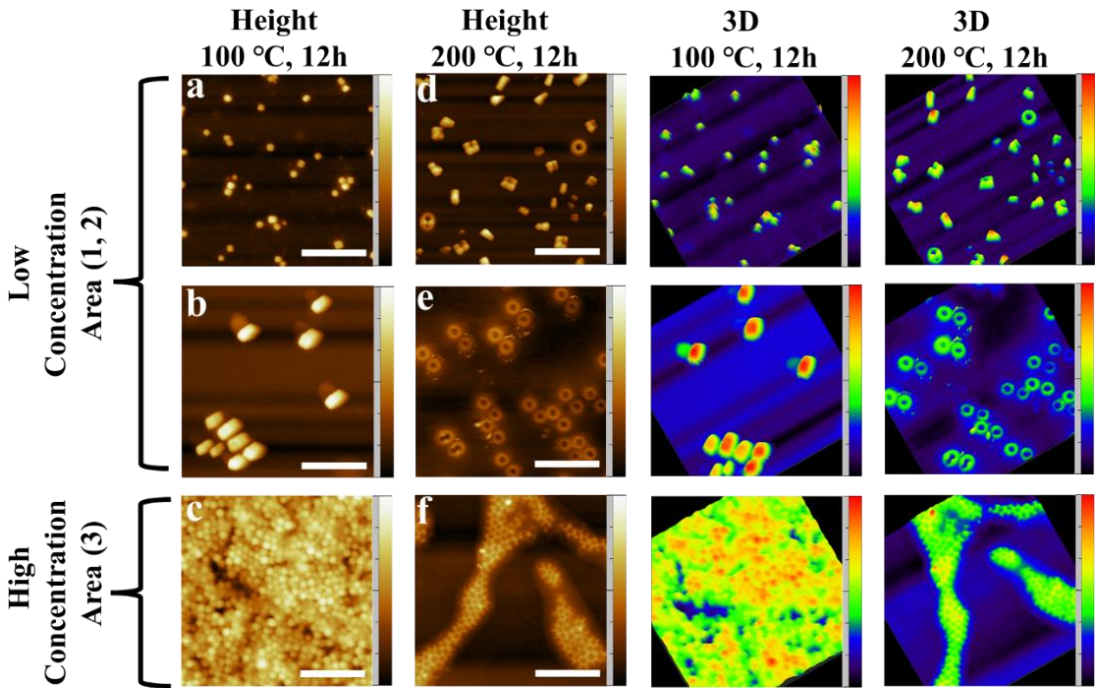

Figure 12. AFM height images and 3D images of morphology on the evolution of BR06 GNCs nanostructures at various annealing temperature for 12h. Scan bar in a-f is 1000 nm. (a) 100 ℃ for 12h, 0.00-74.26 nm for height. (b) 100 ℃ for 12h, 0.00-99.11 nm for height. (c) 100 ℃ for 12h, 0.00-132.53 nm for height. (d) 200 ℃ for 12h, 0.00-46.88 nm for height. (e) 200 ℃ for 12h, 0.00-28.35 nm for height. (f) 200 ℃ for 12h, 0.00-71.68 nm for height.

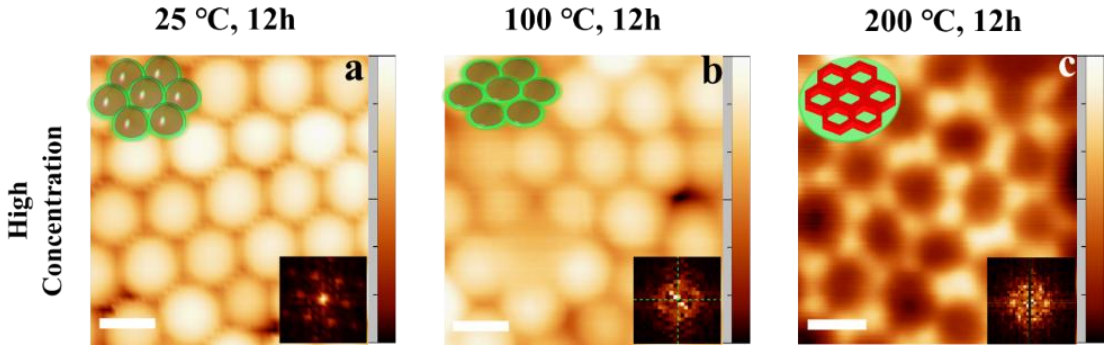

Figure 13. AFM height images and schematic illustration (upper left insert images) of morphology on the evolution of BR06 GNCs nanostructures at various annealing temperature for 12h for the high concentration area of the silicon substration. Scan bar is 100 nm. (a) 25 ℃ for 12h, 0.00-101.70 nm for height. (b) 100 ℃ for 12h, 0.00-74.23 nm for height. (c) 200 ℃ for 12h, 0.00-26.48 nm for height. (a-c) The bottom right insert images are the corresponding Fast Fourier Transform.

providing a simple method for fabricating the tunable morphology of nanoparticles via a post-thermal treatment. Additionally, the substate surface roughness decreases along with the increasing temperature as shown in Figure 14. In conclusion, the drive force for the NCs shape transition from the round through cubic to the donut may ascribe to the minimization of total surface energy to reach the most stable configuration.[31]

Meanwhile, TEM characterization is also carried out to study the BR06 GNCs. As shown in Figure 15b, by drop casting on the copper grid at 100 ℃ for 12h, some core-shell nanoparticles are stretched to be the elongated ones and some begin to melt to be the disk-like shape. Furtherly, extending the time to 96 h at 100 ℃, highly disperse cubic particles with sizes from 10-50 nm can be clearly observed on the TEM grid while a spherical particle is still remained in the Figure 15c. TEM diffraction spots from Figure 15c demonstrate the presence of crystalline domains within these BR06 nanocubes. In comparison to homogenous cubic nanoparticles on the hydrophilic silicon (AFM results), the dispersity of cubic shape on the copper grid may be ascribe to the combination effect of the slower evaporative rate of solvent [34] because the silicon substrate contacts directly the heater while the copper grid is held up by a tweezer in an oven, and the substrate effect on formation of nanocubes due probably to the interaction between the substrate and the GNCs solution.[35] Next, by drop casting on the copper grid at 200 ℃ for 12h, a large amount of rods (diameter:40-80 nm) are connected each other to form the brush-like branch and furtherly have a tendency to construct a hexagonal structure in local. The different morphology between TEM (Figure 15e-f) and AFM (Figure 13c) results might be due to the difference of total amount volume (TEM: 10 μL, AFM: 400 μL) and substrate (TEM: copper, AFM: silicon). We have a reason to assume that honeycomb structures can be obtained on the copper grid when reaching the satisfied concentration of BR06 GNCs after thermal annealing process.

However, the cubic and donut structure from the spherical GNCs by temperature-induced morphology evolution, can be visual on the silicon substrate, there still remains a question as to whether these structures are formed during drying process or it indeed exists in solution. To solve the issue, the GNCs obtained in the deionized water are

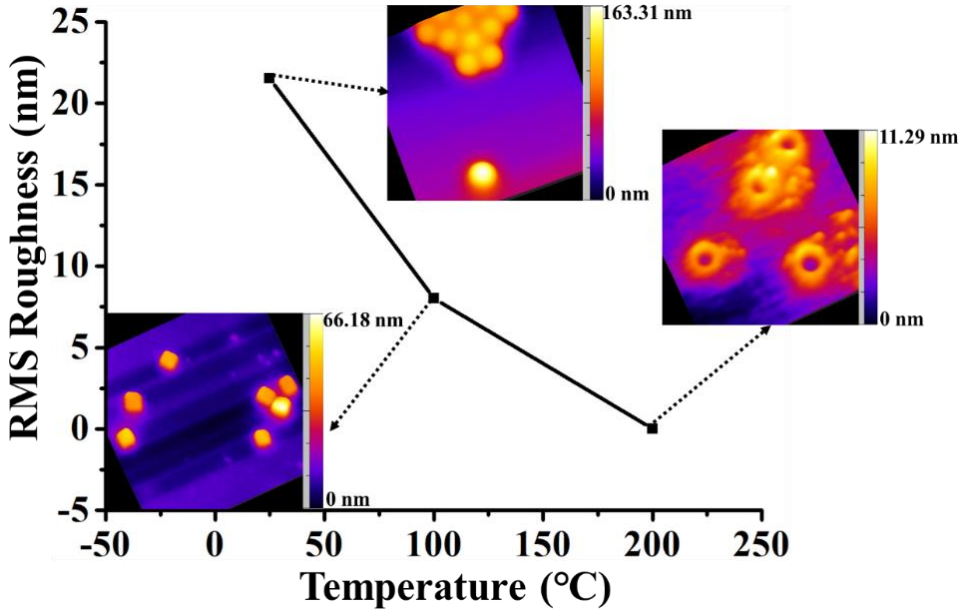

Figure 14. Plot of average RMS roughness collected from the AFM height images of the BR06 nanoparticles (10 drops, 0.69 mg/mL, Figure 3, step 2) under different temperatures dropped casting on the silicon substrates. Three insert images are the 3D images at corresponding temperature.

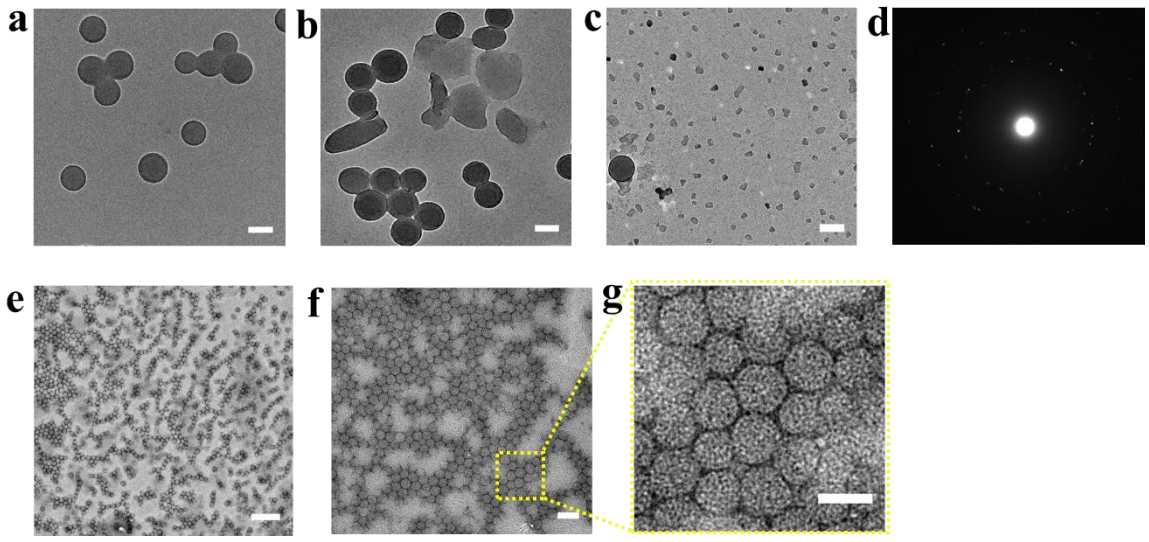

Figure 15. TEM images of BR06 GNCs (0.069 mg/mL in deionized water, 10 µL) by drop casting on a copper grid and then drying at different temperatures and times. (a) at 25 ℃ for 12h. (b) at 100 ℃ for 12h. (c) at 100 ℃ for 96 h. (d) TEM diffraction pattern from c. (e-g) at 200 ℃ for 12 h. (a-c, g) Scale bar for100 nm. (e) Scale bar for 500 nm. (f) Scale bar for 200 nm.

investigated by DLS and TEM experiments before and after thermal treatment in solution. As shown in Figure 16a, upon thermal annealing at 100 ℃ for 12h for BR06 GNCs suspension (0.069 mg/mL in deionized water, 2 mL) contained by a tube in the autoclave, a sharp monomodal relaxation time distribution can be obtained at at the scattering angles of 90° with the $D_{h,90°}$ values of 102 nm. The average diameter of those spheres calculated from TEM in Figure 16c is 93 nm which is closed to the value calculated from DLS results in Figure 16a. Furtherly, upon thermal annealing at 200 ℃ for 12h for BR06 GNCs suspension (0.069 mg/mL in deionized water, 2 mL) contained by a tube in the autoclave, two relaxation time distributions can be observed at the scattering angles of 90° with the $D_{h,90°}$ values of 90 nm and 756 nm respectively, which is consistent with the individual nanoparticle and agglomerate observed in TEM images (Figure 16d,g). We speculate that high temperature causes the degradation of BR06 GNCs shell to a certain extent in water, leading to the shrinking of BR06 GNCs on the whole. TEM tests (Figure 16d,g) confirm the above conjecture in which the concrete spheres with unvisual shell are surrounded with many floccules possible from degradation of BR06 GNCs. Based the above DLS AFM and TEM results, it is reasonable to infer that evaporation of the solvent is able to induce crystallization of BR06 GNCs suspension on the substrates upon thermal annealling.

4.3 Glyconanoparticles preparation from the BR05

As shown Figure 17, another bottlebrush with smaller moleculer weight (BR05) GNCs can be also prepared by following the SDEMS method. To investigate the hydrodynamic radius and size distribution of the resulted nanoparticles (0.069 mg/mL) by diluting the solution (Figure 17, step 3) into deionized water, dynamic light scattering (DLS) measurements are carried out on the nanoparticle dispersions. Figure 17a shows the relaxation time functions at scattering angles at 90° and the autocorrelation functions at the scattering angles of 30°-135° at interval 15°. A monomodal relaxation time distribution can be observed for the nanoparticles from the BR05 (0.069 mg/mL) in deionized water, which indicated the well-defined GNCs with

the $D_{h,90°}$ values of 128 nm. By the Stokes-Einstein relation from the diffusion coefficient values (Ddiff: 3322.13 nm^2ms^{-1}) that is obtained by the linear relationship between the relaxation frequency ($\Gamma = 1/\tau$) and the square of the wavevector (q^2), the D_h is calculated to be 148 nm (Figure 17c). To investigation into structural features of BR05 single particle, AFM experiments are performed to analyze single-particle surface morphology by dropping casting BR05 particle solution (0.069 mg/mL in deionized water, 10 drops) on the hydrophilic modified silicon substrate for 12h at room temperature. As shown in Figure 18a-c, 3D image and the cross-sectional analysis of the AFM images reveal that the individual nanoparticles from BR05 have a round shape with average in size 119 nm and an average height of 95 nm, but not hollow structures like a vesicle. Considering the round shape structure as well as the large diameter, the

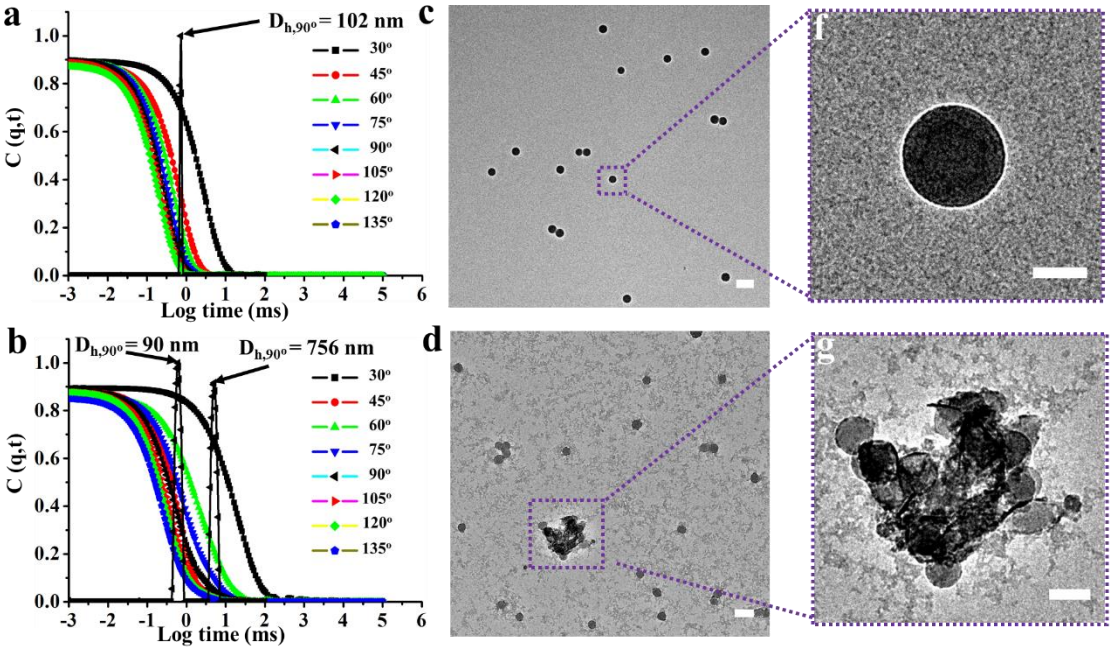

Figure 16. DLS results for the nanoparticles prepared from BR06 GNCs suspension (0.069 mg/mL in deionzied water) after thermal annealling (a) at 100 ℃ for 12h, (b) at 200 ℃ for 12h. Autocorrelation function C(q,t) measured at scattering angles of 30°-135° by step of typically 15° and relaxation time distribution A(t) at 90°. TEM images of BR06 GNCs suspension in a glass tube (0.069 mg/mL in deionized water, 2 mL) after thermal annealling (c,f) at 100 ℃ for 12h, (d,g) at 200 ℃ for 12h. (c, d) Scale bar for 200 nm. (f) Scale bar for 50 nm. (g) Scale bar for 100 nm.

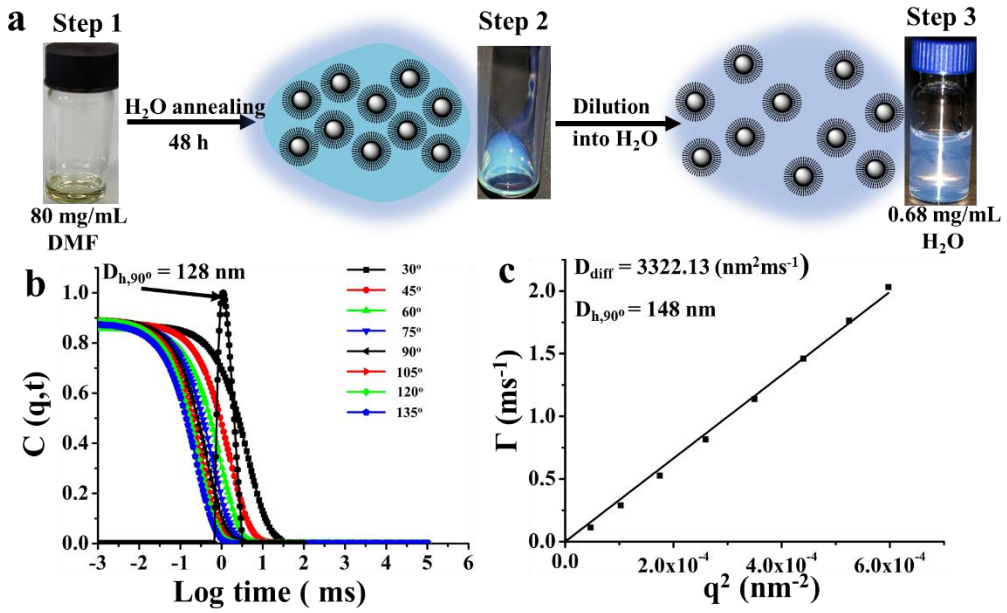

Figure 17. (a) Schematics and photographs of BR05 solution (80 mg/mL, 0.4 mL DMF) and their self-assembly into highly homogeneous core-shell nanoparticles by using the SDEMS method and furtherly diluted in to deionized water. (b) DLS results for the nanoparticles prepared from BR05 (0.069 mg/ml) in deionized water by diluting step 3 solution (0.69 mg/ml). Autocorrelation function C(q,t) measured at scattering angles of 30°-135° by step of typically 15° and relaxation time distribution A(t) at 90°. (c) Dependence of relaxation frequency (Γ) on the square of the wavevector (q^2).

architecture of BR05 GNCs are possible belong to the core-shell shape that core consisted of PS and a thin shell layer consisted of MH. Figure 18d and 18e show the TEM Images for nanoparticles prepared from BR05 under different scan sizes. Individual spherical nanoparticle are clearly observed with thin shell and domain core. The individual nanoparticle and nanoparticles formed fusional structure of several individual nanoparticles without clear boundaries. In specific, the hydrophobic PS core part of GNCs can join together forming a small tube in the junction of GNCs as shown in the insert image of Figure 18e. Furtherly, the core compose of PS can be merged together due to the hydrophobic force. The narrow size distribution observed in the TEM analysis (Figure 18f) is consistent with the sharp and monomodal relaxation time distribution of the nanoparticle dispersion obtained from DLS. The average diameter value of the nanoparticles is calculated to be 77 nm based

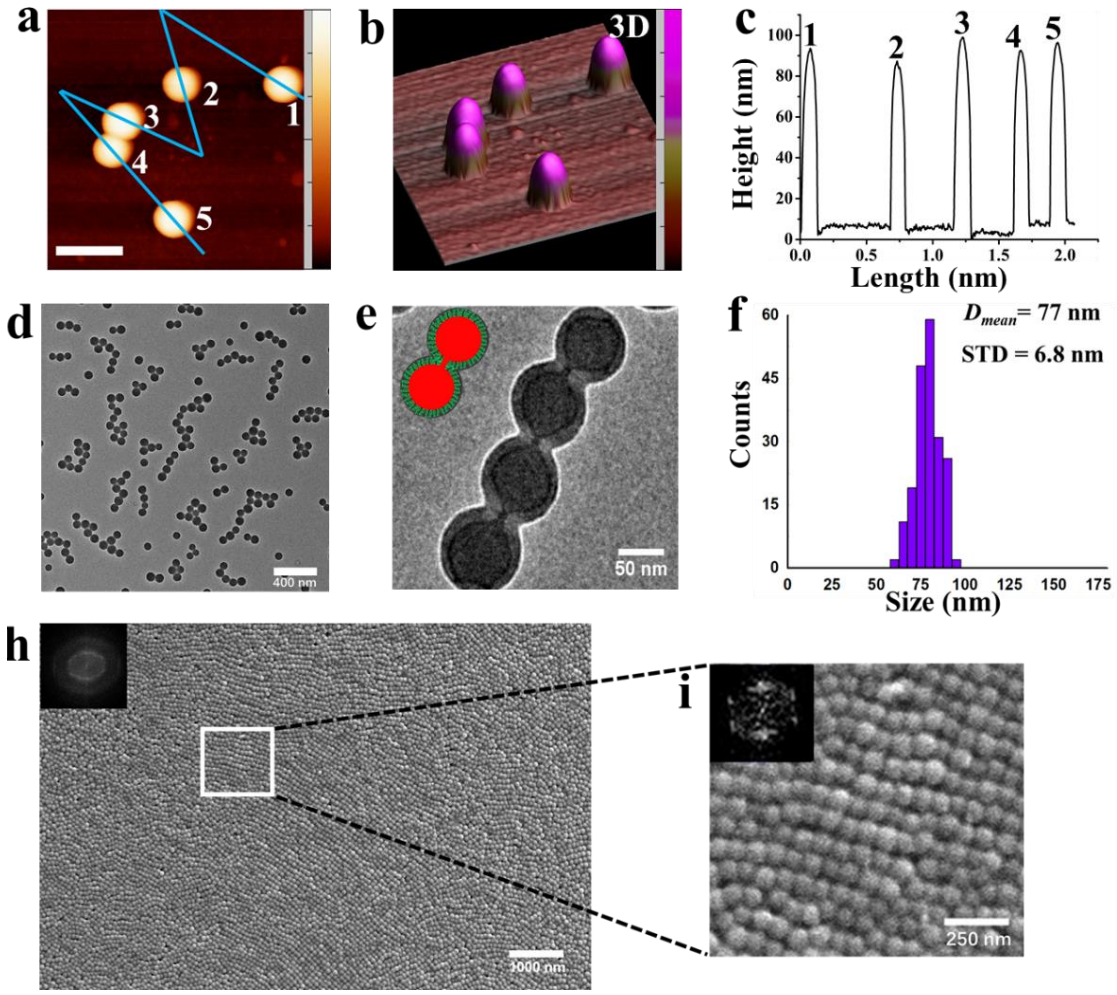

Figure 18. (a) AFM height images of the BR05 NCs (0.069 mg/mL in deionized water from step 3 in Figure 17) dropped casting on a silicon slide with ambient drying for 12h. scale bar for 200 nm (b) the corresponding 3D view of the height image. (c) the corresponding section analysis of the height image by the blue line. (d) TEM images of the BR05 NCs (Figure 17, step 3) with different scale size, scale bar for 400 nm. (e) scale bar for 50 nm (f) the diameter distribution collected from (d), The left-up insert image in (e) is schematic image. green: MH; red: polystyrene. (h) SEM images of the BR05 GNCs (Figure 17, step 3), scale bar for 1000 nm. (i) scale bar for 250 nm in zoon image from (h).

on TEM analysis, which confirms that the particle diameter of BR05 nanoparticles is smaller than those observed by AFM analysis. SEM images (Figure 18h) exhibit homogeneous nanoparticles (75 nm diameter) over the entire scan area. Furthermore, the GNCs pack together to form a hexagonal arrangement in short range as shown in Figure 18i. The 2D Fourier transform of the left bottom portion of the image in short

range shows the six intensity peaks denoting periodicity and hexagonal structure of the nanoparticles with a periodicity of approximately 78 nm (corresponding to the measured averaged diameter of GNCs), indicating that the BR05 nanoparticles are preferentially incorporated into the 2D structure.

4.3.1 Temperature effect on surface morphology of BR05 GNCs

Figure 19 shows the similar morphology evolution of BR05 GNCs on the hydrophilic modified silicon substrate by the control of annealing temperature compared to that of BR06 GNCs. On the whole, the formation of sphere at room temperature, normal cubic, irregular cubic, cylinder, triangular prism and hexagon at 200 ℃ are depicted by the schematic illustration and AFM height images. More specifically, the influence of annealing temperature in the morphology evolution of BR05 GNCs is also studied by the AFM images, line-profiles and surface roughness. Firstly, the BR05 nanoparticle solution (0.069 mg/mL in deionized water, 10 drops) is dropped casting on the hydrophilic modified silicon substrate with ambient drying for 24h as shown in Figure 19. The height and the diameter of the single nanoparticle is analysed by the cross-sectional line-profile in Figure 18c (diameter: 119 nm; height: 95 nm).Upon thermal annealling at 200 ℃ for 6h, a drastic morphology evolution of the BR05 GNCs can be clearly observed in the Figure 19, that is, spherical BR05 GNCs go through a significant flattening to form various irregular architectures as shown in Figure 19 and 20.

As for the low concentration area in Figure 19b and 20 a-f, most of BR05 GNCs have a tendency to form a cubic accompanied with irregular cylinder and triangular prism. The height of cubes in range of 8.5-27.2 nm decreases significantly compared to that of NCs at 25 ℃, and the diameter of cubes in range of 37.7-158.1 nm shows the obviously inhomogeneity in comparison with that of GNCs at 25 ℃. As contrast, the shell of the GNCs composed of MH can be unvisual which may ascribe to that the hydrophilic MH side chains of the BR05 bottle-brush detached from the backbone of bottlebrush macromolecules and further spread out on the flat hydrophilic modified silicon substrate. The drive force for the BR05 GNCs shape transition from the round to the normal cubic, irregular cubic, cylinder and triangular prism may ascribe to

preferentially achieved the minimization of total surface energy to reach the most stable configuration.[31] As for the high concentration area in Figure 19 c and 20 g-i, AFM height images exhibit that the GNCs can order a hexanol structure in short range by drop casting on the hydrophilic substrate at 25 ℃ for 12h. After thermal annealling at 200 ℃ for 6h, a flower-like hexagonal structure composed of a small cavities and hexamer in which six adjacent units connect together. Additionally, the substate surface roughness decreases along with the increasing temperature as shown in Figure 21. More experiments obout the effect of temperature, time and substrate are underway in future.

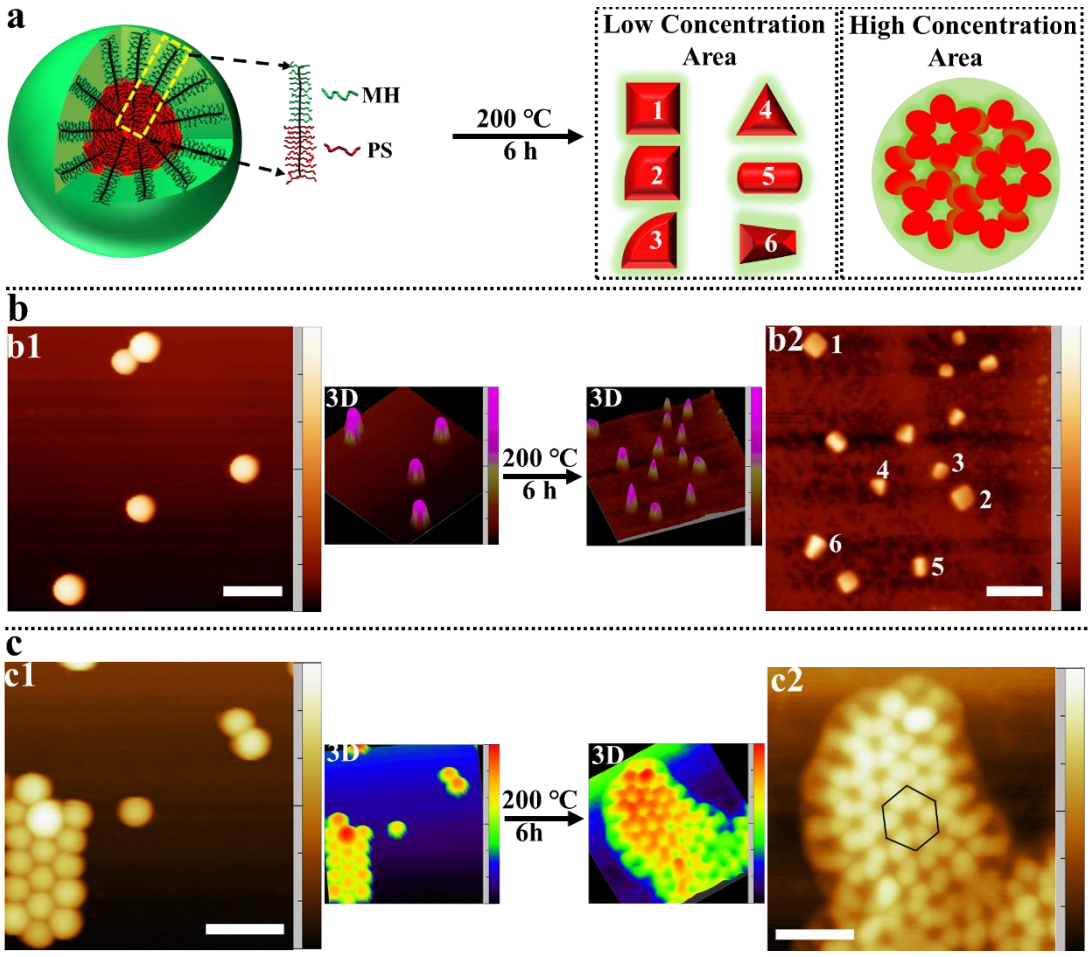

Figure 19. Schematic (a) and AFM height images (b,c) of the BR05 nanoparticles (0.069 mg/mL in deionized water from diluting step 2 solution in Figure 17) dropped casting on a silicon before and after thermal annealing at 200 ℃ for 6h. (b) b1 and b2 scan bar:200 nm; b1: 0.00-99.77 nm for height, b2: 0.00-41.12 nm for height. (c) c1 and c2 scan bar:200 nm; c1: 0.00-100.40 nm for height, c2: 0.00-47.67 nm for height.

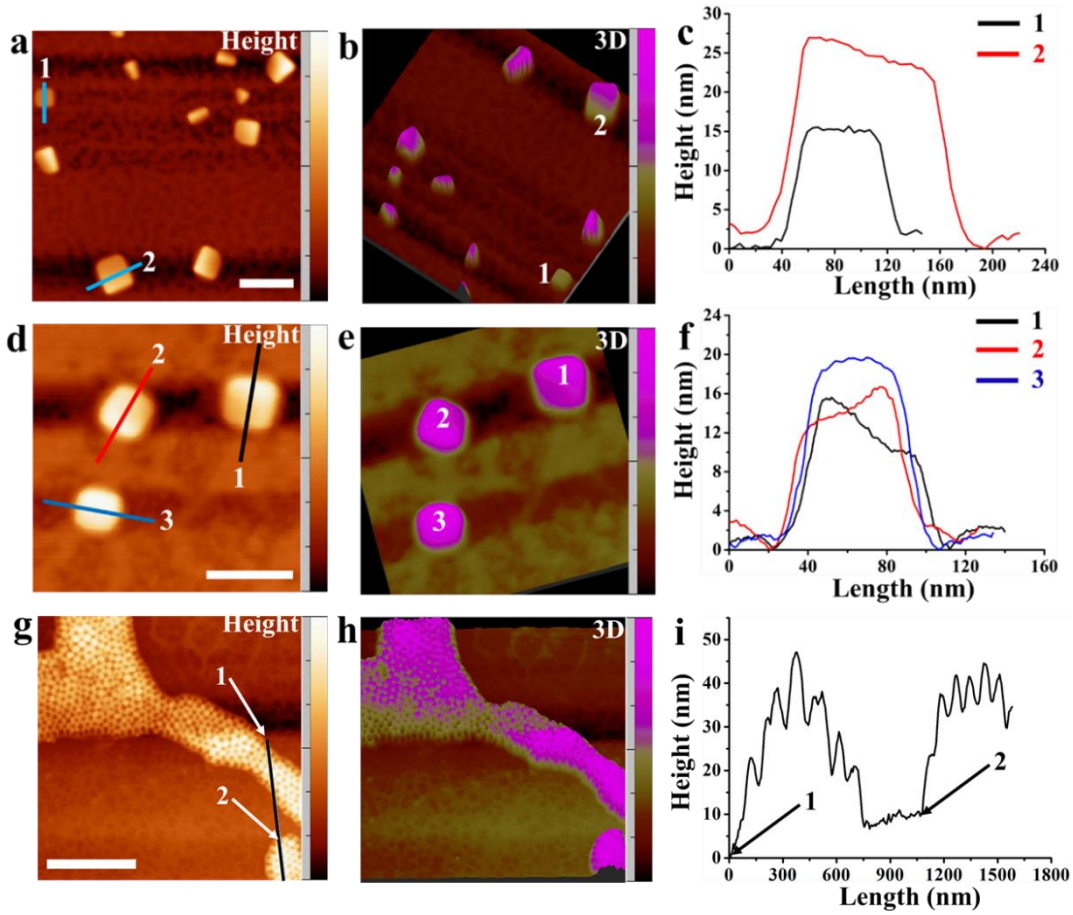

Figure 20. AFM height images, 3D images and profile lines of the BR05 GNCs (0.069 mg/mL in deionized water, Figure 17, step 3) dropped casting on a silicon at 200 ℃ for 6h. (a) scan bar:200 nm; 0.00-44.83 nm for height, (d) scan bar:100 nm; 0.00-26.00 nm for height, (g) scan bar:1000 nm; 0.00-61.88 nm for height, (b, e, h) 3-D side view by the corresponding height image, (c, f, i) the corresponding section analysis of the height images by the lines. (a-f) low concentration area, (g-i) high concentration area.

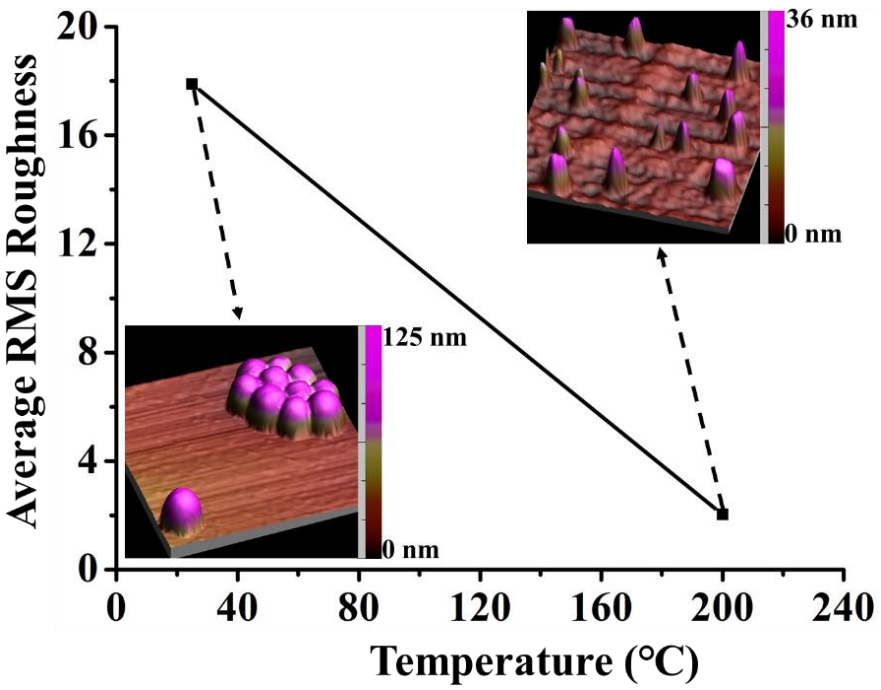

Figure 21. Plot of average RMS roughness collected from the AFM height images of the BR05 GNCs (0.069 mg/mL in the deionized water) dropped casting on the silicon substrates under different temperature anealing by AFM tapping mode. (a). Two insert images are the 3D image of corresponding temperature.

4.4 Experimental Section

The formation of BR01-04 emulsions: BR01-04 (20 mg/mL, DMF, 0.5 mL), PVA and SDS (10 or 20 mg/mL, deionized water, 5 mL) were firstly prepared and then an homogenizer (IKA T25 digital Ultra-Turrax) was used to obtain the BR01-04 emulsions under different setting conditions (speed: 3-15k rpm, time: 5-120 s). Initially, 5 mL PVA solution (20 mg/mL) was added into a glass vial which was fitted with the homogenizer tip. Sequentially, the setting program of homogenizer device started to work while 500 µL BRs solutions (20 mg/mL, DMF) was injected into solutions closed to the spinning impeller of the homogenizer. The obvious emulsion bubbles can be observed at the interface of air/water after finishing the program of the homogenizer. Those solutions were left to stand for 2h and taken photos.

Atomic Force Microscopy (AFM): Nanoparticle solutions (0.069 mg/mL) prepared by diluting solution in deionized water were dropped on a silicon substrate, and then

dried at room temperature. The AFM measurements were realized with a Dimension ICON instrument from Bruker Company. The surface topography was investigated via a soft-tapping mode. Imaging was performed with an App-Nano tip having a radius of less than 10 nm and a spring constant range of 13-77 N/m. AFM images plotting and their data analysis were achieved with the Gwyddion free software.

Dynamic light scattering (DLS): DLS measurements were carried out with the ALV/CGS-8FS/N069 device (from ALV). This apparatus is equipped with a 35 mW red helium-neon linearly polarized laser (from JDSU) operating at a wavelength of 632.8 nm and with the ALV/LSE-5004 multiple τ digital correlator (from ALV) having an initial sampling time of 125 ns. The cylindrical cells (diameter = 10 mm) containing aqueous liquid suspensions were immerged in a toluene bath and thermostated prior to the measurements for few minutes at a temperature of 25.0 ± 0.1°C. Data were collected at different scattering angles ranging from 30 to 135° (modulus of the scattering vector q from 6.85×10^{-3} to 2.44×10^{-2} nm^{-1}) by step of typically 15° for a counting time of 300 s at each angle with the help of the digital ALV correlator control software. The relaxation time distributions were obtained using Contin analysis of the autocorrelation functions $(g(2)^{-1})$.

Transmission Electron Microscope (TEM): Drops of nanoparticle suspensions were deposited on glow-discharged carbon-coated copper grids and dried in air. Transmission electron microscopy was performed using a JEM-2100 Plus (JEOL Ltd., Japan) operated at an accelerating voltage at 200 kV. All electron micrographs were recorded on a Gatan Rio 16 camera (Gatan Inc., USA).

Glyconanoparticles preparation: As shown in Figure 3, water vapor in the atmosphere would diffuse into the DMF solution of BRs in a vial in a sealed chamber under water vapor, with DMF evaporating into the atmosphere. As the water content within the DMF solution was increasing along with time, the self-assembly of could be initiated from the air-solution interface where the water content was presumably highest. We assumed that the formation of GNCs of the BRs could proceed downwards from the interface caused by diffusion of water. After 24h, the vial was removed from the

chamber and dilute it into water to quench the assembly process. we obtained the nanoparticle solutions of BR06 in water. This method was named solvent diffusion-evaporation-mediated self-assembly (SDEMS, Figure 3).

4.5 Conclusion

A series of carbohydrate-based bottlebrushes consisting of MH and PS side chins can self-assemble into homogenous GNCs having outer shell made of MH by using SDEMS. The diameter of core-shell GNCs is increasing with the molecular weight of BRs (2.4-3.0 million) by incorporation of branching in the MH and PS, which were proved by a combination of DLS, AFM, SEM and TEM, allowing to characterize the nanoparticle morphology and to follow the structural evolution. Interestingly, the investigation on evolution of various morphology of BRs nanostructures is successfully demonstrated by the variation of the annealing temperature, time as well as by the molecular weight of BRs. By dropping casting BR06 GNCs suspension on the hydrophilic-modified silicon substrate, at low concentration area, AFM images reveal that BR06 GNCs show the spherical nanostructure at room temperature and the BR06 GNCs domain morphology can be altered for the flattened uniform cubic nanostructure upon thermal annealing at 200 ℃ for 12h. Upon increasing temperature to 200 ℃, various nanostructures including irregular rod, cubic, triangle and homogenous donut are clearly observed after the evaporation of solvent. As constrast, at high concentration area, the hexangonal struture in short range at low temperature can be tansformed into honeycomb structure with cavities upon upon thermal annealing at 200 ℃ for 12h. Based on above results, these BR06 glycol-nanoparticles, with the stabilizing MH shell and a PS core, are able to degrade, reorganize and possibly self-assemble upon increasing the annealing temperatures. Additionally, these BR05 glycol-nanoparticles have a similar property at various temperature. Understanding how functional core-shell NCs maintain or alter their particle morphology during annealing allowed controlling the morphology at both nano- and macro-scale.

References:

1. Walsh, D. J.; Dutta, S.; Sing, C. E.; Guironnet, D., Engineering of molecular geometry in bottlebrush polymers. *Macromolecules* **2019,** *52* (13), 4847.
2. Lin, T. P.; Chang, A. B.; Chen, H. Y.; Liberman-Martin, A. L.; Bates, C. M.; Voegtle, M. J.; Bauer, C. A.; Grubbs, R. H., Control of grafting density and distribution in graft polymers by living ring-opening metathesis copolymerization. *J Am Chem Soc* **2017,** *139* (10), 3896.
3. Miyake, G. M.; Piunova, V. A.; Weitekamp, R. A.; Grubbs, R. H., Precisely tunable photonic crystals from rapidly self-assembling brush block copolymer blends. *Angew Chem Int Ed Engl* **2012,** *51* (45), 11246.
4. Hu, B.; Carrillo, J. M.; Collins, L.; Silmore, K. S.; Keum, J.; Bonnesen, P. V.; Wang, Y.; Retterer, S.; Kumar, R.; Lokitz, B. S., Modular approach for the synthesis of bottlebrush diblock copolymers from poly(glycidyl methacrylate)-block-poly(Vinyldimethylazlactone) backbones. *Macromolecules* **2022,** *55* (2), 488.
5. Ji, E.; Cummins, C.; Fleury, G., Precise synthesis and thin film self-assembly of PLLA-b-PS bottlebrush block copolymers. *Molecules* **2021,** *26* (5), 1412.
6. Xia, Y.; Olsen, B. D.; Kornfield, J. A.; Grubbs, R. H., Efficient synthesis of narrowly dispersed brush copolymers and study of their assemblies: the importance of side chain arrangement. *J Am Chem Soc* **2009,** *131* (51), 18525.
7. Hong, S. W.; Gu, W.; Huh, J.; Sveinbjornsson, B. R.; Jeong, G.; Grubbs, R. H.; Russell, T. P., On the self-assembly of brush block copolymers in thin films. *ACS Nano* **2013,** *7* (11), 9684.
8. Patel, B. B.; Walsh, D. J.; Kim, D. H.; Kwok, J.; Lee, B.; Guironnet, D.; Diao, Y., Tunable structural color of bottlebrush block copolymers through direct-write 3D printing from solution. *Sci Adv* **2020,** *6* (24), 7202.
9. Li, Z.; Tang, M.; Liang, S.; Zhang, M.; Biesold, G. M.; He, Y.; Hao, S. M.; Choi, W.; Liu, Y.; Peng, J.; Lin, Z., Bottlebrush polymers: from controlled synthesis, self-assembly, properties to applications. *Prog Polym Sci* **2021,** *116*.
10. Niu, W.; Zhang, L.; Wang, Y.; Zhang, S., Multicolored one-dimensional photonic crystal coatings with excellent mechanical robustness, strong substrate adhesion, and liquid and particle impalement resistance. *J Mater Chem C* **2019,** *7* (12), 3463.
11. Guo, T.; Yu, X.; Zhao, Y.; Yuan, X.; Li, J.; Ren, L., Structure memory photonic crystals prepared by hierarchical self-assembly of semicrystalline bottlebrush block copolymers. *Macromolecules* **2020,** *53* (9), 3602.
12. Liu, S.; Yang, Y.; Zhang, L.; Xu, J.; Zhu, J., Recent progress in responsive photonic crystals of block copolymers. *J Mater Chem C* **2020,** *8* (47), 16633.
13. Song, D. P.; Zhao, T. H.; Guidetti, G.; Vignolini, S.; Parker, R. M., Hierarchical photonic pigments via the confined self-assembly of bottlebrush block copolymers. *ACS Nano* **2019,** *13* (2), 1764.
14. Li, Y. L.; Chen, X.; Geng, H. K.; Dong, Y.; Wang, B.; Ma, Z.; Pan, L.; Ma, G. Q.; Song, D. P.; Li, Y. S., Oxidation control of bottlebrush molecular conformation for producing libraries of photonic structures. *Angew Chem Int Ed Engl* **2021,** *60* (7), 3647.

15. Wong, C. K.; Qiang, X.; Müller, A. H. E.; Gröschel, A. H., Self-assembly of block copolymers into internally ordered microparticles. *Prog Polym Sci* **2020,** *102*, 101211.
16. Yang, Y.; Kang, T. H.; Wang, K.; Ren, M.; Chen, S.; Xiong, B.; Xu, J.; Zhang, L.; Yi, G. R.; Zhu, J., Tunable photonic microspheres of comb-like supramolecules. *Small* **2020,** *16* (29), 2001315.
17. Zhao, T. H.; Jacucci, G.; Chen, X.; Song, D. P.; Vignolini, S.; Parker, R. M., Angular-independent photonic pigments via the controlled micellization of amphiphilic bottlebrush block copolymers. *Adv Mater* **2020,** *32* (47), 2002681.
18. He, Q.; Ku, K. H.; Vijayamohanan, H.; Kim, B. J.; Swager, T. M., Switchable full-color reflective photonic ellipsoidal particles. *J Am Chem Soc* **2020,** *142* (23), 10424.
19. Chen, X.; Song, D. P.; Li, Y., Precisely tunable photonic pigments via interfacial self-assembly of bottlebrush block copolymer binary blends. *Macromolecules* **2022,** *55* (17), 7438.
20. Jacucci, G.; Vignolini, S.; Schertel, L., The limitations of extending nature's color palette in correlated, disordered systems. *Proc Natl Acad Sci U S A* **2020,** *117* (38), 23345.
21. Park, C.; La, Y.; An, T. H.; Jeong, H. Y.; Kang, S.; Joo, S. H.; Ahn, H.; Shin, T. J.; Kim, K. T., Mesoporous monoliths of inverse bicontinuous cubic phases of block copolymer bilayers. *Nat Commun* **2015,** *6*, 6392.
22. Blanco, E.; Shen, H.; Ferrari, M., Principles of nanoparticle design for overcoming biological barriers to drug delivery. *Nat Biotechnol* **2015,** *33* (9), 941.
23. Zhu, L.; Zhao, B., Transmission electron microscopy study of solvent-induced phase morphologies of environmentally responsive mixed homopolymer brushes on silica particles. *J Phys Chem B* **2008,** *112* (37), 11529.
24. Isono, T.; Miyachi, K.; Satoh, Y.; Nakamura, R.; Zhang, Y.; Otsuka, I.; Tajima, K.; Kakuchi, T.; Borsali, R.; Satoh, T., Self-assembly of maltoheptaose-block-polycaprolactone copolymers: carbohydrate-decorated nanoparticles with tunable morphology and size in aqueous media. *Macromolecules* **2016,** *49* (11), 4178.
25. Li, H.; Mumtaz, M.; Isono, T.; Satoh, T.; Chen, W. C.; Borsali, R., Self-assembly of carbohydrate-based block copolymer systems: glyconanoparticles and highly nanostructured thin films. *Polym J* **2022,** *54* (4), 455.
26. Shao, Y.; Jia, Y. G.; Shi, C.; Luo, J.; Zhu, X. X., Block and random copolymers bearing cholic acid and oligo(ethylene glycol) pendant groups: aggregation, thermosensitivity, and drug loading. *Biomacromolecules* **2014,** *15* (5), 1837.
27. Wanka, G.; Hoffmann, H.; Ulbricht, W. J. M., Phase diagrams and aggregation behavior of poly (oxyethylene)-poly (oxypropylene)-poly (oxyethylene) triblock copolymers in aqueous solutions. *Macromolecules* **1994,** *27* (15), 4145.
28. Wolff, N.; Gerth, S.; Gutfreund, P.; Wolff, M., Temperature dependent cubic and hexagonal close packing in micellar structures. *Soft Matter* **2014,** *10* (42), 8420.
29. He, X.; Schmid, F., Spontaneous formation of complex micelles from a homogeneous solution. *Phys Rev Lett* **2008,** *100* (13), 137802.

30. Margulis, K.; Zhang, X.; Joubert, L. M.; Bruening, K.; Tassone, C. J.; Zare, R. N.; Waymouth, R. M., Formation of polymeric nanocubes by self-assembly and crystallization of dithiolane-containing triblock copolymers. *Angew Chem Int Ed Engl* **2017,** *56* (51), 16357.
31. Pandey, P.; Kunwar, S.; Sui, M.; Bastola, S.; Lee, J., Investigation on the morphological and optical evolution of bimetallic Pd-Ag nanoparticles on sapphire (0001) by the systematic control of composition, annealing temperature and time. *PLoS One* **2017,** *12* (12), 0189823.
32. Huang, H.; Chung, B.; Jung, J.; Park, H. W.; Chang, T., Toroidal micelles of uniform size from diblock copolymers. *Angew Chem Int Ed Engl* **2009,** *48* (25), 4594.
33. Jiang, Y.; Zhu, J.; Jiang, W.; Liang, H. J., Cornucopian cylindrical aggregate morphologies from self-assembly of amphiphilic triblock copolymer in selective media. **2005,** *109* (46), 21549.
34. Howard, M. P.; Reinhart, W. F.; Sanyal, T.; Shell, M. S.; Nikoubashman, A.; Panagiotopoulos, A. Z., Evaporation-induced assembly of colloidal crystals. *J Chem Phys* **2018,** *149* (9), 094901.
35. Zhang, W.; Shi, L.; An, Y.; Shen, X.; Guo, Y.; Gao, L.; Liu, Z.; He, B., Evaporation-induced aggregation of polystyrene-block-poly(acrylic acid) micelles to microcubic particles. *Langmuir* **2003,** *19* (15), 6026.

Chapter 5: Shape-changing in Individual Macromolecules of Carbohydrate-based Brush Block Copolymers

5.1 Introduction

Bottlebrush polymers, anchored with high density of side chains on a linear-polymeric backbone, gives prominence to the unique shape and individual characteristic of macromolecules.[1-4] The repel force between high-grafted density of side chains can support these macromolecules to elongate the linear backbone and reduce entanglement happened frequency to their linear analogues. As a result, brush molecules have a tendency to exhibit the worm-like or cylindrical conformation with an outstanding spatiality.[5] Cylindrical architecture are anisotropic owning to their high aspect ratio. High surface areas and large volume of cylindrical objects in comparison with spherical objects, result in an excellent performance in surface adsorption and encapsulation.[6] Upon response to external stimuli such as pH,[7] solvent,[8] temperature,[9] mechanical[10] and magnetic flied[11] so on, bottlebrush polymers individual macromolecular is able to show a dynamic change in the conformation. In addition, the tunability of side chain density and length and special crystal behavior make them to a promising candidate for diverse of applications such as drug delivery. Therefore, it is interesting/challenge for researchers to design and characterize responsive bottlebrush polymers accompanied with conformations transform under various condition.[12] To date, the conformation transition of brush molecules exposed to external stimuli have been extensively investigated on the substrate by using AFM. For example, in 2006, Sheiko Group reported that conformation transforms and spontaneous scission of covalent bonds of the homo-brushes backbone took place upon adsorption of macromolecules on mica.[13] As shown in Figure 1, the homopolymer brush molecule attached with long side chains poly(n-butyl acrylate) was spontaneously imaged by using AFM for a period of time on the water/propanol (99.8/0.2 wt/wt %) mica. As a function of time, the shorter and increasing number of brush molecules at same region can be clearly presented in Figure 1 a, indicating the fracture of carbon-carbon bonds in the backbone. This behavior of brush molecules can be ascribed to the maximizing interplay between the mica and

extending side chains, causing the strong tension enough to break C-C bonds. Unlike the homopolymer brushes, the conformations of block brush moleclues can present diverse of association pattern as reported by Matyjaszewski and colleagues in 2008.[14] As shown in Figure 1c, individual macromolecular of block brushes composed of a bare visual tail poly(ε-caprolactone) and brighter head poly(n-butyl acrylate) can be clearly observed on the substrate. Furtherly, by manipulating the dense film of this block brush, dumbbell-like and flower-like architectures can be characterized by AFM phase images.

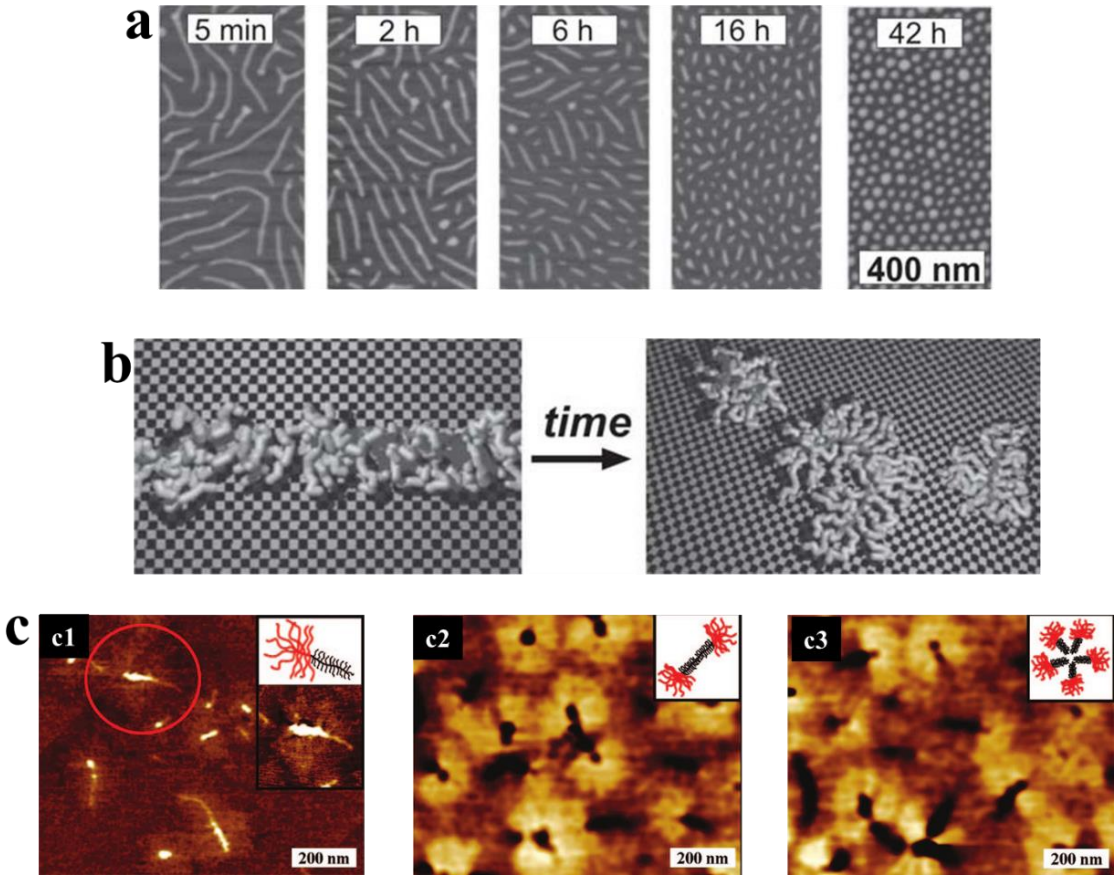

Figure 1. (a) Real-time monitoring AFM height images of individual homopolymer brushes upon adsorption onto mica as function of time, resulting in the scission of carbon-carbon bonds. (b) Schematic illustration of single adsorbed homopolymer brush (left) and continuous fracture of C-C bonds in the backbone (right). Backbone (dark grey) and side chains (light grey).[13] (c) AFM images of single macromolecules (c1) and dense films (c2, c3) from hetero-grafted block brushes.[14]

In case, we are also interested in study the conformation behavior of block brushes on the substrate since a series of well-defined bottlebrush block copolymers (BRs) are in

hands. As we know, BRs endow with two distinct blocks of side chains attached with a linear backbone, leading to a new spatiality of the individual macromolecular on surfaces. Their single molecular brushes adsorption onto planar substrates can disrupt their cylindrical symmetry leading to the assignment of side chains (Figure 2). Furthermore, interplay with substrates is able to prompt the organization of adsorbed macromolecules with specific conformations. The conformation of macromolecules adsorbed on the surface is dominated by two factors :(1) the distribution of side chains adsorbed on the surface relative to the main chain; (2) the number of adsorbed side chain on the surface. By manipulating the above two factors, the globular, curved, ribbon-like, and cylindrical conformations can be achieved from block brush molecules

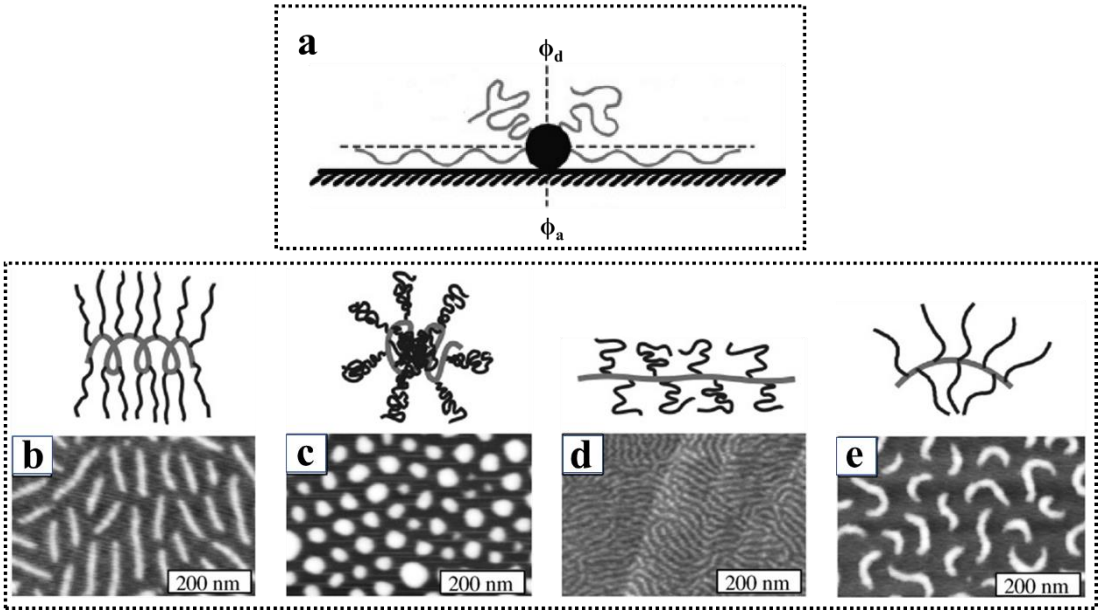

Figure 2. (a) Scheme for the confined conformation of brush-like macromolecules upon adsorption on the substrate is influenced by cylindrical symmetry of side chains and its interconnectivity. (b) ribbon-like ($\phi_a \approx 1$), (c) globe-like ($\phi_a < 1$, desorbed side chains appeal each other), and (d) cylinder-like ($\phi_a < 1$, desorbed side chains repel each other) and (e) spontaneous-curved (asymmetry side chains of two distinct block brushes) conformations (down) and schematic illustrations (upper) of brush-like macromolecules on the substrate can be dominated by the interplay between side chains and ambient environment and substrates as shown in AFM images.[1,12]

adsorbed on the surface (Figure 2 b-e). If the ratio of side chains adsorbed on the surface is prominent, the brush molecules have a tendency to exhibit the energetically-favored conformation (ribbon-like) (Figure 2b) owing to providing efficient surface contact in lager number. If the ratio of side chains desorbed on the surface is prominent, brush molecules will tend to change into other shapes influenced by ambient atmosphere. When exposed to the poor environment (solvent or air), the side chains desorbed on the surface try to join together, bring about the backbone coil, finally get a conformation of globe (Figure 2c). In contrast, there is still possible for desorbed side chains to be cylinder due to steric repel force between side chains in a good solvent (Figure 2d).[12] Moreover, the spontaneous-curved conformation tends to happen to the block brushes with asymmetry two distinct side chains (Figure 2e).[1]

In this context, a series of glycol-BRs (BR01-07) attached with the solvophilic maltoheptaose (MH) and solvophobic polystyrene (PS) side chains, are used to investigate their morphologies on the mica along with the time or highly oriented pyrolytic graphite (HOPG) by atomic force microscopy (AFM). Expectedly, an increase in the average length from about 25 nm, 35 nm to 100 nm can be observed along with BR02, BR03, BR04 and BR07 on micas, which are consistent with increasing the backbone polymerization of BRs. The height and width of the adsorbed polymers on micas are 1.0 ± 0.3 nm and 25 ± 5 nm respectively, and remains similarity across all the images. Impressively, multiple morphologies including worm-like, S- or C-shape, tadpole-like, helical-like, pearl-necklacelike, Globular-like, hair-like, droplet-like and island-like, are able to be observed along with the time from a single BR07 high dilution solution by spin coating on mica. In contrast, globe-shape, toroid-shape and crystal-like conformation can be obtained by spin coating on the HOPG substrate at same condition. Herein, diverse of conformation and dynamic shape-changing of BR07 hierarchical molecular architecture, show a potential application for drug delivery.

5.2 Results and Discussion

In this section, individual molecules of BR07 (table 1, detail information) and their conformational changes along with time are successfully visualized by atomic force microscopy (AFM). The shape and dimensions of individual PS brush-MH brush and their assemblies are investigated by AFM, which provides spatial resolution down to the sub-nanometer scale. In the context, highly diluted solution of brush-like block copolymer BR07 (0.001 mg/mL) is prepared in dimethylformamide (DMF), a good solvent of PS and MH branches, and spin-casted on mica to form deposits of individual macromolecules. Figure 3 shows the topographic and phase images of BR07 in which diversity of conformations including worm-like, helical-like, spontaneous curved, tadpole-like and globular shapes, can be clearly observed by AFM after spinning coating on mica due to the tendency to equilibrium conformation (minimum free energy)

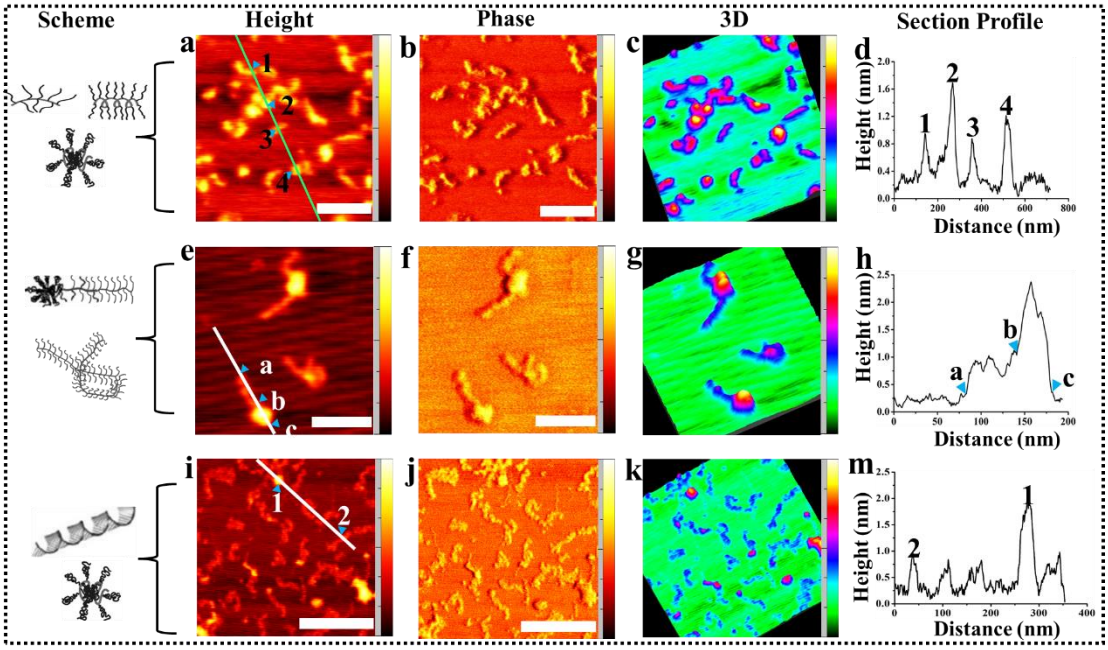

Figure 3. Schemes and AFM Images of the BR07 high diluting solution (0.001 mg/mL in DMF, 20 uL) dropped casting on a mica at room temperatures by spinning coating for 10 mins under blowing air. (a, e, i) height. (b, f, j) phase. (c, g, k) 3-D view by the corresponding height images a and e. (d, h, m) the corresponding section analysis of the height images a, e and m by the lines. (a, b, i, j) Scan bar for 200 nm. (e, f) Scan bar for 100 nm. (a, c) 0.00-2.61 nm for height. (e, g) 0.00-2.69 nm for height. (i, j) 0.00-2.81 nm for height.

depend on the interplay of the intramolecular and surface force.[15] In specific for worm-like conformation (height: 0.55 nm; length: 90 nm; width: 37 nm), the white threads correspond to the backbone, whereas the corona area around the threads is covered by extended side chains at the periphery of backbone. Changes in the colors of 3D height image, Figure 3c (red: backbone, blue: side chain), allowed visualizing better the two constitutive moieties of the macromolecules. The height profile of height images is shown in Figure 3d. The coil-like or globe-like macromolecular presents a range height of 1.00-1.46 nm, while the worm-like macromolecular is more flattened and exhibits an average height of about 0.54 nm, because the free energies of these two conformations vary differently with respect to the contact area and interaction strength.[16]

As shown in Figure 3e-g, head-head self-assembly of two tadpole-shaped macromolecules, a twisted worm-like macromolecular and a tadpole-shaped macromolecular can be clearly observed and the schematic representations of them are left alongside the corresponding individual macromolecular of height image. Specifically, a light brown cylindrical object of the tadpole-shaped macromolecular corresponding to MH moiety is capped by a bright-white sphere corresponding to the PS moiety (Figure 3e). The MH part preferred to adopt an overall worm-like conformation with a length of 61.11 nm and a height of only 0.51 nm, indicating that the MH branches are lying completely flat on the substrate due to their strong affinity toward mica. The PS moieties can be observed as white circular domains with a height of 2.03 nm, which is about 4 times higher than the MH. The two constitutive moieties of the macromolecules can be better distinguished in 3D images. This result can be ascribed to the lower affinity of the PS side chains for the polar mica surface, which in turn reduce their surface of contact with the support.[17] For the twisted worm-like conformation, the contour length of it is roughly calculated to be 144 nm by measuring part-by-part with an average height length of 0.47 nm, which is smaller than the fully extended BR07 macromolecular assumed by theoretical formula.[18]

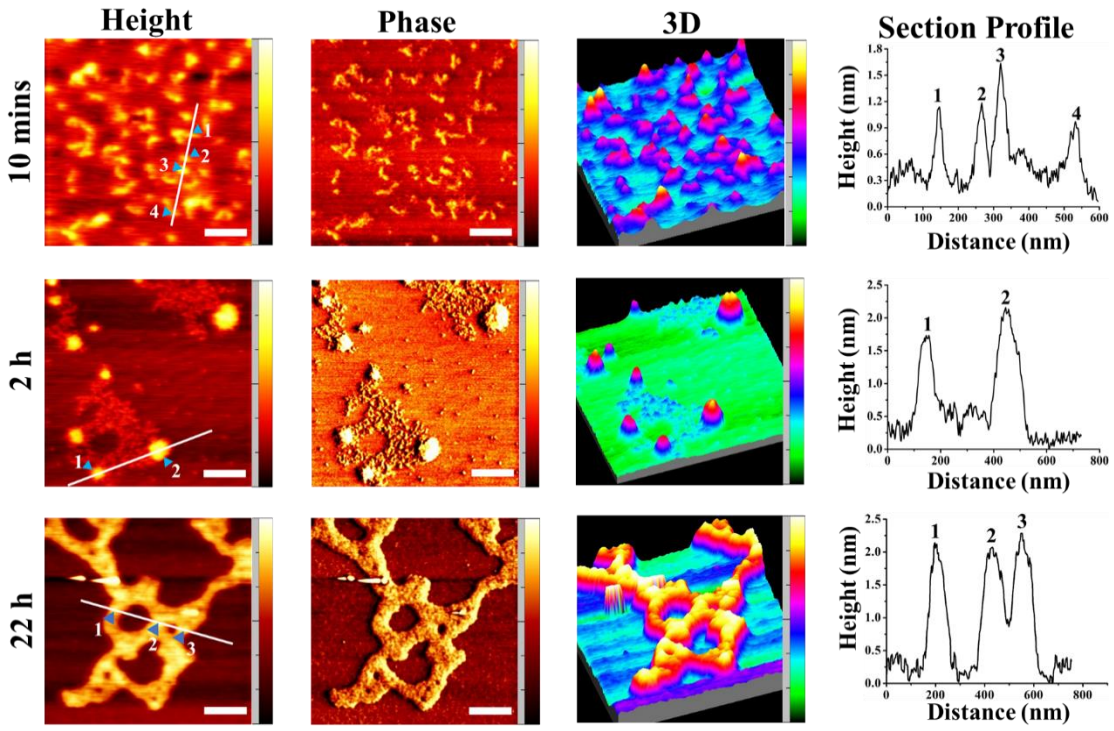

Figure 4. Dynamic AFM Images of the BR07 high diluting solution (0.001 mg/mL in DMF, 20 uL) on a mica at room temperature after spinning coating for 10 mins under blowing air. Columns from left to right are the height, Phase, 3-D view by the corresponding height images and the corresponding section analysis of the height images by the lines, respectively. Scan bar for 200 nm.

As shown in Figure 4, after spinning coating BR07 high diluting solution on mica, a continuous transformation of BR07 conformation can be clearly observed exposed to ambient environment at room temperature by using AFM. Some macromolecules are curved and present the characteristic S-like conformation with an average height of 0.56 nm while some macromolecules contract with a range height of 0.82-1.11 nm, indicating that the assembly process of BR07 macromolecules takes place probably on the mica during DMF solvent evaporation. The observed conformation transition from wormlike conformation to globules is consistent along with time because the surface of mica is still wet by DMF and the DMF may absorb water from the surrounding atmosphere, resulting in a poor local environment. The BR07 macromolecules are able to gain mobility and diffuse the mica surface due to the wet surrounding. In order to the avoidance of hydrophilic mica surface by the hydrophobic PS side chains, the BR07

macromolecules prefer to form spheres with MH corona shell and PS inner core, further aggregate to cluster of spheres when the sample exposed to the ambient atmosphere for longer times. After 2h, all of BR07 macromolecules form small spheres (height :0.3-0.6 nm) spreading out the scan area in which most of them bead up into the cylinder as tiny hairs at periphery of the larger droplets from the aggregation of some spheres. The droplets with a height of about 1.22-1.81 nm are higher dramatically than the initial height of BR07 individual macromolecular. After 22 h, this aggregation droplets further try to join together and final lead to the formation of an island-like 2D structure with an average height of 2.23 nm.[19] In a word, dynamic conformation changes of the adsorbed brush macromolecules along with time can be clearly observed on the mica, providing their dynamic hierarchical molecular architecture.

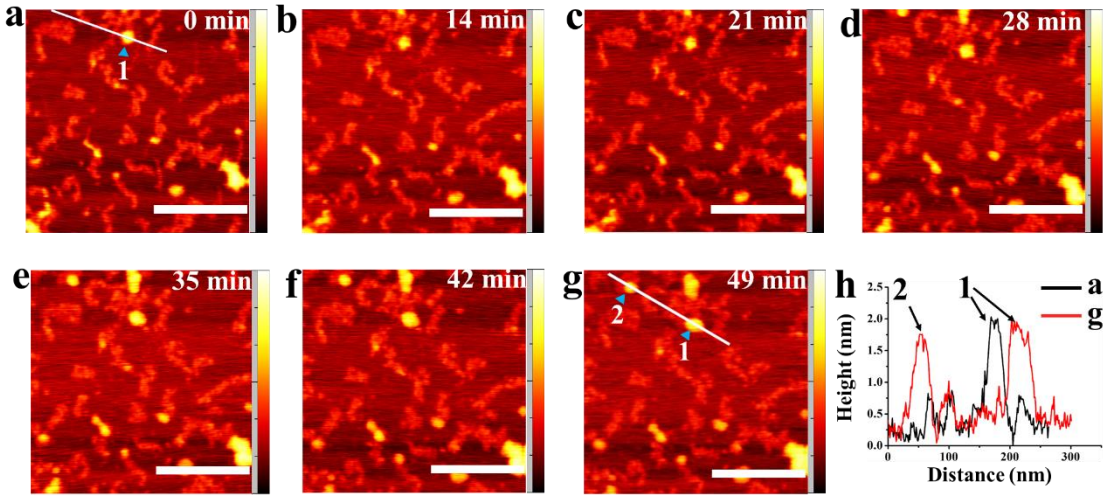

Figure 5. Real-time AFM Height Images in 1h of the BR07 high diluting solution (0.001 mg/mL in DMF, 20 uL) on a mica at room temperature after spinning coating for 10 mins under blowing air. Scan bar for 200 nm.

To real-time monitor shape-changing of BR07 brush molecules on mica in short range of time, a continuous AFM images focusing on the same area is carried on in 1h as shown in Figure 5. In the beginning, many helical-like brush molecules (average height: 0.45 nm) and a few globe-like objects (average height: 1.41 nm) can be clearly observed in the heigh AFM images. As time goes on, the small globe-like object marked 1 in the Figure 5a is growing into bigger one with lager widths and moving down a little bit (in Figure 10a and 10d). Meanwhile, several new globular objects emerge in the same area

in the Figure 10a which is probably due to the aggregation of the neighboring helical-like macromolecules. In this context, it is reasonable for BR07 block brush molecules to have a capability to move around on mica due to the wet surface.

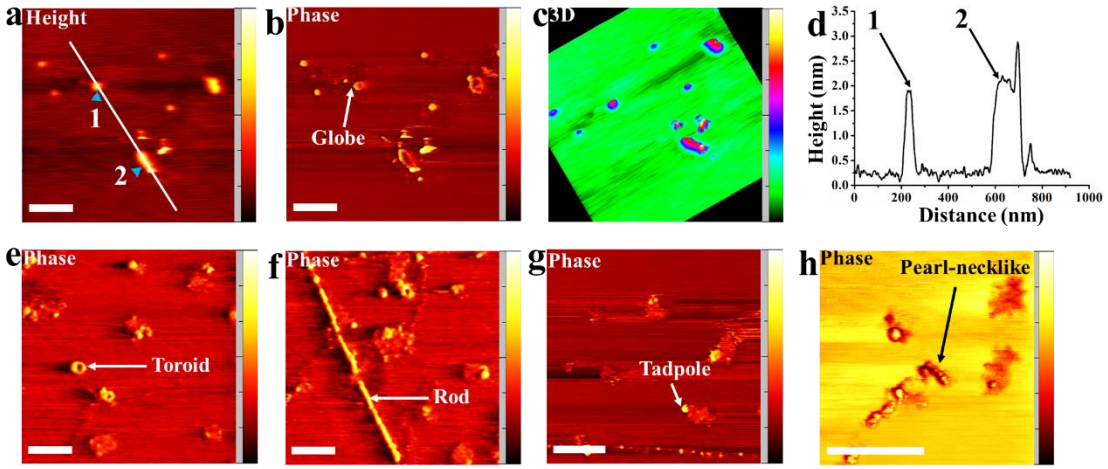

Figure 6. AFM Images of the BR07 high diluting solution (0.001 mg/mL in DMF, 20 uL) on HOPG substrate at room temperature after spinning coating for 10 mins under blowing air. (a-d) The first row from left to right are the height, Phase, 3-D view by the corresponding height images and the corresponding section analysis of the height images by the lines, respectively. (e-h) Phase images in different region. (a) 0.00-3.30 nm for height. (a, b, e-h) Scan bar for 200 nm.

To investigate the substrate effect for the conformation of BR07 block brush molecules on surfaces. Meanwhile, by spinning coating BR07 high diluting solution on HOPG substrate, AFM images are subsequently carried out by a soft-tapping mode. As shown in Figure 6, globe-shape, tadpole-shape, toroid-shape, rod-shape and pearl-necklacelike conformations can be observed on the HOPG substrate at same condition. In comparison with its conformation on mica (Figure 3), BR07 macromolecules are more prone to form globular-related conformations which can be ascribed to the combination effect of larger molar ratio of hydrophilic MH (0.67) and highly hydrophobic HOPG surface, resulting in reducing contact area between MH branches and HOPG surface, further segregating on the surface and finally coil into globes. These neighboring globes are able to join together with some association pattern into the toroid-shape, pearl-necklacelike and rod. Based on the above results, the conformation of single BR07 macromolecules on surface can be indeed affected by different substrates.

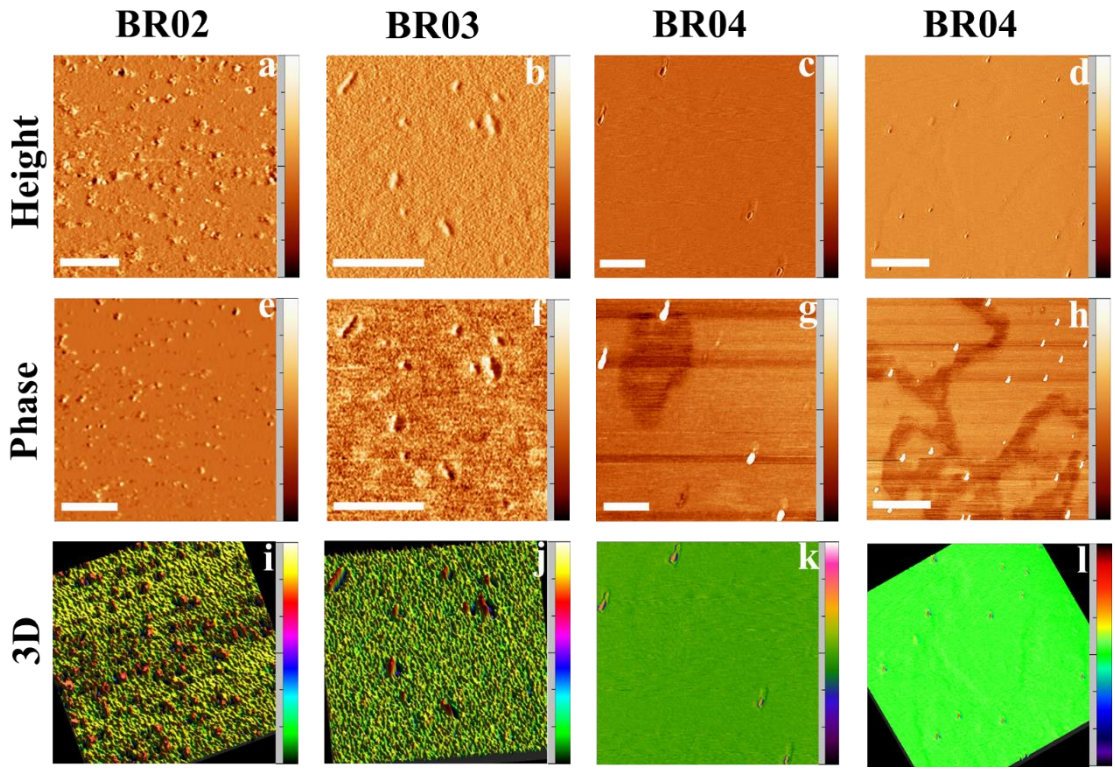

Figure 7. AFM Images of the BR02, BR03 and BR04 high diluting solution (0.001 mg/mL in DMF, 20 uL) on mica at room temperature after spinning coating for 10 mins under blowing air. The first column from up and down is the height, Phase, 3-D view, respectively. (a, i) 0.00-2.93 nm for height. (b, j) 0.00-3.48 nm for height. (c, k) 0.00-3.60 nm for height. (d, l) 0.00-3.45 nm for height. (a-c, e-h) Scan bar for 200 nm. (d, h) Scan bar for 500 nm.

To investigate the composition of side chains effect on the conformation of individual macromolecular on surface, the shape and dimensions of BR02, BR03, and BR04 free chains on mica are also carried out by using soft mode AFM, expecting spatial resolution down to the sub-nanometer scale and strong contrast of different chemical composition (PS and MH). With regards to this, highly diluted solutions of BR02, BR03, and BR04 (0.001 mg/mL in DMF, 20 uL) are spin-casted on mica for 10 mins to form deposits of individual brush molecule. As shown in Figure 7, an increase in the average length from about 25 nm, 35 nm to 100 nm can be observed along with BR02, BR03, and BR04 on micas, which are consistent with increasing backbone polymerization of brush block copolymers. The height and width of the adsorbed polymers on micas are 1.0 ± 0.3 nm and 25 ± 5 nm respectively, and remains similarity across all the images.

In comparison with BR03 and BR04, most of BR02 brush molecules with the lowest polymerization of backbone have a tendency to form a globule conformation possible due to its highest mobility among them. For BR03 brush molecules, the inhomogeneity of these macromolecules can be clearly observed on mica which may ascribe to the inherent polydispersity in the backbone length[20] and macromolecules deformation on adsorption to the mica surface.[21, 22] One can further be observed that BR04 with the largest backbone polymerization have an extended cylinder conformation composed of two distinct parts, that is, a bare visual tail MH and brighter head PS. Taking advantage of 3D image, two distinct constitutive moieties of BR04 brush molecules can be better visualized in Figure 7k. The polynorbornene-g-maltoheptaose moiety corresponded to slightly-raised green part, have an average length of 50 nm with a height of only 0.20 nm, indicating that the MH branches are lying completely flat on the substrate due to their strong affinity toward mica. The polynorbornene-g- polystyrene moieties are observed as stand-up red rods with an average length and height of 50 nm and 0.61 nm respectively, i.e., about 3 times higher than the PS ones. This is due to the lower affinity of the PS branches for the hydrophilic mica surface, which in turn tend to reduce their surface of contact with mica.

For these three polymers, the Length of individual macromolecular increases significantly with increasing backbone polymerization. Although we cannot draw strong conclusions from these three polymers, we note that there is a modest increase in persistence length with increasing backbone polymerization.

5.3 Experimental section

Atomic Force Microscopy (AFM): Highly dilution solutions (0.001 mg/mL in DMF) were prepared by diluting initial BRs solution (0.1 mg/mL in DMF) 100 times, dropped on substrates (mica and HOPG), and then spin-coated (20 μL, 500 rpm/sec, 10 mins) under blowing air at room temperature. The AFM measurements were realized with a Dimension ICON instrument from Bruker Company. The surface topography was investigated via a soft-tapping mode. Imaging was performed with an App-Nano tip

having a radius of less than 10 nm and a spring constant range of 13-77 N/m. AFM images plotting and their data analysis were achieved with the Gwyddion free software.

5.4 Conclusion

A series of BRs (BR02-04, 07) can be used to investigate their morphologies on surface (mica) or highly oriented pyrolytic graphite (HOPG) as a function of time using atomic force microscopy (AFM). Expectedly, an increase in the average length from about 25 nm, 35 nm to 100 nm can be observed along with increasing molar mass on mica, which are consistent with increasing the backbone polymerization of BRs. Impressively, multiple morphologies including worm-like, S- or C-shape, tadpole-like, helical-like, Globular-like, hair-like, droplet-like and island-like, can be observed at high dilution solution by spin coating on mica. In contrast, globe-shape, tadpole-shape, toroid-shape rod-like and pearl-necklacelike conformations are obtained by spin coating on the HOPG substrate. Herein, diverse of conformation and dynamic shape-changing of BRs hierarchical molecular architecture, show a potential in different applications.

References:

1. Xie, G.; Martinez, M. R.; Olszewski, M.; Sheiko, S. S.; Matyjaszewski, K., molecular bottlebrushes as novel materials. *Biomacromolecules* **2019,** *20* (1), 27.
2. Liu, Y.; Vancso, G. J., Polymer single chain imaging, molecular forces, and nanoscale processes by atomic force microscopy: the ultimate proof of the macromolecular hypothesis. *Prog Polym Sci* **2020,** *104*, 101232.
3. Liu, W. B.; Xu, X. H.; Kang, S. M.; Song, X.; Zhou, L.; Liu, N.; Wu, Z. Q., Bottlebrush polymers carrying side chains on every backbone atom: controlled synthesis, polymerization-induced emission, and circularly polarized luminescence. *Macromolecules* **2021,** *54* (7), 3158.
4. Qi, H.; Liu, X.; Henn, D. M.; Mei, S.; Staub, M. C.; Zhao, B.; Li, C. Y., Breaking translational symmetry via polymer chain overcrowding in molecular bottlebrush crystallization. *Nat Commun* **2020,** *11* (1), 2152.
5. Zhao, B., Shape-changing bottlebrush polymers. *J Phys Chem B* **2021,** *125* (24), 6373.
6. Foster, J. C.; Varlas, S.; Couturaud, B.; Coe, Z.; O'Reilly, R. K., Getting into shape: reflections on a new generation of cylindrical nanostructures' self-assembly using polymer building blocks. *J Am Chem Soc* **2019,** *141* (7), 2742.
7. Kent, E. W.; Zhao, B., Stimuli-induced star-globule shape transitions of dually responsive binary heterografted three-arm star molecular brushes in aqueous solution. *Macromolecules* **2019,** *52* (17), 6714.
8. Gallyamov, M. O.; Tartsch, B.; Mela, P.; Borner, H.; Matyjaszewski, K.; Sheiko, S.; Khokhlov, A.; Moller, M., A scanning force microscopy study on the motion of single brush-like macromolecules on a silicon substrate induced by coadsorption of small molecules. *Phys Chem Chem Phys* **2007,** *9* (3), 346.
9. Li, C.; Gunari, N.; Fischer, K.; Janshoff, A.; Schmidt, M., New perspectives for the design of molecular actuators: thermally induced collapse of single macromolecules from cylindrical brushes to spheres. *Angew Chem Int Ed Engl* **2004,** *43* (9), 1101.
10. Xu, H.; Sun, F. C.; Shirvanyants, D. G.; Rubinstein, M.; Shabratov, D.; Beers, K. L.; Matyjaszewski, K.; Sheiko, S. S., Molecular pressure sensors. *Adv Materi* **2007,** *19* (19), 2930.
11. Zhang, M.; Estournès, C.; Bietsch, W.; Müller, A. H. E., Superparamagnetic hybrid nanocylinders. *Adv Funct Mater* **2004,** *14* (9), 871.
12. Sheiko, S. S.; Sumerlin, B. S.; Matyjaszewski, K., Cylindrical molecular brushes: synthesis, characterization, and properties. *Prog Polym Sci* **2008,** *33* (7), 759.
13. Sheiko, S. S.; Sun, F. C.; Randall, A.; Shirvanyants, D.; Rubinstein, M.; Lee, H. I.; Matyjaszewski, K., Adsorption-induced scission of carbon-carbon bonds. *Nature* **2006,** *440* (7081), 191.
14. Lee, H. I.; Matyjaszewski, K.; Yu-Su, S.; Sheiko, S. S., Hetero-grafted block brushes with PCL and PBA side chains. *Macromolecules* **2008,** *41* (16), 6073.
15. Potemkin, I. I.; Khokhlov, A. R.; Prokhorova, S.; Sheiko, S. S.; Möller, M.; Beers, K. L.; Matyjaszewski, K., Spontaneous curvature of comblike polymers at a flat interface. *Macromolecules* **2004,** *37* (10), 3918.

16. Sheiko, S. S.; Prokhorova, S. A.; Beers, K. L.; Matyjaszewski, K.; Potemkin, I. I.; Khokhlov, A. R.; Möller, M., Single molecule rod-globule phase transition for brush molecules at a flat interface. *Macromolecules* **2001,** *34* (23), 8354.
17. Tang, C.; Dufour, B.; Kowalewski, T.; Matyjaszewski, K., Synthesis and morphology of molecular brushes with polyacrylonitrile block copolymer side chains and their conversion into nanostructured carbons. *Macromolecules* **2007,** *40* (17), 6199.
18. Chiang, J. F.; Chiang, R.; Lu, K. C.; Sung, E. M.; Harmony, M. D., The molecular structure of norbornene as determined by electron diffraction and microwave spectroscopy. *J Mol Struct* **1977,** *41* (1), 67.
19. Gallyamov, M. O.; Tartsch, B.; Potemkin, II; Borner, H. G.; Matyjaszewski, K.; Khokhlov, A. R.; Moller, M., Individual bottle brush molecules in dense 2D layers restoring high degree of extension after collapse-decollapse cycle: directly measured scaling exponent. *Eur Phys J E Soft Matter* **2009,** *29* (1), 73.
20. Romio, M.; Grob, B.; Trachsel, L.; Mattarei, A.; Morgese, G.; Ramakrishna, S. N.; Niccolai, F.; Guazzelli, E.; Paradisi, C.; Martinelli, E.; Spencer, N. D.; Benetti, E. M., Dispersity within brushes plays a major role in determining their interfacial properties: the case of oligoxazoline-based graft polymers. *J Am Chem Soc* **2021,** *143* (45), 19067.
21. Klein, J., Surface interactions with adsorbed macromolecules. *J Colloid Interface Sci* **1986,** *111* (2), 305.
22. Xin, Y.; Kielar, C.; Zhu, S.; Sikeler, C.; Xu, X.; Moser, C.; Grundmeier, G.; Liedl, T.; Heuer-Jungemann, A.; Smith, D. M.; Keller, A., cryopreservation of DNA origami nanostructures. *Small* **2020,** *16* (13), 1905959.

General Conclusions and Perspectives

Conclusions

Carbohydrates as a promising building block, have aroused researchers' interest for designing a new smart polymer system for application in photonic crystals and nanoparticles due to its natural abundance and green properties. Recently, bottlebrush block copolymers have exhibited unparalleled advantages to fabricate photonic crystals compared to linear block copolymers via self-assembly. Taking consideration of previous study on carbohydrate-based linear block copolymer system in our group over the last decade, the combination of carbohydrates and UV-responsive polystyrene into bottlebrush block copolymers (BRs) as side chains could assemble into diverse of polymeric nanostructures in films and solution for optical and biological medicine applications. The purpose of my Ph.D. project is to fabricate the responsive one-dimensional photonic crystals reflecting structural coloration in films or solution via self-assembly.

Firstly, a series of well-defined BR01-07 attached with MH and PS as the branches, have been successfully synthesized at range of $0.82x10^6$-$5.01x10^6$ g/mol via the combination of grafting-through and grafting-to approach by M. Mumtaz (a post-doc. in our group). Sequentially, the self-assembly of these bottlebrushes into one-dimensional photonic crystals (1D-PCs) is investigated by UV-vis spectrum, microscopy, SEM and SAXS. The full-color of the 1D-PCs prepared from BR01-04 individually or blending BR04 with sorbitol, can be obtained from colorless, blue, green, orange to grey covering the entire UV-vis. spectrum range which is consistent with domain spacing ranged from 89-245 nm from SEM results. Impressively, the optical appearance of the BR01or BR02 1D-PCs can be changed from blue, green, yellow, orange to pink, through the whole visible spectral range, by simply controlling preparation techniques and solvent annealing, showing the tunability, responsiveness , and reversibility of BR01 and BR02 1D-PCs. The wavelength of BR04 absorbance and transmission scales linearly increased with weight sorbitol ratios, ranging from the orange, through red, to grey, allowing for the modulation of photonic properties by

blending bottlebrushes with short linear polymers, as well as providing a route to obtaining tailorable photonic crystals without synthesizing new carbohydrate-based bottlebrushes.

In order to obtain the photonic crystals in solution, the confined self-assembly of BRs in the emulsified water is also carried out under various conditions including molecular weight, surfactants, concentrations, homogenizer speed and time. Unfortunately, only blue color can be observed in these solutions. Surprisingly, highly homogenous core-shell glyconanoparticles can be easily obtained via the self-assembly of carbohydrate-based BR05-06 under the water vapor environment. The diameter of core-shell glyconanoparticles with precisely position and highly density of MH composed of shell, can be adjustable by manipulating the molecular weight of BRs. Specifically, AFM images showed that the surface morphology of the sphere glyconanoparticles from a single BR06 on the hydrophilic-modified silicon can be tunable into multiple conformations such as cubic and donut structure after thermal annealing treatments, which may put forward new insight into the design and synthesis of functional materials with unique structures, properties, and applications by using post-treatments of the glyconanoparticles.

In the last chapter of the PhD project, the conformation of BRs individual macromolecular on surface are investigated by atomic force microscopy (AFM). Expectedly, an increase in the average length from about 25 nm, 35 nm to 100 nm can be observed on mica along with increasing backbone polymerization of BRs. Impressively, multiple morphologies including worm-like, S- or C-shape, tadpole-like, helical-like, Globular-like, hair-like, droplet-like and island-like, can be clearly observed from a single BR07 at high dilution solution by spin coating on mica. In contrast, globe-shape, tadpole-shape, toroid-shape, rod-like and pearl-necklacelike conformations are obtained by spin coating on the highly oriented pyrolytic graphite substrate. As function of time, dynamic shape-changing of BR07 individual

macromolecular conformation on mica, exhibit a promising application for encapsulation and delivery of substances.

In conclusion, the rapid self-assembly of these carbohydrate-based block copolymers (BRs) into 1D-PCs with larger periodicity demonstrates outstanding strengths in comparison with their linear block copolymers of high molecule weight, showing promising applications as optical devices. Upon treatment by external stimuli such as solvent and UV light, the optical properties of 1D-PCs fabricated from BRs are able to be tunable, showing the responsiveness and reversibility of 1D-PCs in structural colorations. Furtherly, homogenous core-shell glyconanoparticles prepared from these amorphous polymeric brush-like BRs can be transferred into diverse of nanostructures such as the symmetrical crystal structure cubic upon evaporation of solvents at elevated temperature. Lastly, the multiple conformations of BRs individual macromolecules composed of hydrophilic MH and hydrophobic PS have a tendency to show a worm-to-globe transition as function of time.

Perspectives

In Chapter 2, bottlebrushes composed of whole biomaterials will be explored for applications in photonic crystals and glycol-nanoparticles.

In Chapter 3, responsive photonic crystals of uniform thickness from water-soluble brush-like block copolymers will be highly desired due to its increasing practical use.

In Chapter 4, photonic crystals in solutions prepared from glycol nanoparticles under UV exposure will be investigated by DLS, AFM and TEM.

In Chapter 5, responsive conformations of uniform individual bottlebrushes in solution and on the substrates will be real-time studied by DLS and AFM.

Publications

1. **Li, H.**; Mumtaz, M.; Isono, T.; Satoh, T.; Chen, W.; Borsali, R. Self-assembly of Carbohydrate-based Block Copolymer Systems: Glyconanoparticles and Highly Nanostructured Thin Films. *Polym. J.* 2022, **54**, 455.

2. Brachi, M.; Buzzetti, M.; Gorgy, K.; Shan, D.; Audebert, P.; Goff, A.; **Li, H.**; Borsali, R.; Cosnier, S. Trialkoxyheptazine-Based Glyconanoparticles for Fluorescence in Aqueous Solutions and on Surfaces via Controlled Binding in Space. *ACS Macro Lett.* 2022, **11**, 135.

3. Zhang, H.; Zhu, X.; **Li, H.**; Liu, G.; Wang, J.; Wang, A.; Kong, L.; Zhu, W.; Zhou, H., A RNA-Targeted Two-Photon Bioprobe with High Selective Permeability into Nuclear Pore Complexes for Dynamically Tracking the Autophagy Process among Multi-Organelles, *Anal. Chem.* 2019, **91**, 14911. (co-first author)

4. **LI, H.**; Mumtaz, M.; Putaux, J.; Ogawa, Y.; Borsali**,** R. Highly Homogenous Core-shell Nanoparticles into Multiple Morphologies from a Single Carbohydrate-based Bottlebrush Block Copolymer. (submitting)

5. **LI, H.**; Mumtaz, M.; Borsali, R. Carbohydrate-based Bottlebrushes and Their Self-assembly: Tunable Full-color Reflective to Photonic Crystals. (submitting)

Meetings

1. Poster: Hong LI, Muhammad MUMTAZ, and Redouane BORSALI, Self-Assembly of Bottle-Brush Glycopolymers into Nanoparticles, Journée de printemps 2022 du GdR DUMBIO, 11-13 May 2022.

2. Oral presentation: The 7th ed. of Nanotech France 2022 Int. Conference and Exhibition, 15 Jun to 17 Jun 2022 Paris-France.